

AD-785 398

SAR IMAGE QUALITY ANALYSIS MODEL

Ralph H. Mitchel

Environmental Research Institute of  
Michigan

Prepared for:

Air Force Avionics Laboratory

May 1974

DISTRIBUTED BY:

**NTIS**

National Technical Information Service  
U. S. DEPARTMENT OF COMMERCE  
5285 Port Royal Road, Springfield Va. 22151

UNCLASSIFIED



AFAL-TR-74-114, Volume II

193900-  
ERIM No. ~~19360~~-10-F

Final Technical Report

# SAR IMAGE QUALITY ANALYSIS MODEL

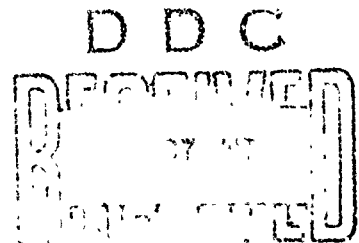
1 July 1972 Through 31 August 1973  
Volume II

R. H. MITCHEL, D. A. AUSERMAN, H. W. DOSS,  
M. B. EVANS, B. H. FRIBERG, and W. D. HALL

Radar and Optics Division

MAY 1974

Approved for public release: distribution unlimited



Air Force Avionics Laboratory  
Air Force Systems Command  
Wright-Patterson Air Force Base, OH 45433  
Contract F33615-72-C-1996



UNCLASSIFIED 11

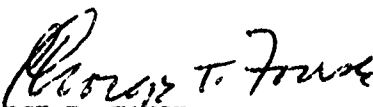
AD785398

## NOTICE

When Government drawings, specifications, or other data are used for any purpose other than in connection with a definitely related Government procurement operation, the United States Government thereby incurs no responsibility nor any obligation whatsoever; and the fact that the government may have formulated, furnished, or in any way supplied the said drawings, specifications, or other data, is not to be regarded by implication or otherwise as in any manner licensing the holder or any other person or corporation, or conveying any rights or permission to manufacture, use, or sell any patented invention that may in any way be related thereto.

Copies of this report should not be returned unless return is required by security considerations, contractual obligations, or notice on a specific document.

This report has been reviewed and is approved for publication.

  
GEORGE T. FOUSE  
Acting Division Chief  
Navigation & Weapon Delivery Div

11-a

UNCLASSIFIED

SECURITY CLASSIFICATION OF THIS PAGE (When Data Entered)

AD-785398

REPORT DOCUMENTATION PAGE		READ INSTRUCTIONS BEFORE COMPLETING FORM
1. REPORT NUMBER AFAL-TR-74-114, Volume II	2. GOVT ACCESSION NO.	3. RECIPIENT'S CATALOG NUMBER
4. TITLE (and Subtitle)  SAR Image Quality Analysis Model		5. TYPE OF REPORT & PERIOD COVERED Final Technical Report 1 Jul 72 - 31 Aug 73
		6. PERFORMING ORG. REPORT NUMBER ERIM Report No. 193900-10-F
7. AUTHOR(s)  Ralph H. Mitchel		8. CONTRACT OR GRANT NUMBER(s)  F33615-72-C-1996
9. PERFORMING ORGANIZATION NAME AND ADDRESS Environmental Research Institute of Michigan Beck Road, P.O. Box 618 Ann Arbor, Wayne County, Michigan 48107		10. PROGRAM ELEMENT, PROJECT, TASK AREA & WORK UNIT NUMBERS Project 698DF Task 03 Work Unit 22
11. CONTROLLING OFFICE NAME AND ADDRESS Air Force Avionics Laboratory AFAL/NVA-698DF Wright-Patterson AFB, Ohio 45433		12. REPORT DATE May 1974
14. MONITORING AGENCY NAME & ADDRESS (if different from Controlling Office) ONRRR/University of Michigan 121 Cooley Bldg. Ann Arbor, Michigan 48105		13. NUMBER OF PAGES 184
		15. SECURITY CLASS. (of this report) Unclassified
15a. DECLASSIFICATION/DOWNGRADING SCHEDULE N/A		
16. DISTRIBUTION STATEMENT (of this Report)  Approved for public release; distribution unlimited		
17. DISTRIBUTION STATEMENT (of the abstract entered in Block 20, if different from Report)		
18. SUPPLEMENTARY NOTES		
19. KEY WORDS (Continue on reverse side if necessary and identify by block number) Synthetic Aperture Radar Image Quality Analysis Threshold Quality Factor Operator Performance Research		
20. ABSTRACT (Continue on reverse side if necessary and identify by block number) This report describes a Synthetic Aperture Radar (SAR) image quality analysis and a model incorporating the conclusions of the analysis into a SAR system digital simulation. The objective of the model and its development program is to provide a fundamental approach for SAR image quality analysis via a model containing sufficient sophistication to quantify image quality effects for specific SAR systems (parameter combinations performing specific missions). The model thus provides a relatively economical (over)		

DD FORM 1473 1 JAN 73 EDITION OF 1 NOV 65 IS OBSOLETE

UNCLASSIFIED

SECURITY CLASSIFICATION OF THIS PAGE (When Data Entered)

NATIONAL TECHNICAL  
INFORMATION SERVICEU.S. Department of Defense  
Springfield, VA 22151

UNCLASSIFIED

SECURITY CLASSIFICATION OF THIS PAGE(When Data Entered)

Block 20 Continued:

prediction of the information which can be extracted from a specified radar-mission configuration.

The model output is a collection of image quality assessment functions, in particular the TQF (Threshold Quality Factor). Other parameters, which indicate the performance of the SAR system, are available from the digital simulation. These include the point target responses along with their locations for a preselected target field configuration.

i-a

UNCLASSIFIED

SECURITY CLASSIFICATION OF THIS PAGE(When Data Entered)

## ABSTRACT

This report describes a SAR (Synthetic Aperture Radar) image quality analysis and an image quality model incorporating the conclusions of the image quality analysis into a SAR system digital simulation. The objective of the model and its development program is to provide a fundamental approach for SAR image quality effects for specific SAR systems (parameter combinations performing specific missions). The model thus provides a relatively economical prediction of the information which can be extracted from a specified radar-mission configuration.

The model output is a collection of image quality assessment functions, in particular the TQF (Threshold Quality Factor). Other parameters, which indicate the performance of the SAR system, are available from the digital simulation. These include the point target response (both range and azimuth) along with their locations for a preselected target field configuration.

## FOREWORD

This study was conducted by the Environmental Research Institute of Michigan beginning in July 1972. The work, under contract F33615-72-C-1996, was sponsored by the Air Force Avionics Laboratory, Air Force Systems Command, at Wright-Patterson Air Force Base, Dayton, Ohio. The project engineer was Sgt. T. F. Stipulkosky.

The project was directed at ERIM by Dr. L. J. Porcello of the Institute's Radar and Optics Division. The principal investigators were Dr. W. D. Hall and Dr. R. H. Mitchel. Other contributors to the project included Mr. M. Evans and Mr. B. Friberg who are responsible for the AIRMOD module, Mr. H. Doss who generated the RSMOD, and Dr. D. Ausherman who devised the IRMOD module. The image quality analysis and IQMOD development were performed by Dr. R. Mitchel.

This final report consists of two volumes. Volume I is CONFIDENTIAL and describes the image quality analysis and its conclusions along with an overview of the SAR simulation. The second volume is Unclassified and contains detailed descriptions of each of the modules composing the simulation.

Details of the technical effort for the period 1 July - 31 December 1972 are contained in the interim report, "Image Quality Analysis," ERIM Report 193900-1-P, Ralph H. Mitchel, July 1973.

## TABLE OF CONTENTS

Introduction . . . . .	1
5.0. AIRMOD Module Description . . . . .	3
5.1. Mode Description. . . . .	3
5.2. Computer Program . . . . .	12
6.0. Radar, Recorder and Processor Simulation . . . . .	18
6.1. Introduction and Background . . . . .	18
6.2. Main Program and Input Models . . . . .	24
6.2.1. Targets . . . . .	24
6.2.2. Aircraft Parameters. . . . .	28
6.2.3. Transmitter-Receiver . . . . .	29
6.2.4. Motion Compensation. . . . .	34
6.2.6. Processor . . . . .	42
6.2.7. Displays . . . . .	45
6.3. Signal Generation . . . . .	46
6.3.1. Timer . . . . .	47
6.3.2. Table . . . . .	51
6.3.3. Point . . . . .	51
6.3.4. MOCOMP . . . . .	54
6.3.5. AMPR . . . . .	54
6.3.6. CHIRPX . . . . .	60



6.3.7. LIMIT . . . . .	60
6.3.8. MTF's . . . . .	63
6.4. Processor . . . . .	64
6.4.1. Focusing for Signal Histories . . . . .	64
6.4.2. Optimization Choices . . . . .	73
6.4.3. Image Location . . . . .	76
6.4.4. Geometrical Distortion. . . . .	77
6.4.5. Processor Subroutines. . . . .	79
6.5. Output . . . . .	80
6.6. Conclusions. . . . .	95
7.0. Impulse Response Generation. . . . .	97
7.1. Introduction. . . . .	97
7.2. Theory of Operation . . . . .	97
7.2.1. Received Signal Generation. . . . .	100
7.2.2. Reference Function Generation. . . . .	104
7.2.3. Performing the Convolution . . . . .	106
7.3. Target Response Software Description. . . . .	109
7.4. Processing Examples . . . . .	119
7.4.1. Demonstration of Motion Errors . . . . .	132
7.4.2. Demonstration of Amplitude Weighting Effects . . . . .	141
7.5. Summary. . . . .	156
Appendix . . . . .	157

## LIST OF ILLUSTRATIONS

1. Single Channel of Inertial Platform . . . . .	13
2. Vertical Channel . . . . .	14
3. Beam Velocity Computer . . . . .	15
4. Ground Speed Channel. . . . .	16
5. Model Block Diagram. . . . .	19
6. Radar Beam and Target Geometry. . . . .	21
7. Main Program Generalized Flow Chart . . . . .	25
8. Amplitude of Target Return vs. Time . . . . .	32
9. Forward Squint Angle . . . . .	37
10. SIGGEN Generalized Flow Diagram . . . . .	48
11. Antenna Beam Width . . . . .	50
12. Subroutine Table . . . . .	52
13. Antenna Gain - Vertical Position . . . . .	57
14. Horizontal Beam Structure $(\text{sinc})^2$ . . . . .	58
15. Amplifier-Limiter Function . . . . .	62
16. Range Response MTF . . . . .	65
17. Azimuth Response MTF. . . . .	66
18. Modulation Transfer Function . . . . .	67
19. Recorder Limiting Function. . . . .	68

# LIST OF ILLUSTRATIONS (continued)

20.	Sample Plots FS vs. Z . . . . .	71
21.	Corrections for Squint and Distortion . . . . .	78
22.	PROCES Generalized Flow Diagram . . . . .	81
23.	Signal Pulse Amplitude as a Function of Film Position. . . . .	121
24.	Doppler Frequency of Return as a Function of Azimuth Position . . . . .	123
25.	Signal Phase as a Function of Azimuth Position. . . . .	124
26.	One-Dimensional Zone Plate Section Constructed Using Signal Phase . . . . .	125
27.	Quadratic Reference Phase as a Function of Azimuth Position	127
28.	Point Target Response. . . . .	128
29.	An Example of the Three Plot Options Associated with the Point Target Response. . . . .	129
30.	Idealized System Impulse Response. . . . .	131
31.	Far Range, No Motion Point Target Response . . . . .	134
32.	Mid Range, No Motion Point Target Response . . . . .	135
33.	Near Range, No Motion Point Target Response. . . . .	136
34.	Far Range Point Target Response with Motion Error . . . . .	137
35.	Mid Range Point Target Response with Motion Error. . . . .	138
36.	Near Range Point Target Response with Motion Error . . . . .	139
37.	Uniform Amplitude Weighting for Returned Signal Pulse . . . . .	142
38.	Sin x/x Amplitude Weighting (out to -3 dB) for Returned Signal Pulse . . . . .	143

LIST OF ILLUSTRATIONS  
(continued)

39.	Uniform Amplitude Weighting Far Range Response. . . . .	145
40.	Uniform Amplitude Weighting Mid Range Response. . . . .	146
41.	Uniform Amplitude Weighting Near Range Response . . . . .	147
42.	Non-Uniform Weighting Far Range Response . . . . .	148
43.	Non-Uniform Weighting Mid Range Response . . . . .	149
44.	Non-Uniform Weighting Near Range Response . . . . .	150
45.	Three Sidelobe Sin x/x Antenna Weighted Doppler History . . .	152
46.	Far Range Target Response . . . . .	153
47.	Mid Range Target Response . . . . .	154
48.	Near Range Target Response. . . . .	155

## INTRODUCTION

This is the second volume of a report describing a SAR (Synthetic Aperture Radar) image quality analysis and an SAR image quality model incorporating the conclusions of the image quality analysis into a SAR digital simulation. The objective of the model and its development program is to provide a fundamental approach for SAR image quality analysis via a model containing sufficient sophistication to quantify image quality effects for specific SAR systems (parameter combinations performing specific missions). The model thus provides a relatively economical prediction of the information which can be extracted from a specified radar-mission configuration.

The approach used to define an image quality figure of merit and the description of the resulting image quality model is the subject of this report. The report is written in two volumes. The first volume describes the image quality analysis and its conclusions along with an overview of the SAR simulation. The second volume contains detailed descriptions of each of the modules composing the simulation.

Sections 5, 6, and 7 in this volume describe the details of the simulation modules. Section 5 discusses the AIRMOD module, used to compute the airframe dynamics. Section 6 describes the RSMOD module which simulates the radar, recorder (storage), and processor. Section 7 details the theory and implementation

of the IRMOD module which computes the impulse response characteristics of the entire SAR system.

## 5.0 AIRMOD MODULE DESCRIPTION

The aircraft model (lateral channel only) was originally programmed on the IBM 360 digital computer to simulate the University of Michigan C-131 aircraft. Later simulations included the autopilot, a simplified doppler navigator, and a single axis inertial platform.

The current model is an expansion of the previous program that includes the longitudinal and vertical dynamics, a more complex autopilot and a turn command generator. The aircraft can be commanded to fly a straight line or a complex three dimensional flight path. The model for the inertial platform includes the roll, pitch and yaw axes, the dynamics for three accelerometers mounted on the X, Y, Z axes, and platform tilt errors. The model has the built in flexibility to simulate most modern aircraft plus the flexibility to simulate many aircraft radar configurations.

### 5.1 MODEL DESCRIPTION

The aircraft is considered a rigid body, and the path of the aircraft is determined by the aerodynamic forces, the angular acceleration about the three orthogonal axis, the inertia characteristic, the propulsive force, and the air density. The equations of motion

are derived from the basic force and moment equations for each degree of freedom. These force equations are then written in partial differential form. Closed loop operation of the aircraft is maintained through the control of the aileron, rudder and elevator. Control surface deflections produce the desirable moments along the principal axes. These deflections also generate cross moments and forces along the principal axes that do not always contribute positively to the control of the aircraft.

The model simulates the aircraft using nine degrees of freedom, the lateral, vertical, and along track accelerations, the roll, pitch, and yaw rotations, and the three control-surface deflections. The six differential equations can be divided into two groups of three. The first three equations are the lateral side force equation, the roll equation, and the yaw equation. These equations are written in terms of the variables  $\beta$  (drift angle),  $\psi$  (yaw angle),  $\phi$  (roll angle),  $\delta a$  (aileron deflection angle), and  $\delta r$  (rudder deflection angle). The second three equations are the longitudinal force equation, the vertical force equation, and the pitch angle equation. The variables are  $V$  (aircraft



velocity),  $\alpha$  (angle of attack),  $\theta$  (pitch angle), and  $\delta e$  (elevator angle). The nine degree of freedom equations are written below:

$$1) \quad \dot{\beta} + \dot{\psi} = \frac{G}{V} \sin \phi + \frac{1}{2} \frac{\rho V S}{M} \left( C_{yB} \beta + C_{y\delta a} \delta a + C_{y\delta r} \delta r \right)$$

$$2) \quad \ddot{\phi} = \frac{1}{2} \frac{\rho V^2 S b}{I_x} \left[ C_{l\beta} \beta + C_{l\delta a} \delta a + C_{l\delta r} \delta r + \frac{.5b}{V} \left( C_{lp} \dot{\phi} + C_{lr} \dot{\psi} \right) \right]$$

$$3) \quad \ddot{\psi} = \frac{1}{2} \frac{\rho V^2 S b}{I_z} \left[ C_{n\beta} \beta + C_{n\delta a} \delta a + C_{n\delta r} \delta r + \frac{.5b}{V} \left( C_{np} \dot{\phi} + C_{nr} \dot{\psi} \right) \right]$$

$$4) \quad \ddot{\theta} = \frac{\left( \frac{1}{2} \right) \rho V^2 S \bar{c}}{I_y} \left[ C_{m\alpha} \Delta \alpha + C_{m\delta e} \delta e + \frac{\bar{c}}{2V} \left( C_{m\dot{\alpha}} \dot{\alpha} + C_{m\dot{\theta}} \dot{\theta} \right) \right]$$

$$5) \quad mV(\dot{\alpha} - \dot{\theta}) = \frac{1}{2} \rho V^2 S \left[ \frac{W}{\frac{1}{2} \rho V_o^2 S} + C_{L\alpha} \Delta \alpha + C_{L\delta e} \Delta \delta e \right] - [mW]$$

$$6) \quad m\dot{V} = - \frac{1}{2} \rho V^2 S \left[ \left( \frac{W}{\frac{1}{2} \rho V_o^2 S} + C_{L\alpha} \Delta \alpha + C_{L\delta e} \Delta \delta e \right)^2 - \left( \frac{W}{\frac{1}{2} \rho V_o^2 S} \right)^2 \right] \div (2.5A) - W(\theta - \alpha)$$

The static stability derivatives  $C_{y\beta}$ ,  $C_{l\beta}$ ,  $C_{n\beta}$  etc., and the dynamic stability derivatives  $C_{lp}$ ,  $C_{lr}$ ,  $C_{np}$  and  $C_{nr}$  etc. are some of the parameters that describe the aircraft under investigation. These plus other constants such as the mass, the moment of inertia about each axis, etc. are calculated, measured, and/or determined from wind tunnel tests and then substituted in the above equations. Most conventional aircraft can then be readily simulated using the above equations. The equations can then be solved by using classical techniques, a rather formidable task, or the equations can be programmed into a computer. There are several second order and nonlinear effects that have been assumed negligible. The control surface dynamics are approximated by second order differential equations, and the resulting errors are assumed to have little influence on the radar, but may affect the aircraft handling qualities. A selection from any of the above variables can be listed as a function of time in the output file.

The aircraft motions are available from the system dynamics and are related to a system of coordinates. A flight path coordinate system is labeled  $X_f$  - along track,  $Y_f$  - lateral direction,  $Z_o$  - vertical direction, and the fixed axes are labeled  $X_o$ ,  $Y_o$ ,  $Z_o$ . The transformation matrix between the two can then be written.

$$\begin{bmatrix} X_f \\ Y_f \\ Z_f \end{bmatrix} = \begin{bmatrix} \\ \\ \end{bmatrix} \begin{bmatrix} X_o \\ Y_o \\ Z_o \end{bmatrix}$$

and the inverse matrix written

$$\begin{bmatrix} X_o \\ Y_o \\ Z_o \end{bmatrix} = \begin{bmatrix} \\ \\ \end{bmatrix} \begin{bmatrix} X_f \\ Y_f \\ Z_f \end{bmatrix}$$

An aircraft oriented reference frame is also written labeled  $X_a$ ,  $Y_a$ ,  $Z_a$ , and the transformation matrix is written with respect to the "f" reference system.

$$\begin{bmatrix} X_a \\ Y_a \\ Z_a \end{bmatrix} = \begin{bmatrix} \\ \\ \end{bmatrix} \begin{bmatrix} Z_f \\ Y_f \\ Z_f \end{bmatrix}$$

The matrix is also written for the transformation between the "a" and the "o" axis by

$$[A_{"o"}] = [T_{of}] [A_{"f"}]$$

The velocity matrix for the "o" reference frame is written by integrating the acceleration signals

$$[V_{"o"}] + \left[ \int \right] [A_{"o"}]$$

and a displacement matrix is written by a second integration

$$[D_{"o"}] = \left[ \int \right] [V_{"o"}]$$

A turn command generator is integrated in the model that has the capability of introducing simple or complex turns in the lateral axis and/or the vertical axis.

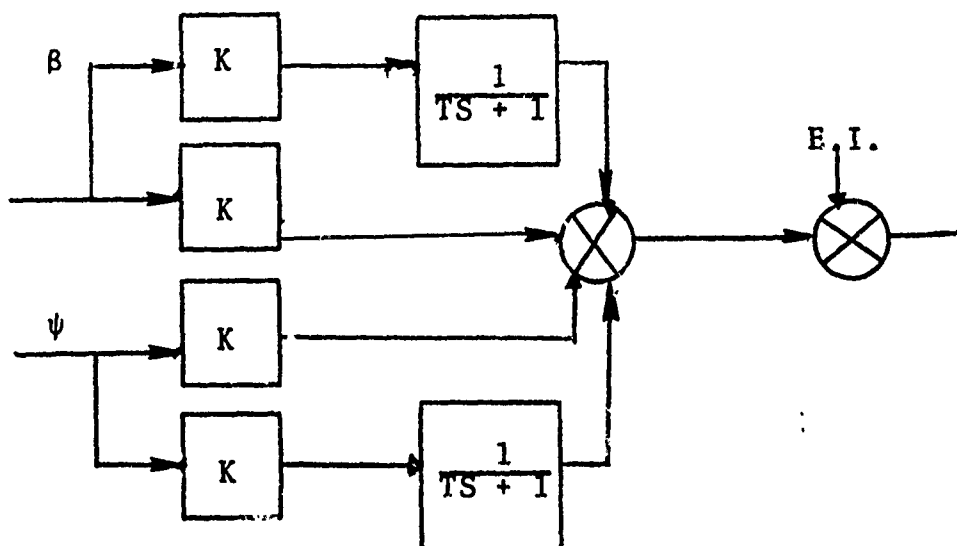
The model is commanded to a straight flight path (subject to atmospheric turbulence) when the turn generator is off. The turn generator is switched "ON" by selecting a non zero value for one or more of the constants in the following expression

$$a = K_1 + K_2 t + K_3 t^2 + K_4 \sin (W_1 t + \phi_1) + K_5 \sin (W_2 t + \phi_2)$$

As an example, a selection of a  $K_1$  value initiates a constant acceleration command at time  $t = 0$ . The aircraft control surface is deflected and a transient is initiated in the aircraft. A settling period is required before the acceleration error signal reaches a steady state value. The model also has the capability of starting at  $t = 0$  in a settled condition, i.e., the autopilot error signal maintains a steady state value. The complex turn command also includes a second expression that is used to control the vertical channel, and is independent from the lateral channel.

The doppler navigator is a radar system that measures aircraft ground-speed and drift angle. The model approximates the doppler by a first order system with error inputs (EI) added. A perfect doppler navigator is also modeled to show the possible improvement in

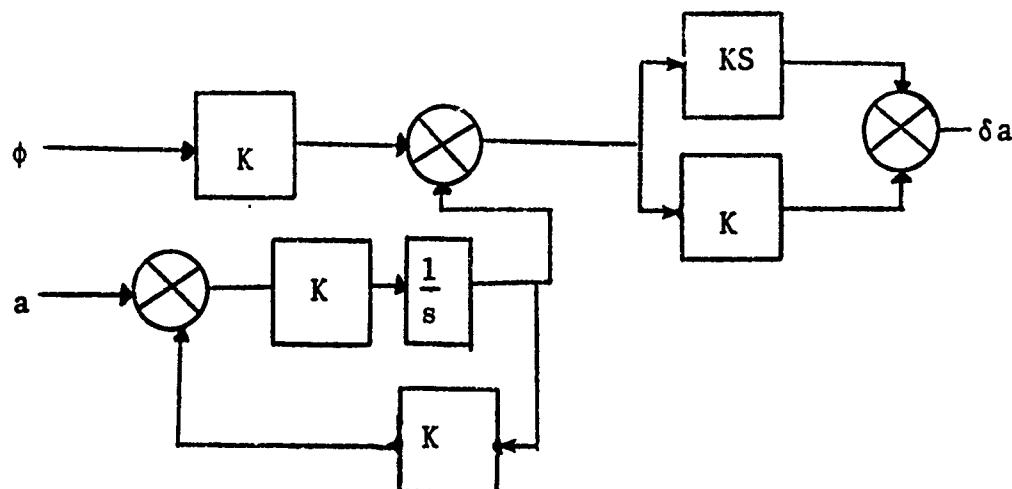
the overall system performance. In the "base" system the doppler drift angle is combined with azimuth angle information, and this signal is sent to a steering gyro. The sensitive axis is mounted to detect yaw motion. (The terminology "base" system refers to an aircraft - inertial navigation subsystem that has been used in a previous model. A comparison can then be made between the new and old models to confirm programming accuracy.) The gyro output is then sent to the autopilot rudder channel.



$\beta$  - drift angle  
 $\psi$  - azimuth angle  
 $K$  - arbitrary gain

The "base" autopilot is very simply approximated by a displacement channel and a rate channel for each control surface. The servo errors, assumed to be small, were not included for the base study. The "base" autopilot is incorporated in the autopilot diagrams shown in the figures. The autopilot block diagrams

for the three channels are given in Figures 2-4 in the computer program section 5.2. The aileron channel has three sets of inputs, the true values (acceleration, velocity, displacement, roll and roll rate), the inertially computed values (acceleration, velocity, and displacement). A vertical gyro is included that is oriented to the local vertical.



The gyro pendulum, being sensitive to lateral accelerations, is torqued off level during a turn, and a settling period is required to restore the aircraft to a straight and level flight path. The autopilot rudder channel also includes three sets of inputs, the ideal signals (acceleration, velocity, displacement, and azimuth rate), the component generated signals (acceleration, velocity, displacement, and azimuth), and the command signals (acceleration, velocity and displacement). The autopilot elevator channel also includes the three sets of inputs. In addition, a pitch gyro, a pitch rate gyro, a barometric altimeter, and a barometric rate unit are approximated

in the model. The above signals are combined according to the gain settings, and sent to the three servo systems to control the elevator, rudder and aileron.

The inertial-platform (INS) model is represented by four subsystems: the lateral channel, the longitudinal channel, the azimuth channel, and the vertical channel. The first two channels are functionally identical. Figure 1 is a diagram for a single channel inertial platform, that includes the accelerometer dynamics and the platform tilt errors that are a function of angle inputs. Accelerations are sensed by the accelerometer mounted on the inner gimbal, and integrated. The velocity signals are either subtracted from the doppler navigator outputs or used directly to torque the gyro, depending upon the choice of doppler damped or Schuler mode of operation. The velocity signals are then integrated to produce displacement information. The model also computes the change in the local vertical as the aircraft travels over the surface of the earth. Gain control is provided to select any degree of doppler damping. The platform azimuth channel senses the azimuth angle information by means of a vertical gyro. The gyro torqueing signal is derived from the computed velocity, earth rate, and latitude information. The platform vertical acceleration, the barometric altitude, and altitude rate are the inputs to the vertical channel in Figure 2. Barometric and barometric rate inputs are provided for damping purposes. The outputs are sent to the autopilot elevator control channel.

Accelerations derived from the platform are sent to the beam-velocity computer (Figure 3). In this subsystem, the aircraft velocity is computed along a predetermined depression angle and squint angle. The feedback loop is the sum of an integrator, a filter, and an arbitrary gain, and is subtracted from the acceleration input. The computer can be operated in either a first, second, or third order damped mode with any choice of loop gain and damping. The second channel receives the true acceleration signals, resolves them along the predetermined angle, and integrates to obtain the true velocity: Three basic outputs are available,  $V_{bm}$ ,  $V_t$ , and  $V_{be}$ .

The ground speed channel in Figure 4 computes the ground speed using the combined inertial-platform-derived ground track acceleration signals  $a_{xm}$ ,  $a_{ym}$  and the doppler-derived ground speed  $V_{go}$ . The combined output velocity contains both doppler (low frequency) and platform (high frequency) data. The error computer channel, indicated by the dashed lines, accepts the true acceleration signals, resolves, integrates and compares with the computed velocity to produce the velocity error signal  $V_{ge}$ .

The error computer is not a separate unit, but is integrated throughout the model. The error computer combines the true values of the system variables with the component derived signals. These signals, representing the subsystem errors as a function of time, are stored in a file and can be printed for documentation.



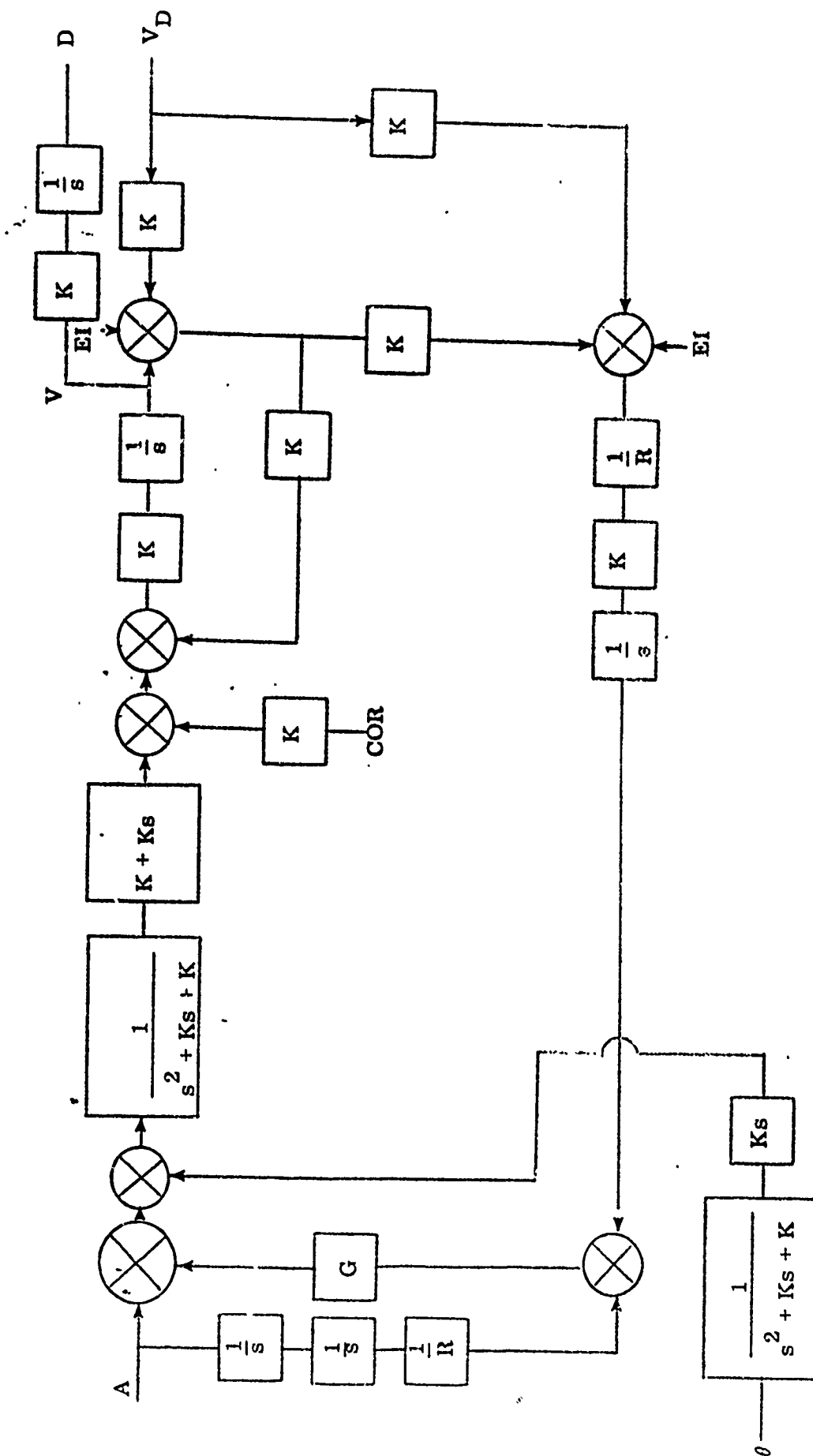


Figure 1. Single Channel of Inertial Platform



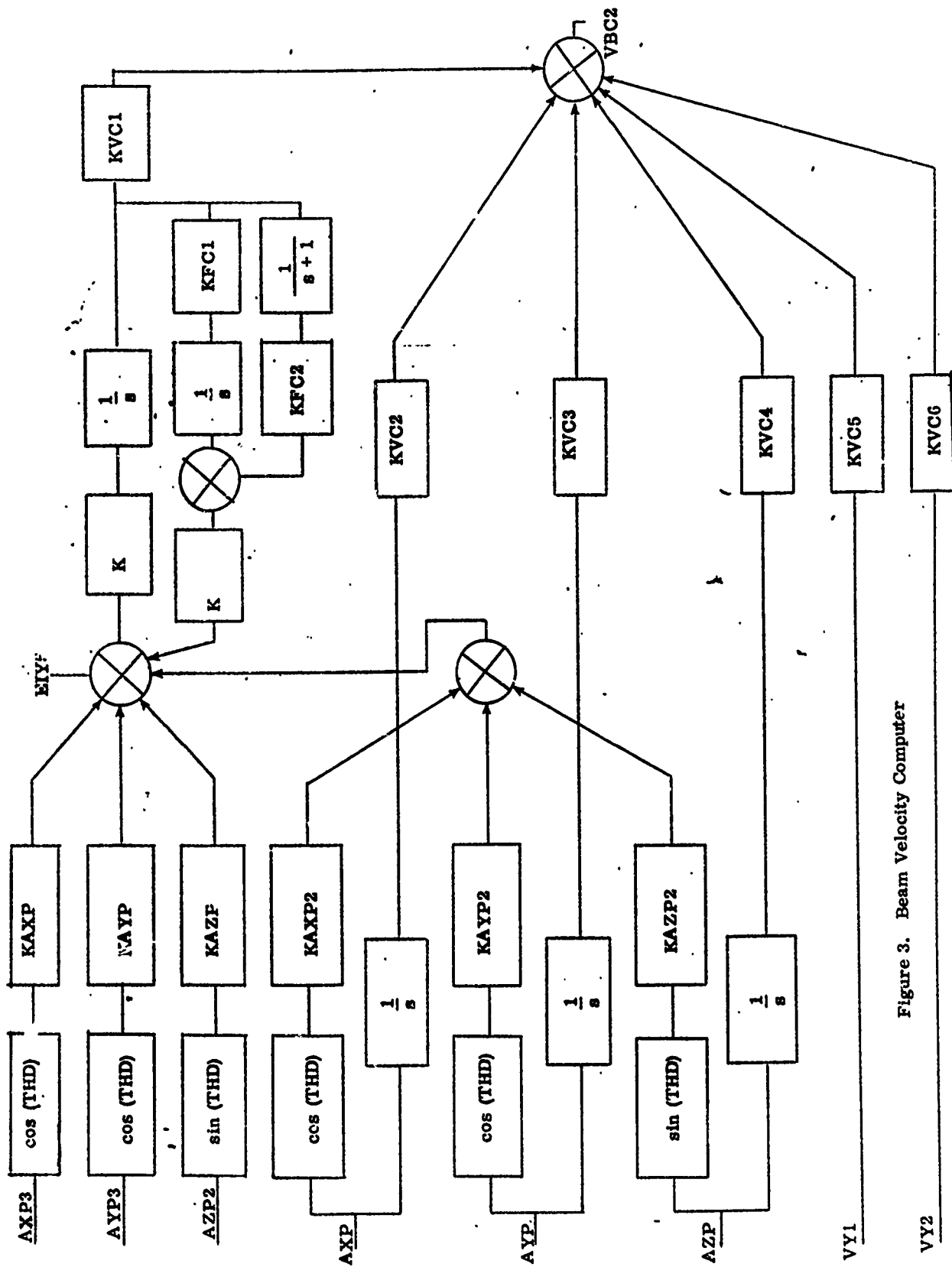


Figure 3. Beam Velocity Computer

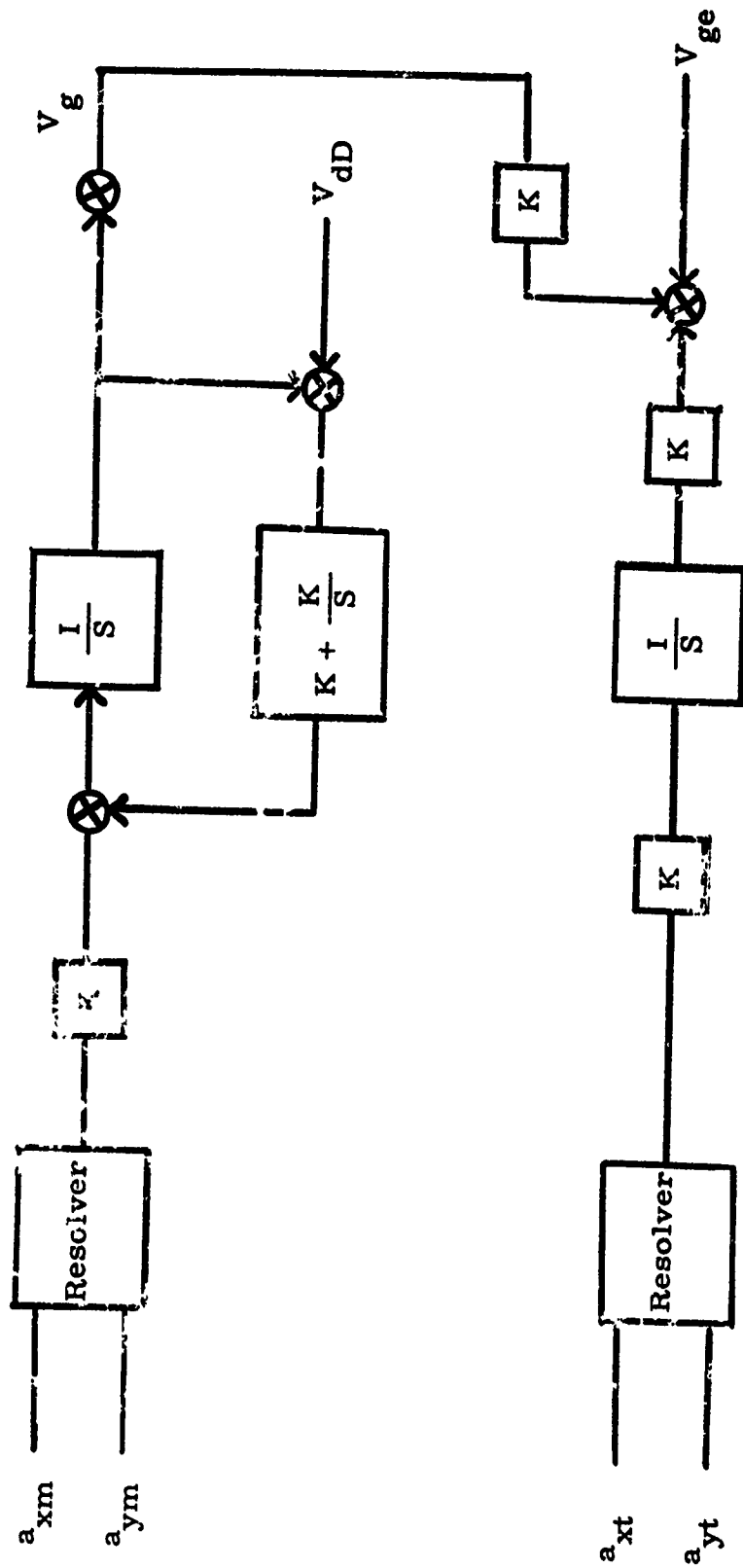


Figure 4. Ground Speed Channel

## 5.2 COMPUTER PROGRAM

The AIRMOD program is written in the CSMP language that is compatible with the IBM 360 computer. The CSMP format has many optional operating modes, that allows for considerable flexibility in the programming. The dynamic section contains the bulk of the program: the set of differential equations that relates to the system under investigation. The use of the initial section is optional but an improvement in computer efficiency is obtained. Other sections include the initial conditions, the timing commands, and the output specifications.

The output file contains the time histories of the many system variables that are used as inputs for the MSTRIP computation. The general organization of this simulation allows the operator to select a variety of configurations, gains, and operational parameters suitable for exercising an aircraft in a multitude of SAR modes. The importance of this simulation is the ability to investigate the results of hardware parameter selection (e.g., platform sophistication) and effects of aircraft maneuvers on the overall SAR mapping performance.

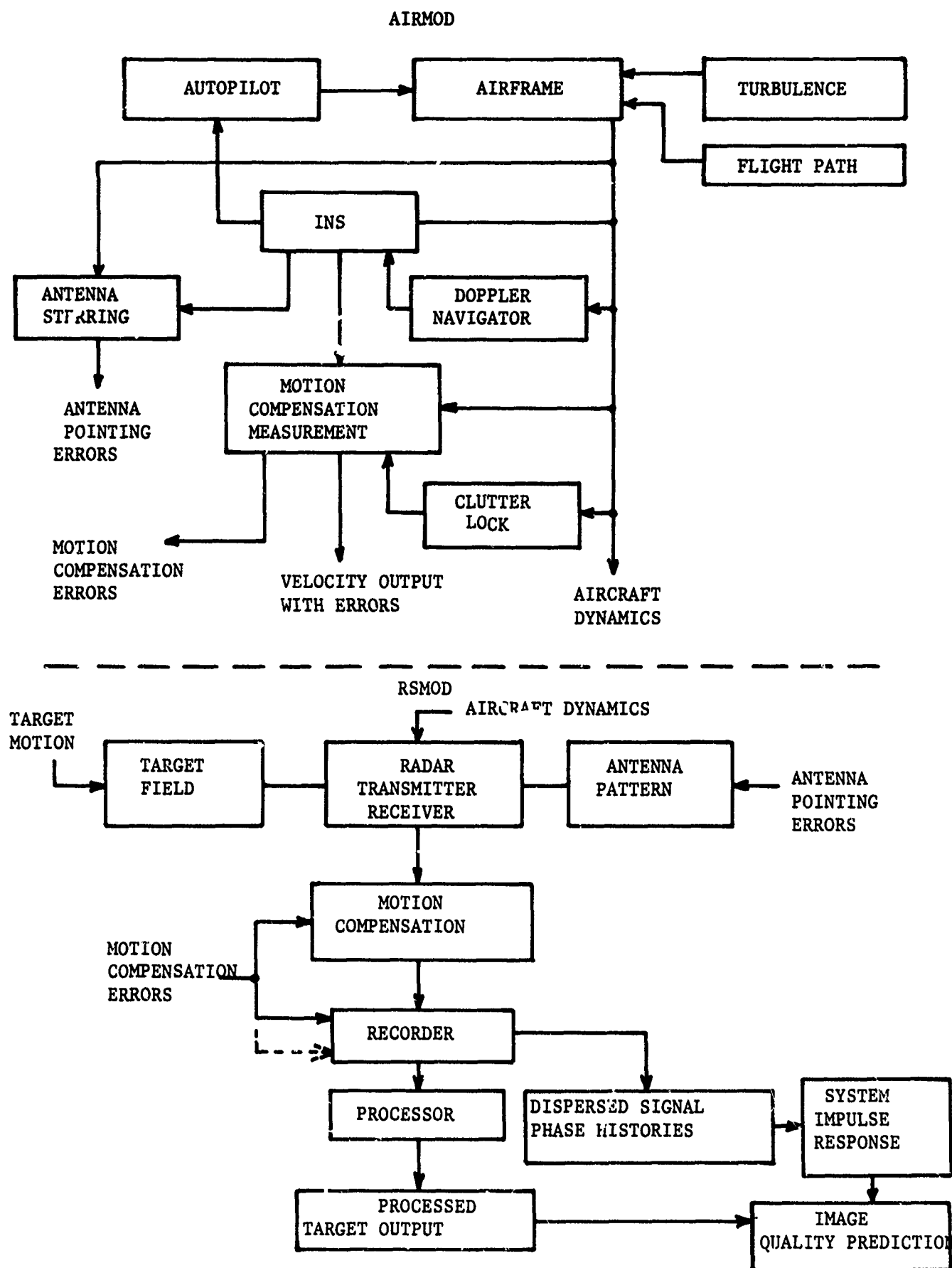
## 6.0 RADAR, RECORDER AND PROCESSOR SIMULATION

### 6.1 Introduction and Background

A digital computer simulation is described in this section. Its basis is a mathematical model in which important hardware components are represented and associated together to form a system simulation. Figure 5 illustrates hardware components and system flow. Inputs and outputs to the simulation are flexible to provide convenience and generality. Input parameter values can be chosen to reflect many different system characteristics and then easily varied from run to run to facilitate parameter studies as required. Outputs include measures of system performance [7.0] and intermediate results that are useful as inputs for additional analysis [2.0]. An original form of this simulation was named MSTRIP (strip-map radar simulation). The present model has been named RSMOD (Radar, recorder and processor simulation).

Aircraft motion and target motion can be either inputted as tables from external sources such as AIRMOD, discussed in a previous section, and logs from aircraft flights, or generated internally by function generators. Motion compensation (e.g., phase shifter, sampling rates, trigger delays, clutter lock) may be generated internally or can be externally generated by a flight simulator such as AIRMOD.

Radar parameters are set up as inputs of wavelength, nominal squint and depression angle, half-power beam width, scanning beam width, and looking beamwidth. Antenna patterns are included



by tabular input and/or through the use of the sinc function  $\left(\frac{\sin x}{x}\right)^2$  where  $x = \frac{\pi D}{\lambda} \sin \theta$  with D antenna aperture,  $\lambda$  wavelength, and  $\theta$  as the look angle from the antenna. The antenna pattern is maintained vertically and horizontally, and is directed toward the target field by the instantaneous pointing angles of the radar. Half-power beam widths (BEAM) are used to set-up the sinc function for half-power beam inputs. Scanning beamwidths (BEAMSC) relate the rectangular beamwidth over which point targets will be interrogated for chirp and doppler sampling (i.e., generation of signal history). The looking beamwidth (BEAMLK) is used to obtain background clutter by integrating clutter over the sensible beamwidth and to allow amplitude distortion by target returns entering through side lobes.  $BEAM \leq BEAMSC \leq BEAMLK$ , where equality is not representative. However, one may input equals if desired. Internally generated motion compensation may be driven relative to BEAM or BEAMSC.

Geometry of aircraft, target and radar beam is considered in a realistic manner. Figure 6 illustrates the basic geometry in which the radar is looking out the right-hand side of an aircraft. Looking out the left side is obtained by using a squint angle greater than  $90^\circ$ . A squint of about  $30^\circ$  is illustrated. Three coordinate frames of reference are presented. The a-frame relates aircraft rotation and translation, the s-frame relates target motion, and the (x, y, z) frame is the master frame. Time dependent transformations are maintained to relate all motion to the



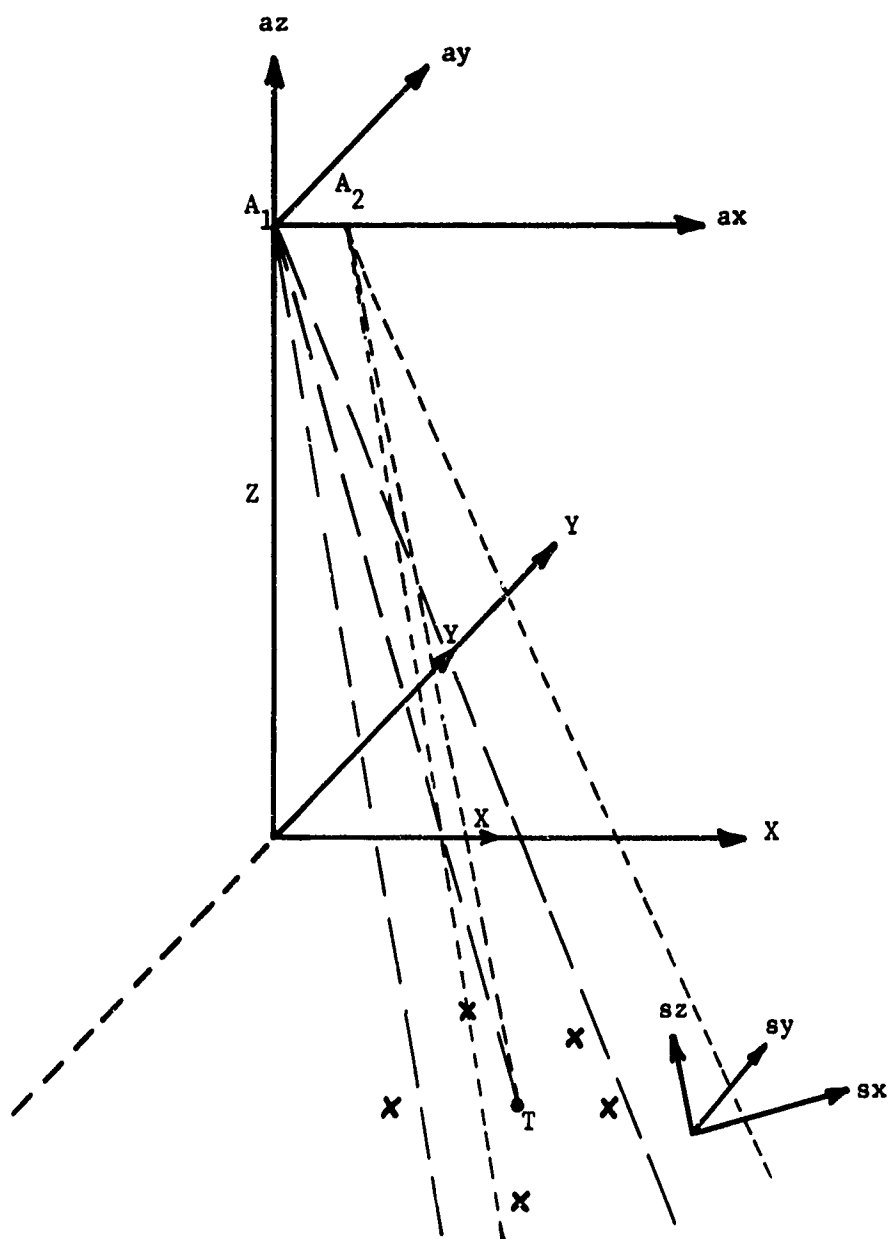


Figure 6. Radar Beam and Target Geometry

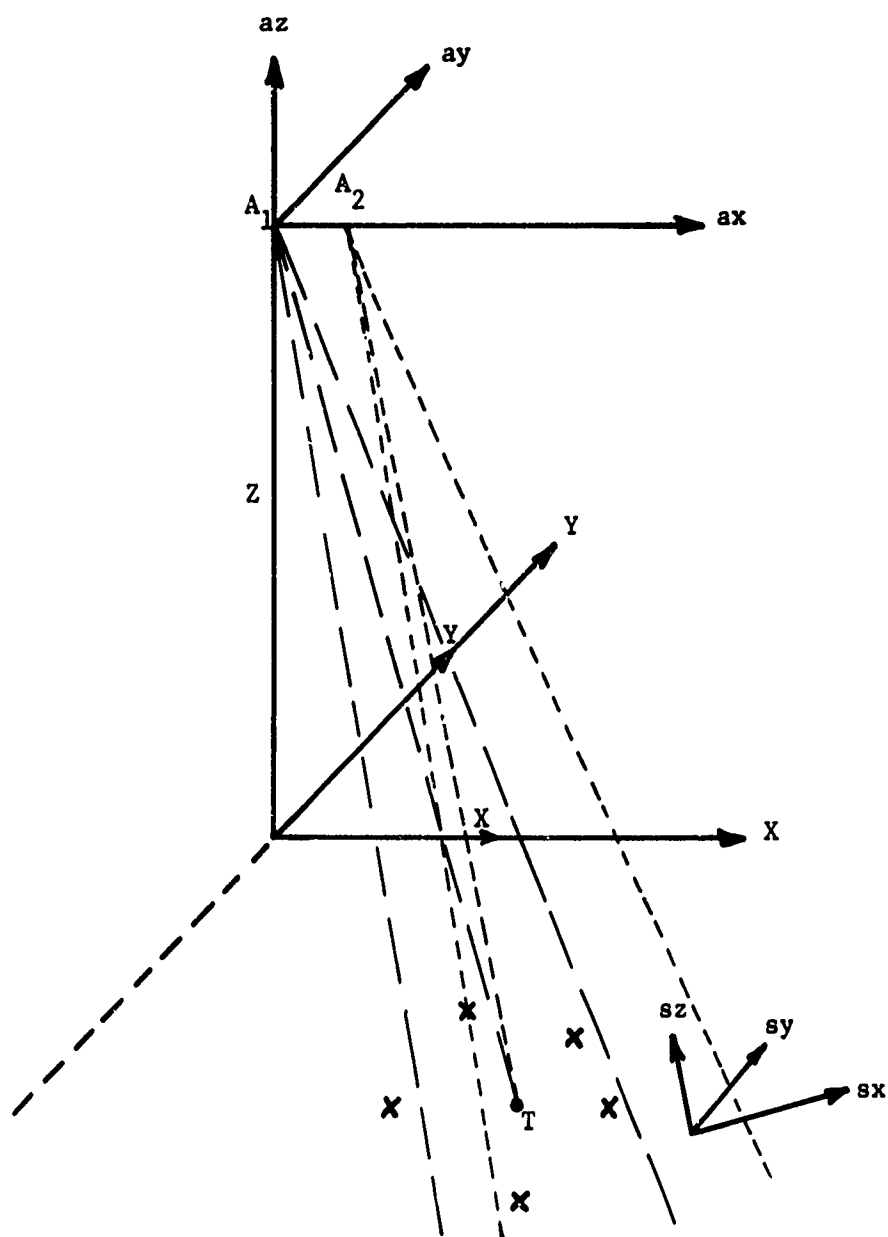


Figure 6. Radar Beam and Target Geometry

master frame. During a simulation run, aircraft velocities, target velocities, and antenna pointing angles are used to compute instantaneous beam velocities from which signal histories, temporal and spatial, are computed. Motion compensation, selectable either from a number of possible functions or from tabular inputs, relates the temporal histories to the recorded spatial histories. Signal histories in doppler and chirp (video) are made dependent on the carrier frequency and the chirp pulse that is transmitted. From the received chirp and doppler a video frequency and amplitude history for each of  $n$  ( $n = 21$  is a present programming limit which can be changed by recompiling the program) point targets. This history reflects signal amplitude, background clutter, and noise level as functions of radar gain, RF gain and limiting, video gain and limiting, modulation transfer functions applied during signal recording, and the transmitted power of the radar. A target pattern of cross-section is provided for each point target.

Output from simulation runs can be varied also. Tables of doppler and video history, and binary coded signal histories for direct input to impulse response calculations can be chosen for outputs. A linear fit processor may be applied to compress (focus) video and doppler histories into range and azimuth positions, and range, azimuth, and RMS (Range and Azimuth) resolutions. The ratio of input distance to output distance, between each pair of point targets, is computed as a measure of geometric distortion. A digital plot of input images and output images of the point targets is also available.

To conclude this introductory discussion, we observe that AIRMOD or real aircraft motion histories along with real target motion (e.g., ships) can be used as inputs to RSMOD. That RSMOD is a hardware oriented, parametric, representation of a strip-map, synthetic aperture, radar. Mathematical approximations are used to restrict computation but are chosen to provide a degree of similitude which gives simulation results that are comparable with real systems. Although an optical recorder and processor are presently represented, modular construction of the computer model allow large or small changes by re-programming. Large changes would be represented by changing from chirp to a different type radar pulse and by changing from one processor type to another. Small changes could involve any number of function generators such as a chirp generation, a limiter function, or the sinc function generator. Wherever possible function generators have been singled out as subroutines to allow easy transition to different or more complex forms. Even so, the present simulation is not tied to any particular hardware. Through the use of a multitude of input parameters, many different aircraft, radars, radar controls, and other system components are represented by RSMOD in its present form.

The remainder of this section is devoted to a comprehensive discussion of simulation modules.

Our present simulation divides naturally into a main program and input section, a signal generation section, a processor section, and an output section. Coupled with these main sections are various second order subroutines which function primarily with signal generation. There are various third order subroutines which operate as function generators or supply computations that are repeated often. These often repeated routines include a basic set of vector and matrix operations which support geometrical computations in the signal generation section.

## 6.2 Main Program and Input Module

Inputs and simulation control (main program) are closely tied together and thus far have been associated in a single module within the computer program. A general flow diagram for this module is shown in Fig. 7.

In many respects, the simulation program can be illustrated best by a discussion of the parameter inputs. We will discuss these inputs in terms of the hardware or real world entities represented by the model. These entities are: targets, aircraft, radar transmitter-receiver, motion compensation, signal recording, processor, and display.

### 6.2.1 Targets

Target inputs are given as  $N$  point targets with coordinates relative to a target frame of reference. This target frame, shown in Fig. 6 as the  $s$ -frame, has coordinates relative to the main frame which may be arbitrarily chosen in position and in

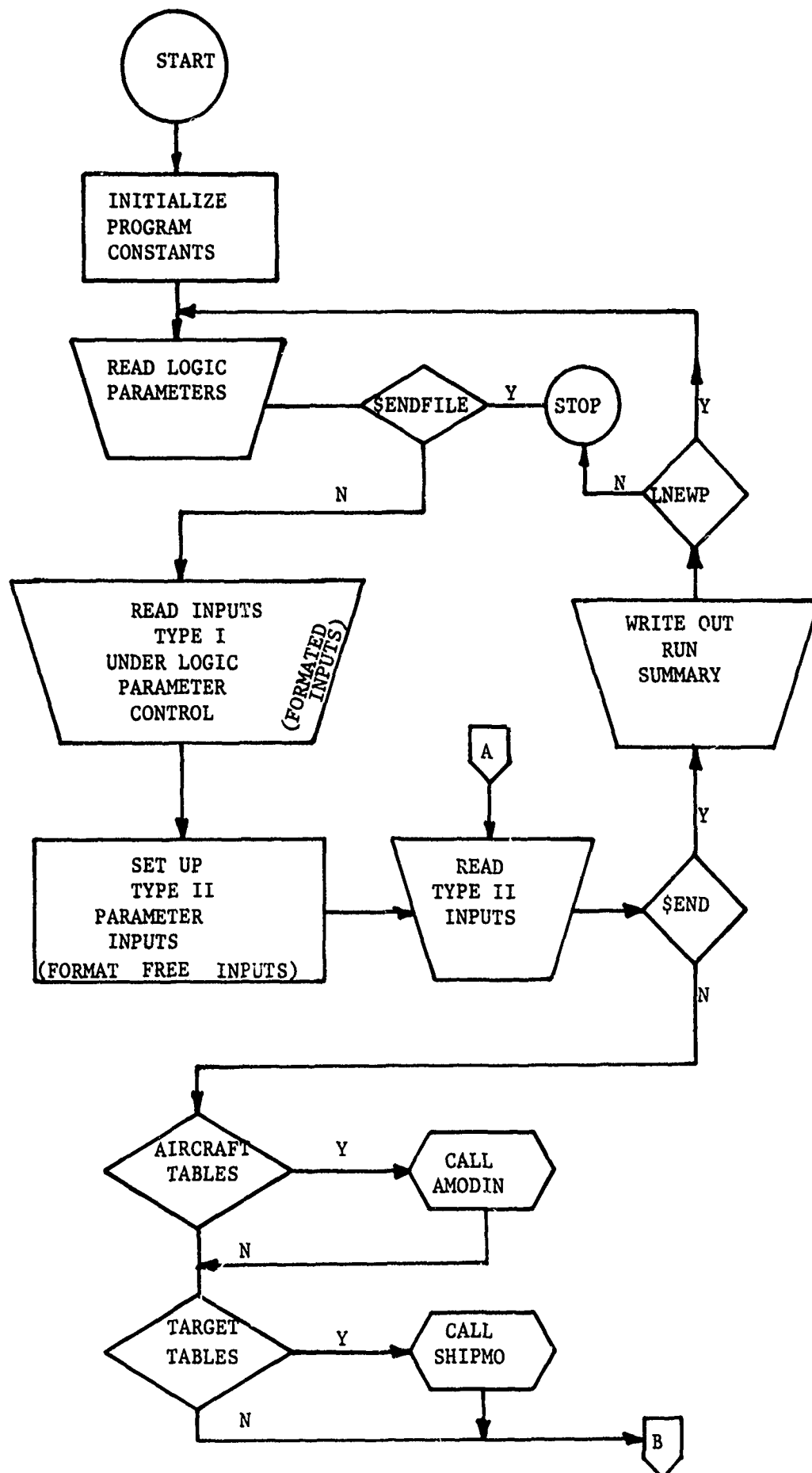


Figure 7. (a) Main Program Generalized Flow Chart

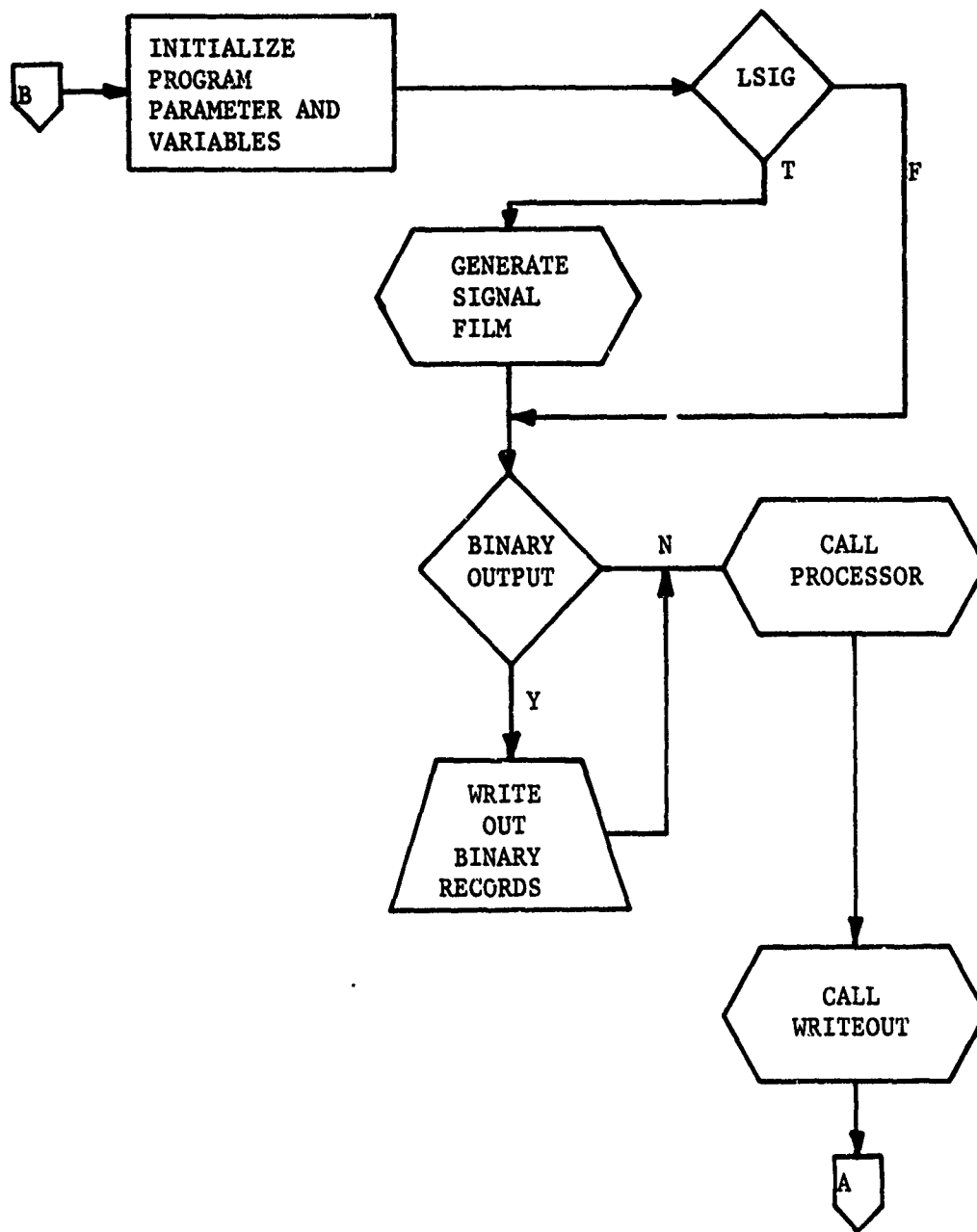


Figure 7(b). Main Program Generalized Flow Chart

angular orientation. Each target point may be given an arbitrary maximum cross-section with a vertical and horizontal beamwidth. What this means is that each target can reflect as if it resembled a flat plate (very narrow beamwidth) or as a corner reflector (very wide beamwidth) or anywhere in between. The cross-section inputs consist of a maximum cross-section, the two beamwidths, and two pointing angles, one in azimuth and the other in elevation, which describe how the target reflects directionally relative to the target frame. A Sinc function is then computed from these inputs which produces a cross-section pattern with a main lobe structure which has vertical and horizontal 1/2-power beam structure corresponding to the input beamwidths.

As noted earlier, individual target locations are input relative to a target frame of reference. Initial inputs set the beginning location and orientation of the target frame. Hence, individual point targets present a motion history that is directly related to position in the target frame.

Target and radar interactions are computed on a per target basis. Amplitude of target returns are dependent on cross-section of targets and the antenna pattern of the radar which in turn are aspect angle dependent. Thus, targets may scintillate to some extent relative to the interaction between two lobed patterns. High frequency scintillation is restricted by the computational load inherent in a large simulation program. Of course, many of the overall effects of a closely knit target complex can be studied



through the description of cross-section vs. aspect of a single target center.

The limitation of having only point targets with amplitude, angle-dependent, return characteristics represents a significant simplification which makes the simulation tractable from a cost and programming point of view. Using previously acquired radar target signature data, various target complexes and target types can be quite easily simulated by arranging the point targets in a suitable configuration representative of these selected target types. This approach precludes the problem of constructing a microwave scattering theory suitably realistic to model targets in the complex world. This approach does introduce some departure from reality in that dispersive targets are not included, but for the problem we are initially addressing, it does not present insurmountable departures from the overall SAR system performance evaluation task.

#### 6.2.2 Aircraft Parameters

Aircraft input parameters may be used in the AIRMOD simulation to provide a time history of aircraft motion. Inputs include:

- a. initial airspeed
- b. altitude
- c. gross weight
- d. stability coefficients
- e. control coefficients
- f. autopilot gains

- g. steering commands
- h. wind velocity
- i. gust profiles
- j. INS (Inertial Navigation System)
- k. doppler errors
- l. trubulence level
- m. antenna stability errors
- n. desired flight path

The AIRMOD simulation can be used to obtain time-histories of aircraft altitude, position, velocities, accelerations or any other AIRMOD parameter and its error. Limitations to AIRMOD are the linear, rigid-body, differential equations used for air-frame representations. Otherwise, this aircraft simulation provides realistic parameters with errors for input to RSMOD.

We note that RSMOD can be run without AIRMOD by limiting aircraft motion to prescribed time-functions of antenna translation and rotations. Inputs to these functions are coefficients which describe position, velocity, magnitude, frequency and phase of a sinusoidal term and magnitude of a step function term. Aircraft motions, recorded in digital format from aircraft flight, may be used as inputs also. In which case, the only difference from AIRMOD inputs would be the pre-processing of records into an acceptable table for input to RSMOD.

#### 6.2.3 Transmitter-Receiver

Inputs to the transmitter-receiver section are:

- a. wavelength (nominal)
- b. squint and depression angles (nominal)
- c. three beamwidths (geometrical)
- d. antenna pattern
- e. chirp function with non-linearities
- f. transmitter power
- g. antenna gain (transmitter and receiver)
- h. receiver front-end noise
- i. RF-amplifier gain and limiting
- j. detector noise
- k. video-amplifier gain and limiting
- l. antenna stabilization errors
- m. PRF
- n. logical switches
- o. background clutter levels.

An explanation of these radar parameters follows. These radar parameters are used in the following manner. For MSTRIP, beamwidth was specified as an angle spreading out from the radar. This pattern was aimed by a specification of squint (forward from broadside) and depression (positive downward from the horizontal). Two times, one for entry into the beam, (T1), and one for exit from the beam, (T2), were computed for each target. Thus, the effective antenna pattern was "on" over a fixed angular spread and "off" otherwise. In RSMOD a similar computation is used to ascertain the times over which each target is to be considered in

a broad field of view. Over this field of view, the antenna pattern (presented as a weighting function), target cross-section (aspect angle and depression angle dependent), and noise level are used to compute an amplitude of the return signal. Transmitter and receiver gain are directly related to the antenna pattern and the maximum gain of the antenna.

Intermediate to the receiver's first amplification stage (receiver gain) and the video recorder, there are various limiting factors: noise limiting and AGC (automatic gain control) are two examples. RF limiting will act with no time delay. When limiting occurs, the limiting level will be a function of the total power level (signal plus background noise level), limiting levels and nominal amplifier gain. The computed gain, under limiting, that is applied to each signal, to noise level, and to clutter will preserve S/N ratios. Similar functions or possibly tabulated weighting functions can be used to relate signal attenuation throughout the radar processor chain. Computation of an AGC requires integration of returns (at the video stage) from several targets. In Fig. 8, example amplitudes of target returns from a number of targets are plotted relative to a time scale. To adjust or set the AGC from this data, it would be necessary to compute a running average (integrate) over these returns under the influence of a time constant (AGC lags the present signal strength) and a corresponding delay which determines the weighting function for decay of old information. Due to the added complexity of the

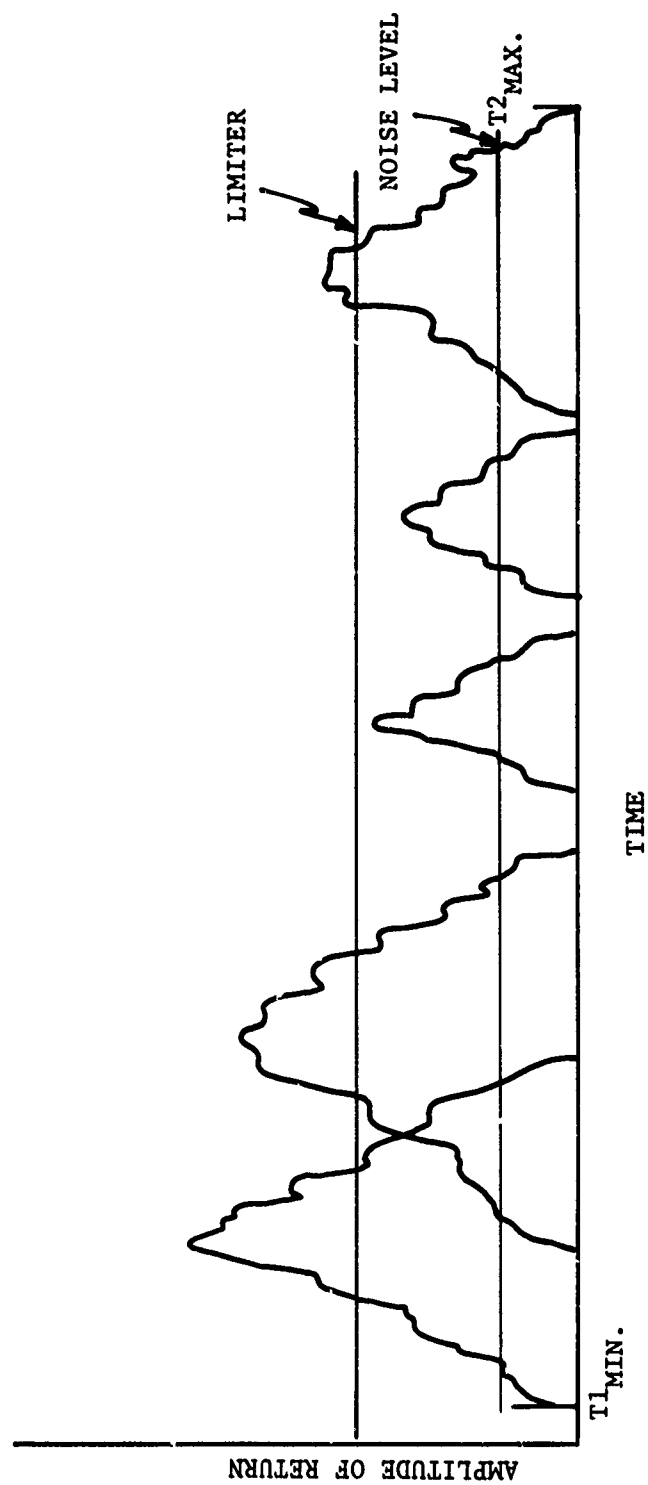


Figure 8. Amplitude of Target Return vs. Time

AGC correction, we have not included this consideration in RSMOD.

Antenna stabilization errors are an input from the aircraft simulation. Without these errors, the target cross-section profile, the antenna pattern, the instantaneous squint and depression angles, and range and range rate to the target, describe an expected history of amplitude, video frequency and doppler frequency. With antenna pointing errors: (a) the antenna pattern will be biased from and/or will oscillate about the expected pattern to create errors in observed amplitudes; (b) the clutterlock function will supply either a low or a high offset frequency, since the doppler returns from the target field observed will be shifted away from the desired doppler.

MSTRIP contains a time slice which is arbitrarily based on dividing the time history for each target into an equal number of slices. That is, if a target is in the beam for 1.5 sec. and the number of slices is 11, then a target history will be generated in each 0.15 sec. beginning with  $T_1 = t_0$  and going to  $T_2 = t_0 + 1.5$ . In the updated RSMOD\* PRF timing is used. Since the limiter functions require a parallel look at targets, background clutter and noise, common time points are required. Time slices are taken as equally spaced (integral multiples of  $1/PRF$ ) at the beginning and then initial times for targets are adjusted to

---

\*As a consequence of the evolving form of RSMOD, it is of some interest to note that MSTRIP is embedded in RSMOD. Consequently, MSTRIP and other simulation forms, intermediate from MSTRIP to RSMOD, can be operated from the same coded program.

correspond with PRF. At first glance, this may seem to be a concern over inconsequential; but, it is a reasonable concern since doppler spatial frequency in the range direction is dependent on chirp frequency and range scale factors. The doppler is also range-rate dependent and will depend on motion compensation which will be time dependant since each record in the range direction begins at a range which is a function of the commanded minimum range and is also a function of the recorder sample rate.

As an interaction between aircraft-target dynamics and the radar frequencies, the simulation model will compute time histories of uncompensated doppler for each target center. Heretofore, these dopplers have been computed as a function of the radar frequency; a single fixed frequency. Now, however, with the addition of chirp frequencies, the doppler is dependent on the chirp. RSMOD computes dopplers as a function of chirp frequencies. Doppler at the leading edge of the chirp pulse is based on

$$\frac{2(f_c + f_l)}{C} \dot{R}, \text{ and } \frac{2(f_c + f_u)}{C} \dot{R}$$

for the trailing edge; where  $f_c$  = center frequency,  $f_l$  = chirp frequency leading edge,  $f_u$  = chirp frequency trailing edge,  $\dot{R}$  = instantaneous range rate to target in question, and  $C$  = velocity of propagation.

#### 6.2.4 Motion Compensation

Inputs to the computation of motion compensation have been:

nominal altitude, nominal sweep-trigger delay, nominal sweep time, a doppler-correction function, trigger delay function, and film-speed function. We have investigated the possibility of adding a reference path as an explicit input. Through the use of AIRMOD this capability has been added to RSMOD. Hence aircraft maneuver considerations can be allowed. In the MSTRIP simulation, a single straight line was assumed as the reference path. If AIRMOD inputs are used, all motion compensation can be brought over as tabular entries. Otherwise, the following internal computations can supply motion compensation.

A phase-shifter rate (doppler correction) is computed as a function of aircraft motion which is used to correct the computed uncompensated dopplers. This rate is obtained by choosing one of several possible motion-compensation rules. Currently, we have ten individual motion compensation rules available for examination. Each set of rules specifies the functions to be used to compute doppler frequency correction, azimuth sampling rate, and range-delay correction.

In the use of pure broadside (unsquinted) strip-mapping, questions of proper motion-compensation rules do not arise (except for the relatively straightforward question of single-range compensation versus multi-range or continuous-range compensation, for which most of the trade-offs are known). For squinted (non-broadside) strip-map operation, however, determination of the best signal mix for motion compensation is not at all clear-cut,



except for the case of a single point target at zero depression angle. Moreover, even the one-degree squint angle resulting from the use of azimuth (doppler) offset in "broadside" mapping can be appreciably non-zero at steep depression angles. Consider the forward-squint case, with single-range motion compensation.

The sketch, Fig. 9, shows velocity components in four directions: beam velocity ( $V_B$ ) down the squinted radar beam to swath center; cross-beam velocity ( $V_{CB}$ ) normal to the radar beam; along-track velocity ( $V_T$ ) in the direction of the reference path; and cross-track velocity ( $V_{CT}$ ) normal to reference path. In the broadside case,  $V_T$  and  $V_{CB}$  are identical, and this quantity is used to control azimuth sampling (thus locking actual displacement to ground displacement, to eliminate along-track geometric distortion in the map); similarly,  $V_B$  and  $V_{CT}$  are identical, and this is the quantity required for frequency-correction of the doppler returns (to eliminate cross-track distortion and smear in processing). But in the squinted case, which quantity,  $V_B$  or  $V_{CT}$ , should be used for doppler correction? And if  $V_B$  is chosen, should not the orthogonal velocity,  $V_{CB}$ , be used instead of  $V_T$  to control azimuth sampling? (If so, azimuth sampling is no longer slaved to ground-speed). Which-ever combination is chosen, what happens to the image quality of targets appreciably distant from the swath center?

The simplified problem of a single point target at swath center, and zero depression angle, has been solved analytically--

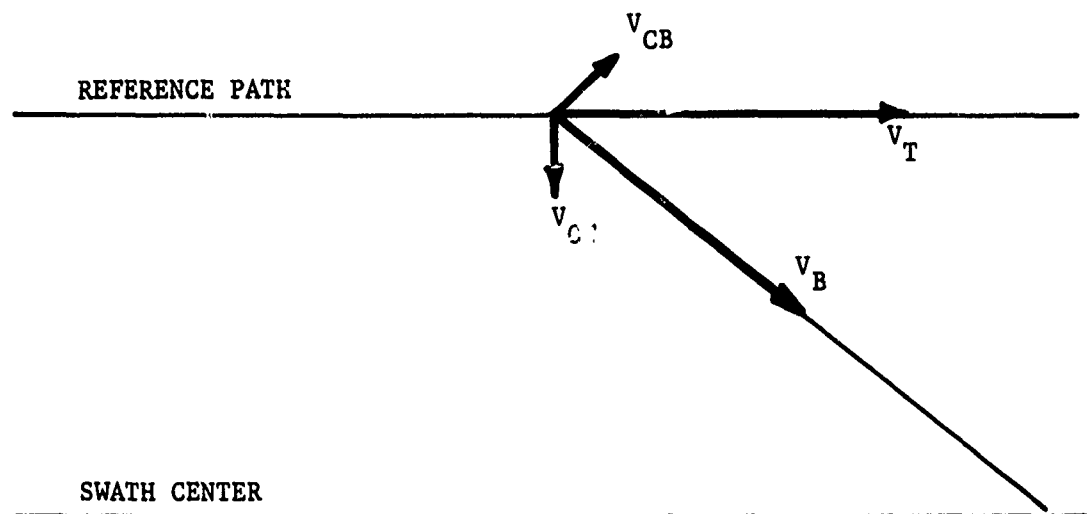


Figure 9. Forward Squint Angle

the answer in this case is that, for best azimuth resolution,  $V_B$  should be used for doppler correction and  $V_{CB}$  for control of azimuth sampling. But the more realistic cases of non-zero swath width and/or non-zero depression angle are not easily analyzable-- it was specifically for the purpose of studying these cases that the SAR simulation model was originally developed. A variety of motion-compensation rules can be entered as alternate subroutines. (For example, MOCOMP 1 might use  $V_B$  for doppler correction,  $V_{CB}$  to drive azimuth sampling, and cross-track displacement for range-delay correction; MOCOMP 2 might use  $V_B$  for doppler,  $V_T$  for azimuth sampling, and beam-direction displacement for range delay.) The same target array can be mapped (with the same aircraft dynamics) alternately using each of the MOCOMP methods, and the resulting processed imagery compared for resolution and geometric fidelity.

The motion-compensation technique study, described above, is not yet complete. Preliminary results, however, seem to indicate that, for range swaths exceeding 10% of swath-center range, the best combination of signals for single-range compensation is that using  $V_B$  for doppler correction,  $V_T$  for azimuth sampling, and displacement in the beam direction for range-delay correction. This compensation method degrades resolution somewhat at swath center, but resolution at swath edges is better preserved.

Heretofore, these functions have been computed relative to perceived or measured motion of the aircraft. Motion measurements

and generation of motion compensation did not have error sources as inputs. The only errors that existed were involved with the motion compensation rules and the amount of uncompensated motion that ended up on the stored returns, plus an error which was allowed as the difference between actual forward motion and measured forward motion of the aircraft. In the updated model these computations will allow input of RMS errors (deterministic, not random). Thus, motion may be measured with errors and motion compensation can be computed with error. For these reasons, as with the actual systems, the accumulation of motion compensation errors and residual uncompensated motion can cause final images to be degraded below a minimum acceptable level which is to be determined.

The function of the clutterlock is to generate a correction (error signal) to bring the doppler observed after motion compensation, as measured against the target background, into coincidence with a desired band of doppler frequencies. To provide this result, a clutterlock can be designed to shift all doppler frequencies, after phase shifter compensation, so that any target in the center range position at the aft edge of the antenna beamwidth, for example, will record at zero frequency or will record at a prescribed minimum frequency. Other choices of target background are to average over a band of possible target positions, or to average over several bands of possible target ranges and azimuth positions. A residual error will also be allowed to correspond to errors in the clutterlock or to delays in making the corrections, since

the clutterlock has a time constant, settling time, which nominally is fairly long (several beamwidths). Alternatively, clutterlock signals (with errors) can be inserted from the AIRMOD file.

Since we are providing a representation of chirp and are allowing doppler returns to be chirp-dependent, we have included the effect of a range dependent phase shifter on chirp frequencies. Hence, chirp warp is represented by a function generator in the simulation model.

#### 6.2.5 Signal Generation and Data Storage

Generation of signal histories depends on target, aircraft, radar, and motion compensation inputs. Also, we observe that a number of logic variables are brought into play. Some examples are:

a. If LTABMD = .TRUE, then changes in doppler and chirp frequencies due to motion compensation may be obtained from AIRMOD tables depending on whether or not LPSRT, LFLMSP, LCUT and LTDEL - representing phase shifter input, film speed input, clutterlock input, and recorder trigger delay, respectively - are TRUE or FALSE. True means 'use AIRMOD' and false means 'use internally generated function.'

b. If LANG = TRUE, target motion inputs are tabular (e.g., data logs from field experiment). Otherwise function input is used.

c. If LCHIRP = FALSE, one dimensional signal history is generated and stored corresponding to doppler returns only.

Otherwise, two dimensional signal history chirp (video) in range and doppler in azimuth - is generated and stored. If LMAINI is also turned on, equals TRUE, then appropriate binary records are written into a file for future use in computing impulse responses.

A total of fifteen logical (control) parameters are initialized by read in of the first data card. For the purpose of printing out intermediate results during debugging operations, there are an additional nineteen debug controls read-in on the second card. Control cards are most important with respect to actual use of the simulation program. Further discussion of the control or logical inputs is subjugated, for the most part, to the details of program running that are presented in the Appendix on RSMOD programs.

A recording process to produce a digitized signal is employed in MSTRIP, which computes azimuth spatial frequency from compensated doppler and commanded azimuth sampling rate. These doppler histories are attached to storage locations in azimuth and in range by a computed data position. Data position is a function of a commanded range-delay trigger, range sampling rate, and azimuth sampling rate. We have added to these histories a corresponding spatial frequency in the range direction that results from the received chirp signals. Since the chirp frequencies, added to the carrier frequency, produce a variation in doppler across the chirp, the new recorder attaches dopplers

for each chirp pulse that are chirp-frequency dependent. Thus the effect of chirp on azimuth (doppler) frequency is represented. We have a simulated data-storage, then, which records video frequencies in the range direction and doppler frequencies in the azimuth direction. Spatial frequencies in the range (video) direction varies with range sampling rate. Sampling rates are allowed to have slowly-varying and impulse-type nonlinearities.

Another important feature of RSMOD is target amplitude (signal strength of target returns). Gain and limiting functions were mentioned earlier under the radar sub-section. After the signal strength at the receiver front-end has been attenuated by noise limiting, and other system attenuations, we take the resulting signals and record a corresponding intensity for each data point. There is, therefore, a history of recorded signal and noise amplitudes as functions of video amplifier bandwidth (and CRT spot size for optical recording) in range and in azimuth (recorder MTF characteristics).

Finally, the recorded signal histories can provide a two-dimensional "signal-film" output in a format for impulse-response calculations.

#### 6.2.6 Processor

A processor exists in RSMOD (from MSTRIP) which accepts the following input parameters, which are characteristics of the processing:

- a. Focus-target selection
- b. Best-focus criterion (minimum azimuth smear, minimum range smear, minimum real mean smear)
- c. Squint-angle-correction criterion
- d. Depression-correction criterion
- e. Fixed-frequency gate option.

These parameters enter into the azimuth offset processing of doppler histories (azimuth focus). If chirp (video) signals are to be focused a new processing component called RNGPRC for range processor is invoked. In which case, individual video signals for a target are focused (compressed) to form a one-dimensional signal history. This range compressed history is identical in form to the azimuth histories used in MSTRIP. Therefore, the second stage of processing for RSMOD, is identical with MSTRIP processing. Before processing any of the doppler histories, the processor is primed with a fixed band of spatial-frequency-response limitations. Then four optimization procedures are available. Three of these are computed automatically but are dependent on the selection of a focus target (one of the input targets) and the selection of a best-focus criterion. In these cases, the focus target and its location in range and azimuth (its doppler and, eventually, video frequency history) becomes the controlling factor for computing smear and location of other targets. Targets are excluded or included according to the



overlap of signal histories (in the frequency domain) with the focus target. A target can be focused if and only if a minimum history criterion is met. Presently this criterion says that at least 14% (3 points out of 21) of a target's doppler history must overlap with the optimized frequency band and/or the fixed frequency band defined for first looks at the focus target. If the focus target's doppler bandwidth does not meet this criterion, no targets are focused and a comment is printed to the effect that the focus target has no useable doppler history. The focus target signal history is printed out, then, and the program returns to the next computer run.

A fourth method of optimization is allowed--namely a fixed spatial frequency band can be stipulated as before, but this frequency band can be retained for checking and focusing the signals for each target.

If only MSTRIP is used, the processor section focuses in azimuth only. It computes azimuth and range smear based on using data already compressed (focused) in the range direction. Since chirp is already compressed, (short pulse system) nonlinearity of chirp implications on range resolution is fed in as a fixed smear, RRMIN, due to chirp. This RRMIN input is then averaged (RSS) with nonlinearities due to "range walk" to obtain a range resolution. For the expanded version of RSMOD, compression of chirp and the accumulated effects of errors in generating, transmitting,

receiving, and recording chirp signals are computed during each simulation run. In which case, RRMIN becomes a computed number for each range compression. Since range compression can now produce the doppler history for the second stage, there is a corresponding contribution to doppler noise or azimuth smear.

Outputs from the processor are:

- a. A list of all input parameters
- b. Range and azimuth image position for each target
- c. Range, azimuth, and average (RMS) smear for each target.
- d. Geometric distortion between targets, with and without corrections.
- e. Printplot of output image with scale factors.

#### 6.2.7 Displays

Output of video histories, doppler histories, processor results, plotted image positions, input parameter lists, binary inputs for impulse response, and various intermediate parameter values are controlled by integer and logic switches. The switches are input parameters. Logic structure in the four sections of the RSMOD program also control display of information in terms of existence of a particular kind of record. For example, if LCHIRP is off, no video history is computed. As a consequence of this switch setting the program never enters the write out section in which video histories are displayed. Hence, the

writeout switch for 2D video-doppler display could be on but the output of video would not be attempted unless LCHIRP is also on.

### 6.3 Signal Generation

Signal generation as a module in the simulation program consists of a main module (SIGGEN) which calls sub-modules and stores signal history according to logic controls. Choices of limiters, time base, limiter computations, and one or two dimensional histories are represented in these controls. During the signal generation stage, four important sub-modules are involved. These are:

- a. TIMER - a calculation of target-radar interaction times
- b. POINT - a collection of algorithms which supplies translations, rotations, and vector calculations of target points relative to the phase center of the radar
- c. MOCOMP - a group of computations which provide motion compensation values for the determination of signal history
- d. TABLE - a module which generates and tabulates signal history by using results from TIMER and calculations from POINT and MOCOMP.

In TABLE, signal amplitudes are calculated to the receiver front-end and chirp images are developed for video returns. TABLE works on an individual target basis while SIGGEN associates these individual scalar and vector results with time, and stores values

in appropriate arrays indexed by target, by time slice, by range slot, and by chirp sample.

Figure 10 illustrates the order of computation and the options available. These options are determined by logical switches which are: LAMP (for amplitude computation), LNEWT (for timing sequence), LCHIRP (either azimuth only signals or Range and Azimuth Signals), LLIMIT (determines limiting for RF), and LVDAMP (corresponding to video amplification). Other options appear in TABLE, MOCOMP, and POINT relative to tabular inputs vs. function input and choice of procedure. We will now discuss the options and resulting computations in the context of the various subroutines and function routines that are used.

#### 6.3.1 TIMER

TIMER is the subroutine in which the entry and exit time for each target is computed. Either a scanning beam or a scanning beam and a looking beam may be specified. The algorithm for the determination of these times is based on squint angles,  $\theta_{1L}$ ,  $\theta_1$ ,  $\theta_2$ , and  $\theta_{2L}$  as shown in Fig. 11. For purposes of illustration, we let the target point T walk through the beam along the dotted line as shown and assume the velocity of T to be the real velocity of the target minus the aircraft ground speed.  $\theta_T$  the initial squint angle to T is computed by using POINT. Then, if the time to  $\theta_1$ , for example, is desired, an estimated time to close is computed from ground range to target, aircraft ground speed, and

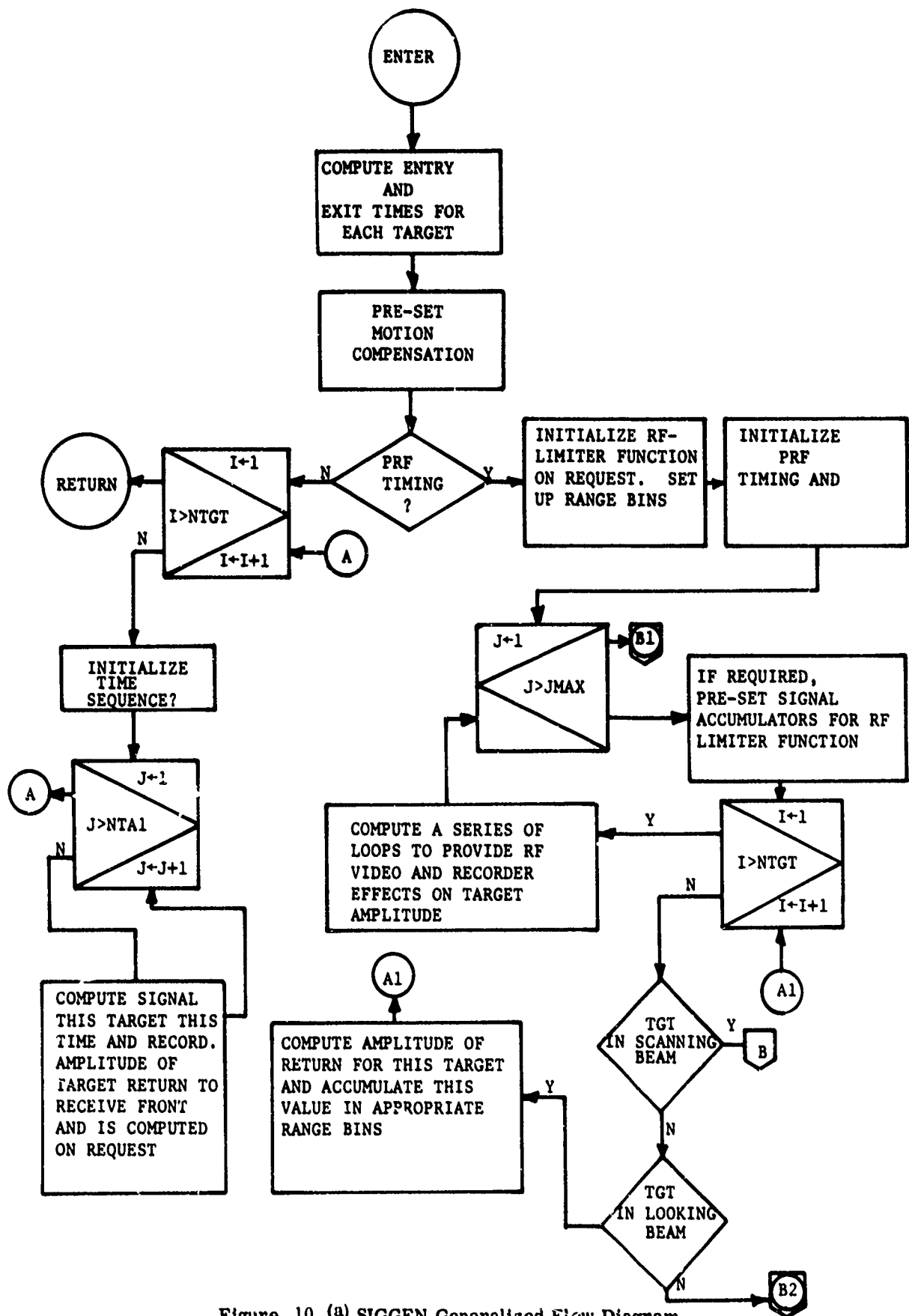


Figure 10. (a) SIGGEN Generalized Flow Diagram

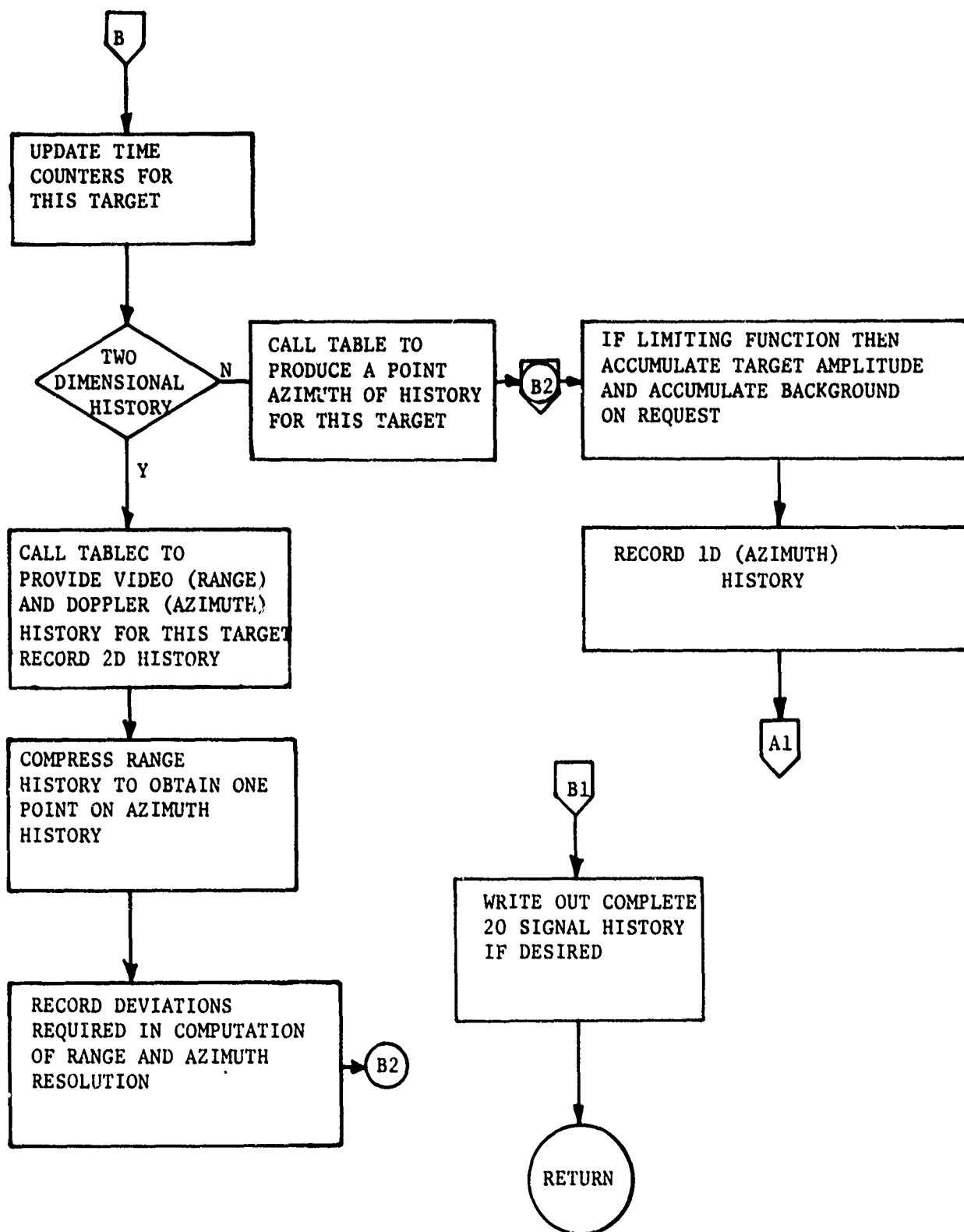


Figure 10 (b) SIGGEN Generalized Flow Diagram (continued).

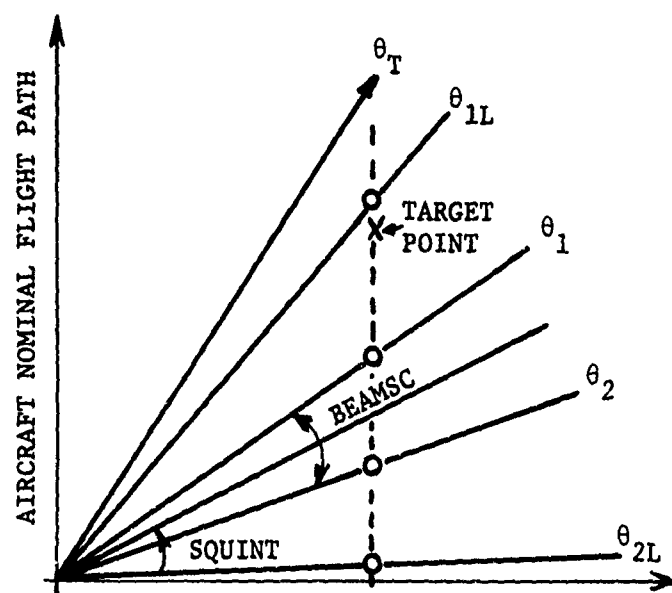


Figure 11. Antenna Beam Width

the angular separation. This process is iterated three or four times until the computed  $\theta$  at some location like X is near enough to  $\theta_1$ . We observe that aircraft and target velocities vary with time and hence an iterative procedure is required.

#### 6.3.2 TABLE

The subroutine TABLE provides control and computations to generate signal histories on a per target and a per time slice basis. Signal history in chirp and doppler (range and azimuth) is computed from transmitted chirp frequencies, beam velocity, and applicable motion compensation. It is these chirp and doppler histories, considered in a spatial orientation that are compressed (focused) to obtain final images and resolutions. In addition to these spatial frequencies, amplitude of target returns, background clutter, and noise figures are also computed. Since the subroutine TABLE involves so many interactive elements it is desirable to show a generalized flow diagram at this hierarchical level also. In Fig. 12, it is observed that subroutines POINT, MOCOMP, and CHIRPX are used along with a function named AMPR.

#### 6.3.3 POINT

Subroutine POINT contains aircraft motion and target motion functions. These are quadratic functions of time with sinusoid and step function terms. Velocity equations and angle generating function for target roll, pitch and yaw are included. Alternatively within this subroutine, calls on AMOD and SHIPMO subroutines



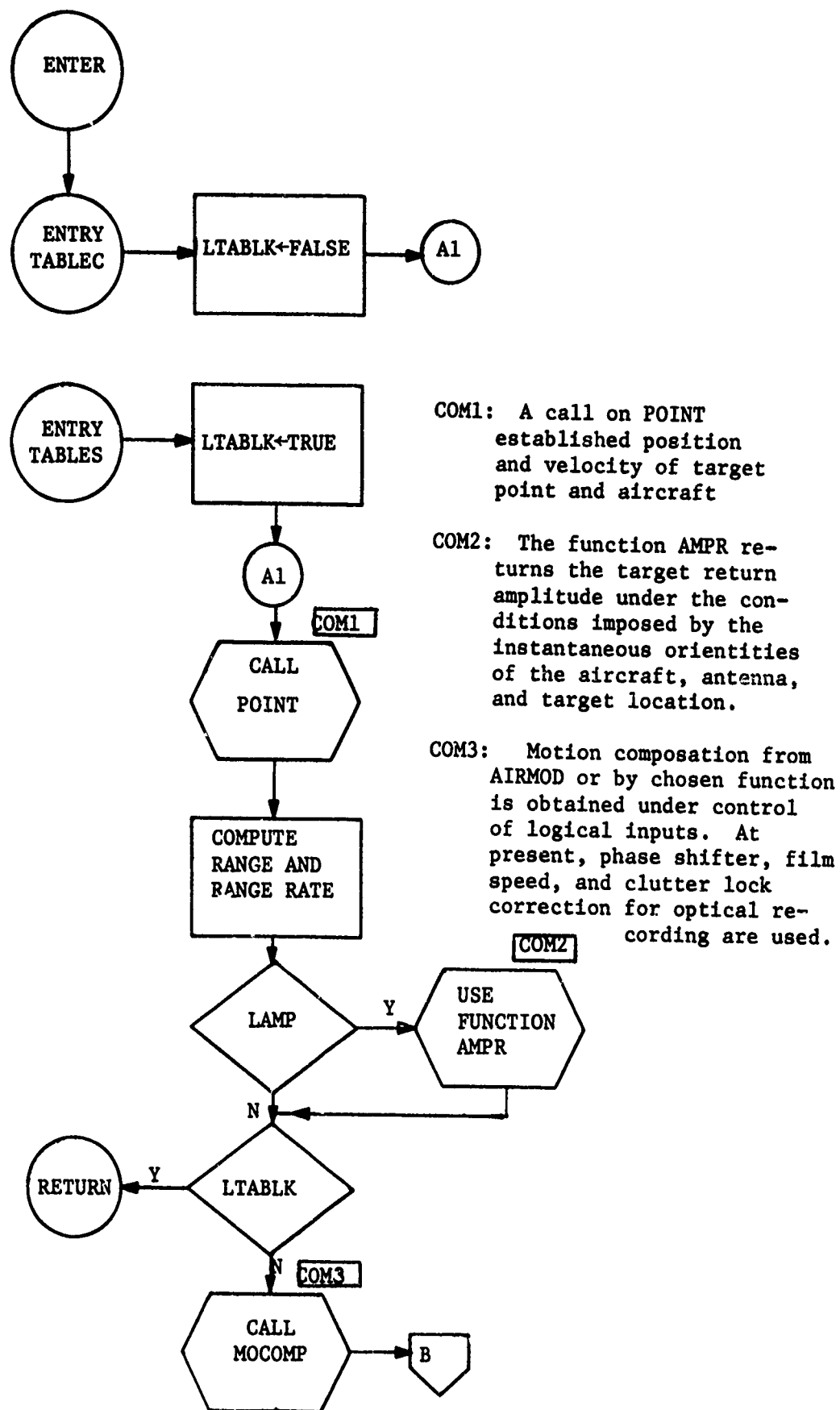


Figure 12. (a) Subroutine Table

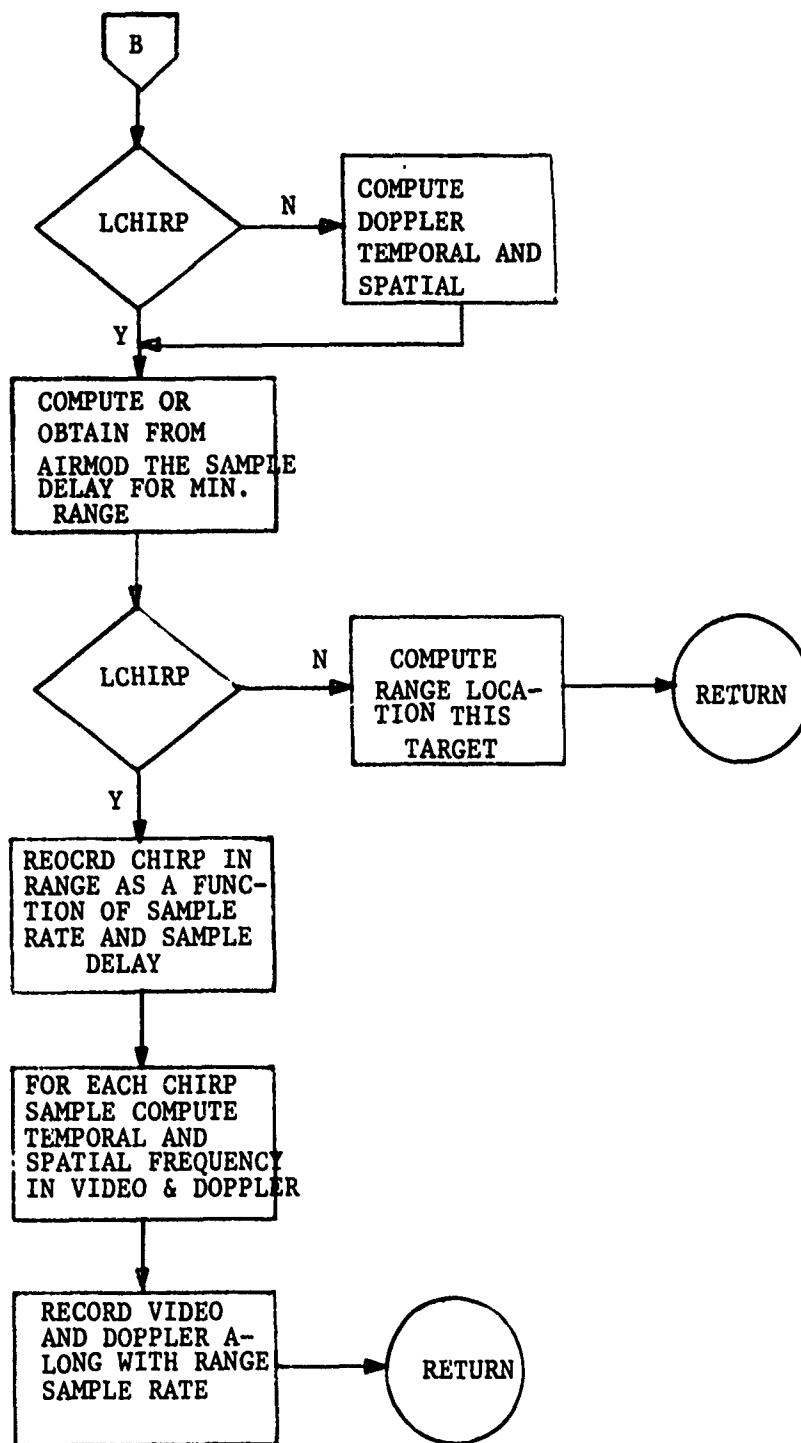


Figure 12 (b) Subroutine Table (continued).

provide more realistic aircraft and target motion. As part of this alternative, one may specify table look-up, linear interpolation, or quadratic interpolation. It is in POINT and in MOCOMP where the aircraft simulator (or aircraft logs) are used extensively.

#### 6.3.4 MOCOMP

Subroutine MOCOMP contains the functions and table look-ups which perform motion compensation. Motion compensation was discussed earlier in terms of input parameters and relative to parametric studies aimed at finding best motion compensation. With the addition of AIRMOD inputs to RSMOD, we can now provide a better input of error sources as well as different forms of motion compensation. Heretofore, (MSTRIP), we studied motion compensation relative to aircraft motion or velocity errors versus different rules for compensation. Now error sources (RMS) can be introduced realistically into AIRMOD and relayed via phase shifter, range delay time, azimuth sample rate, clutter-lock and antenna pointing errors. Moreover, the effect of INS (Inertial Navigation System) errors is introduced via a real INS representation in AIRMOD. Since the error generators are fully controlled by the AIRMOD simulator, all errors with respect to time, as well as the effects of errors, can be an output for subsequent analyses.

#### 6.3.5 AMPR

Computing amplitude of target returns is accomplished through

the use of a number of subroutines and function subroutines. To compute amplitude, in TABLE, it is only necessary to assign AMPR, a function of target number, time, unit range vector, slant range to target, and an attenuation factor, to an appropriate variable. In the coded program, the Fortran Statement is

```
IF (LAMP) AMP = AMPR(NTP, TT, UR, RA, ATEN)
```

Hidden from view, in AMPR, are: the antenna and target pattern functions; antenna and target pointing functions; the radar power equation; tables of antenna patterns; tables of target cross-section, pointing angles, and lobe patterns; a sinc function generator. Detailed equations for the AMPR function are contained in the coded programs that are listed in the RSMOD appendix. Here again AMOD tables from AIRMOD provide an important input by relating antenna pointing angles relative to aircraft frame with respect to time. These angles combined with aircraft roll, pitch and yaw (from AIRMOD) determine the instantaneous squint, depression and pattern orientation for the antenna. There are times when it may be desirable to back-off from AIRMOD realism. One may wish to study some special effect or, during a phase of program development and/or debugging, static antenna patterns may be desirable. For this purpose, idealized routines are provided, via switch controls, to give aircraft and antenna rotations, either fixed or varied with time.

Functions and routines which support AMPR are designed to be easily reprogrammable. For example, the antenna pattern, presently used, is the product of a vertical and a horizontal pattern. To compute antenna gain along a particular direction, these patterns are sampled and the results multiplied together (added in DB). A vertical antenna pattern is shown in Fig. 13. Depicted is a portion of a calibration curve obtained from a  $\text{csc}^2$  antenna pattern. For simulation purposes the peak power point is shown at  $0^\circ$ . Positive depression (down) is plotted to the left of zero. In use the pointing angle of the antenna a pseudo bore sight, corresponds to the zero-angle gain (max. gain) shown. A maximum gain of 30 db above isotropic is representative.

Using a  $\text{sinc}^2 x = \left( \frac{\sin x}{x} \right)^2$  function for the horizontal pattern produces a gain pattern similar to Fig 14. If  $\theta$  is the horizontal aspect angle, then  $x = \frac{\pi D}{\lambda} \sin \theta$ , where  $\lambda$  is wavelength and D is antenna aperture. In Fig. 14. If  $\theta$  is the horizontal aspect to  $\sin \theta$ . The half-power beam width is singled out as  $.88 \frac{\lambda}{D}$ . For convenience in operating the model and since  $\frac{\lambda}{D}$  's often used as an approximation for the rectangular equivalent half-power beamwidth, the simulation mechanizes  $\text{sinc}^2$  functions with the half-power beams as an input. As a consequence of choosing this input, antenna patterns and cross-section of targets can be idealized by the same kind of sinc functions.  $\theta = 1^\circ$  would be a nominal beamwidth for the radar antenna at X-band

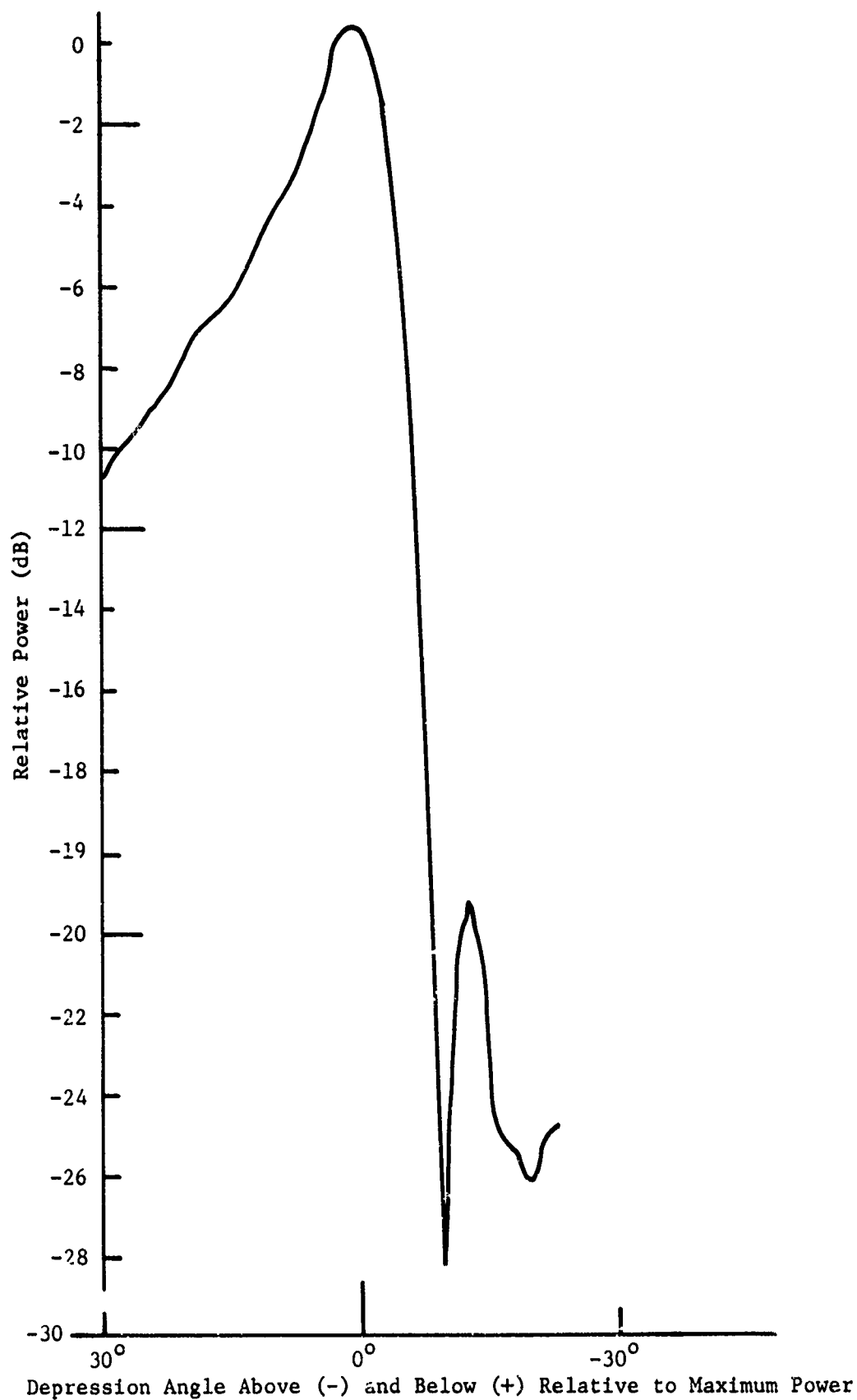


Figure 13. Antenna Gain - Vertical Pattern

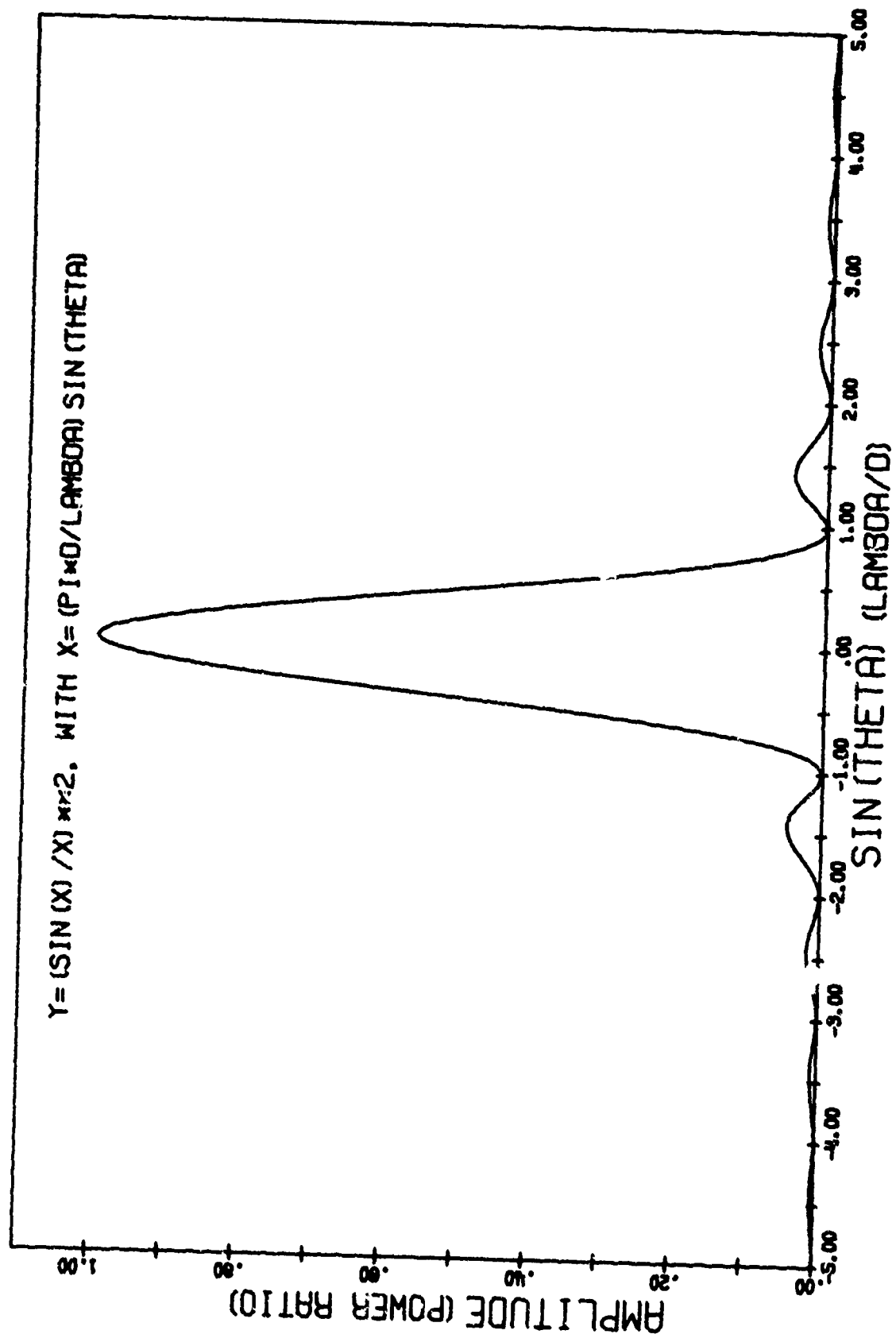


Figure 14. Horizontal Beam Structure  $(\text{sinc})^2$ .

and  $\theta = 10^\circ$  (or  $30^\circ$ ) might be representative for a target cross-section pattern. (It is not desirable, at this time, to entertain any kind of rigorous representation of target signatures in a systems model. Too much rigor in an otherwise, relatively simple representation would not be beneficial).

Before leaving our discussion of antenna patterns, one additional feature can be used to vary the horizontal structure. Coded into the present formulation we admit a weighting function in tabular form which can be used to describe antenna patterns that are asymmetrical in horizontal structure.

Inputs, for each target, describe beamwidths for horizontal and vertical lobing of cross-section, maximum cross-section, and the roll-pitch-yaw orientations of the cross-section pattern. Each point is coordinatized with respect to the target frame, which may be angularly oriented with time. Hence, aspect angle dependence as seen by the radar, may vary with time.

The following, independently coded, functions with outputs noted are used to compute AMPR:

- a. Either AIRANG (AIRMOD) or ANGAIR (function) - angular orientation of the aircraft
- b. Either ANTPNT (AIRMOD) or ANGANT (function) - squint and depression angle of the antenna relative to the air frame
- c. ANPNT - rotation of antenna axes to air frame



- d. ANTDEP - verticle antenna pattern
- e. ANTSQT - horizontal antenna pattern
- f. TGTSIG - target cross-section
- g. RADRDB - Amplitude of a target return in DB.

#### 6.3.6 CHIRPX

In CHIRPX, the transmitted chirp pulse is generated. A beginning chirp frequency, a terminal chirp frequency, a pulse width, and a sample rate are inputs. From these inputs, NCHIRP (the number of chirp samples for simulation) linear samples of the chirped pulse are formed. From either a table (read in) or a function generator (coefficients read in); NCHIRP samples of a non-linear function are added to each linear sample point to form the non-linear pulse that is transmitted. At this time, the only non-linearities which can appear in the chirp as recorded are: transmitter generated and those which result from the geometry and motion compensation. That is, we have not added phase shifts due to the radar receiver or any other function downstream to the recorder. Obviously some phase shifting occurs but it is assumed to be of second order importance to those represented in the model. We have already discussed, phasing shifting and chirp warp in the input section above.

#### 6.3.7 LIMIT

After table generation is accomplished over all targets for a given time slice, the gain and limiter functions are performed.

Either RF amplifier or video amplifier gains can be combined with limiter functions by the following representation. Consider an amplifier gain function as shown in Fig. 15. We have shown a piece-wise linear function with two pieces. The first linear piece, corresponding to Gain 1, relates input power to output power for non-limiting input power. If the total signal from noise, targets and background exceed  $X_{lim}$ , the power input level over a pulse width at which limiting begins, then the following considerations hold. First, after limiting begins, signal-to-noise (S/N) input ratios must be equal to S/N output. That is, a good approximation to limiting in an RF-amplifier or video-amplifier is obtained if a linear model is used in which S/N is preserved. Secondly, the gain after limiting for the total signal is to be GAIN2, while GAIN1 holds prior to limiting. These two conditions are sufficient to establish that:

$$(i) \quad y = \text{GAIN1} * x, X_{total} \leq X_{lim},$$

is the equation of the first linear piece

$$(ii) \quad y_{lim} = \text{GAIN1} * X_{lim}$$

$$(iii) \quad Y_{total} = \text{GAIN2} * X_{total} + Y_o, X > X_{lim},$$

with

$$\begin{aligned} Y_o &= Y_{lim} - X_{lim} * \text{GAIN2} \\ &= X_{lim} (\text{GAIN1} - \text{GAIN2}) \end{aligned}$$

$$(iv) \quad \frac{x_{total}}{N_{in}} = \frac{y_{total}}{N_{out}} = \frac{\text{GAIN2} * X_{total} + y_o}{N_{out}}$$

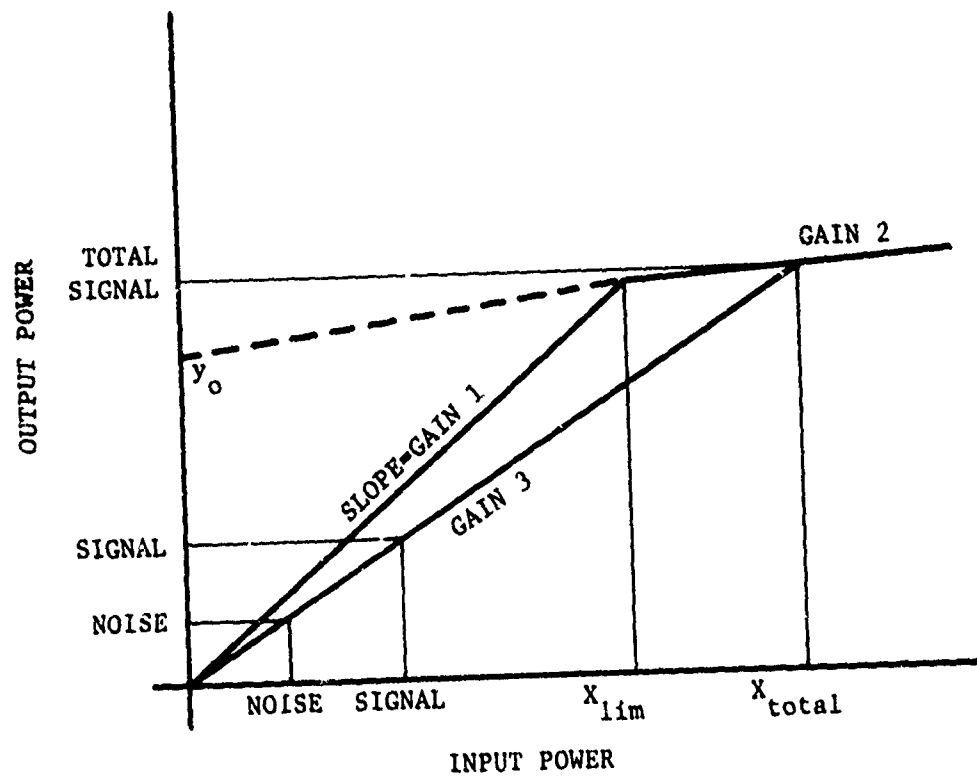


Figure 15. Amplifier-Limiter Function

which implies that for all X, when  $X_{total} > X_{lim}$ ,

$$y = GAIN3 * X = \frac{[GAIN2 * X_{total} + X_{lim} (GAIN1 - GAIN2)] * X}{X_{total}}$$

and

$$GAIN3 = \frac{GAIN2 * X_{total} + X_{lim} (GAIN1 - GAIN2)}{X_{total}}$$

also

$$\text{Noise-out} = (\text{NOISE-IN}) * GAIN3$$

#### 6.3.8 MTF's

As indicated earlier, MTF's (Modulation Transfer Function), particularly in the recording process for an optical processor, are important contributors to recorded amplitudes. It is important in any validation of this simulation model that empirical results can be interleaved with simulation results. We have chosen, therefore, to model an optical recorder. In only these MTF's and in the linear processor of the next section do we find specialization to optical processing. All other representations including the impulse response calculations are not restricted in this way. By disconnecting these MTF's and substituting a particular digital processor representation, the present RSMOD should modify quite readily into a simulation of a digital processor.

There are four MTF's which have been singled out so far. These are CRT-recorder, azimuth and range, response to temporal

and spatial frequency, lens MTF and film MTF. Figures 16, 17, and 18 are samples of calibration curves for three of these MTF's. Since response curves for these transfer functions are available, we can use tabulated values to represent these MTF's.

The basic relations for spot size and spatially dependent transfer functions are illustrated in Figure 19. At an input spatial frequency  $X_1$  (a function of the temporal frequency and sample rate), the attenuation begins to increase as a quadratic function of temporal frequency and continues to an input of  $X_2$  ( $X_1 < X_2$ ). At which point spot size and spatial frequency becomes the dominate factor in determining attenuation. From  $X_2$  to larger  $X$ 's, the attenuation (db) increases almost linearly and is representable as a linear function. A point on the curve at  $X_4$  is required to fit the quadratic function. Without including a specific model, dependent on spot size, we can, therefore, include functions which are described by inputs  $X_1$ ,  $X_2$ ,  $X_3$ , and  $X_4$  along with the level of attenuation at  $X_2$ ,  $X_3$ , and  $X_4$ . In this manner spot size is included implicitly. A logic variable in each of the coded transfer functions enables switching back and forth between a table and a function.

#### 6.4 PROCESSOR

##### 6.4.1 Focusing Signal Histories

Our processor for signal histories in optical form is constructed through the use of a linear fit procedure. Consider

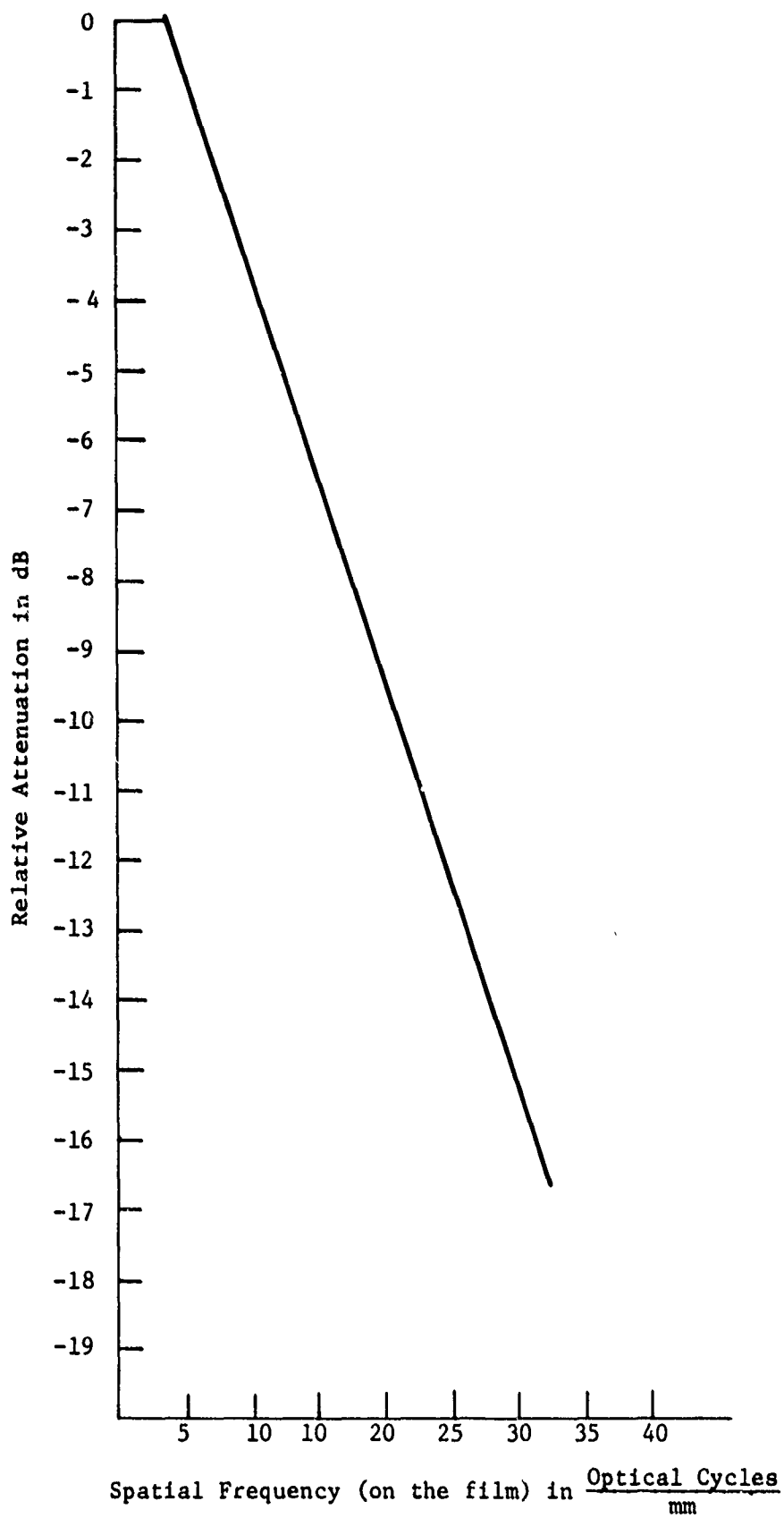


Figure 16. Range Response MTF.

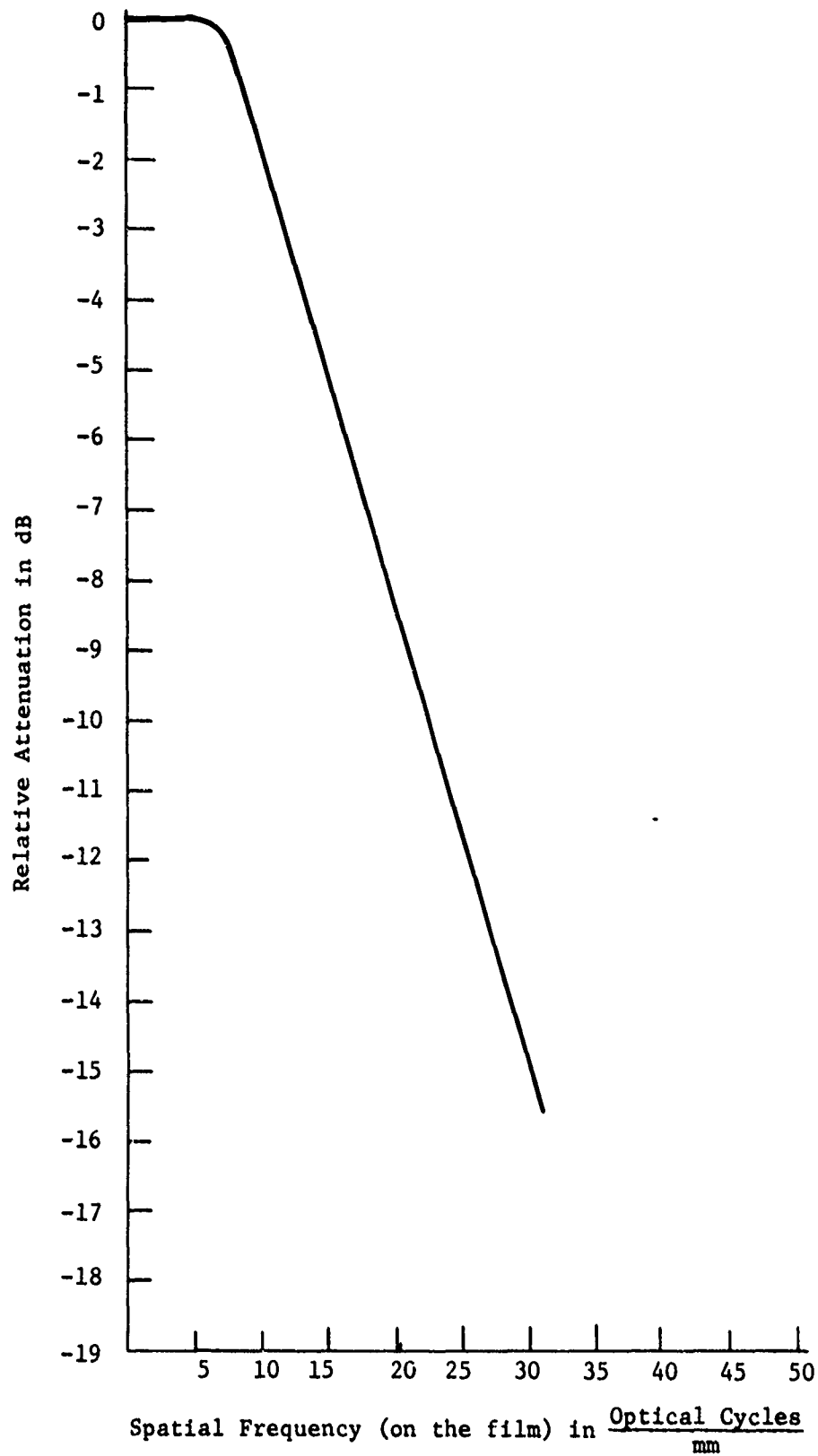


Figure 17. Azimuth Response MTF.

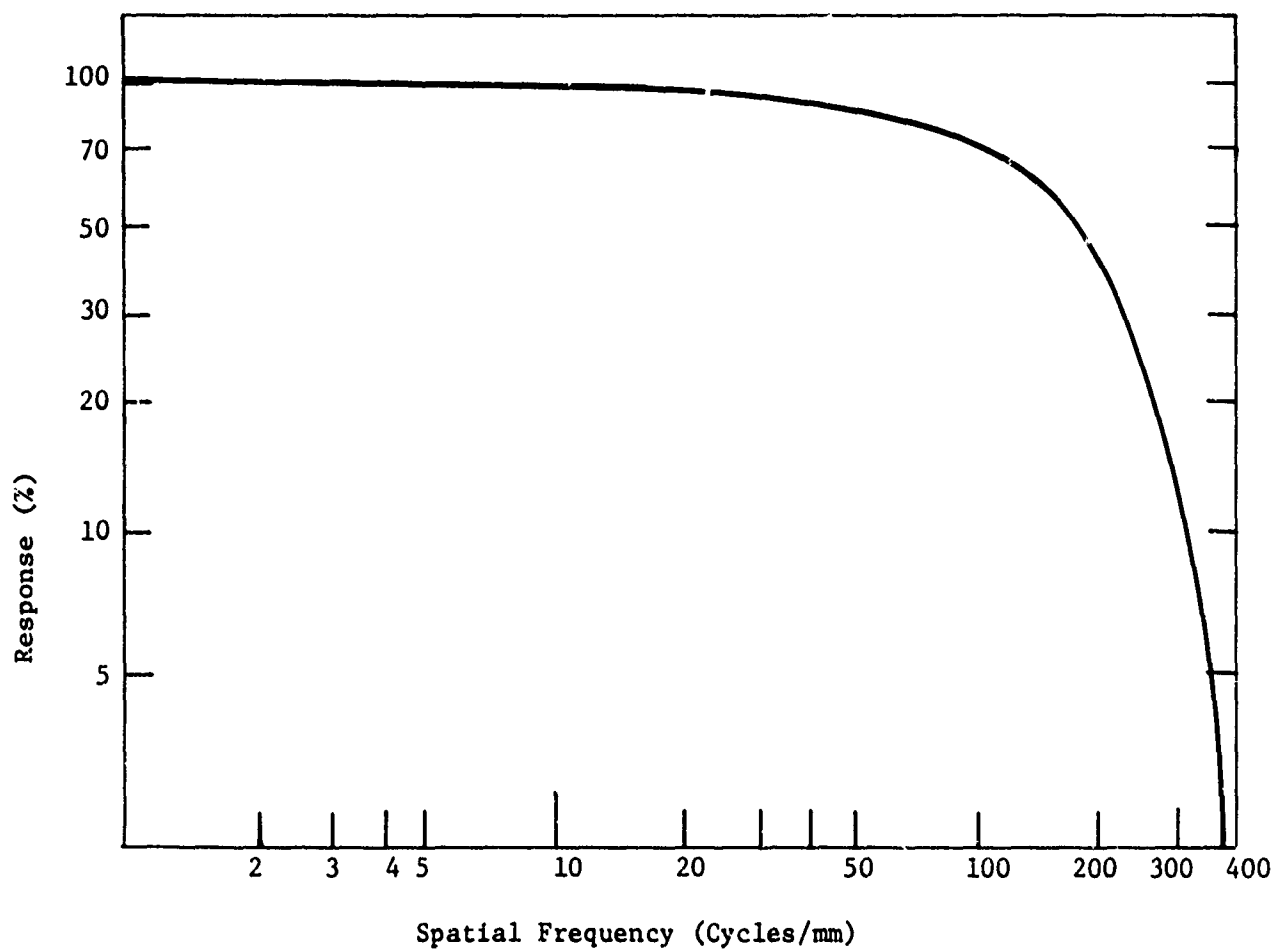


Figure 18. Modulation Transfer Function - Film.



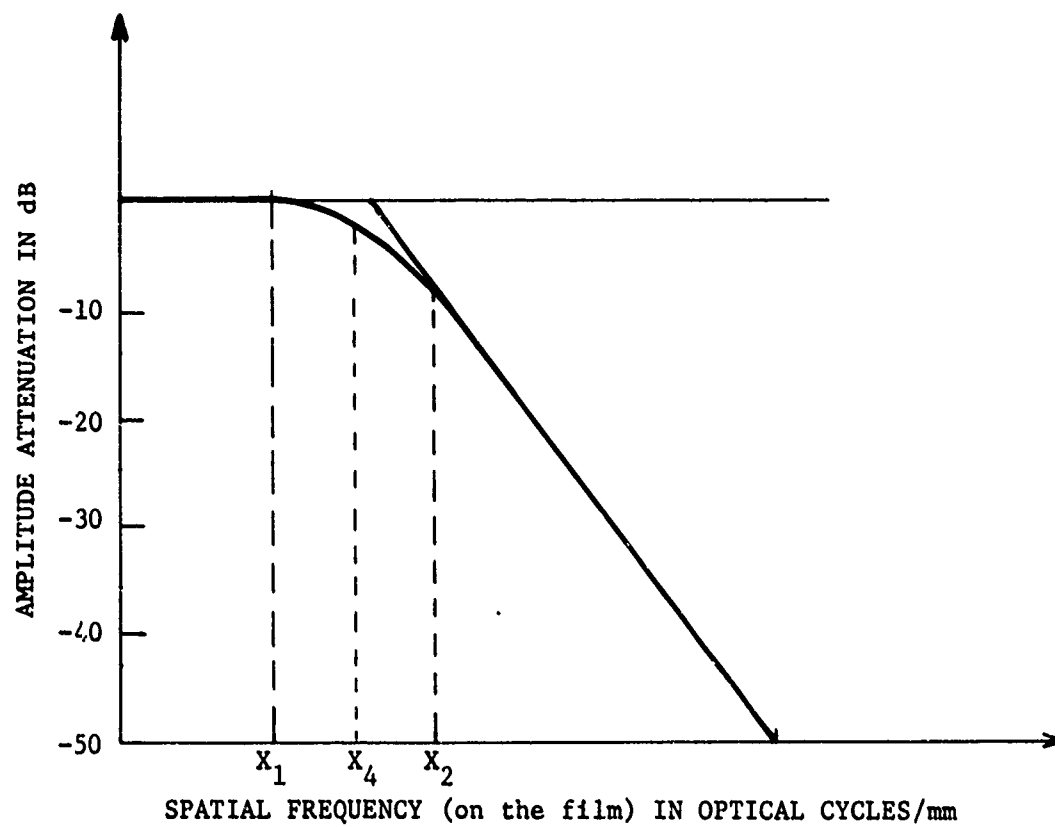


Figure 19. Recorder Limiting Function.

the print out of signal history as shown in Table I and columns FSPAT (FS) and z which denote the spatial frequency and the position along the doppler history for target point 2. For FS vs. Z to correspond to a perfect section of signal film (will focus to a point in the image plane), FS must be a linear function of Z. The sample plot with circles in Fig. 20 corresponding to Table I, is nearly linear. This corresponds to having quadratic phase in a recorded signal of phase history. The amount of non-linearity, deviation, (DEVA), of the actual points of FS to the best linear fit of FS vs. Z is a measure of how much azimuth smear can be attributed to this non-linearity. Azimuth smear SMA from DEVA is then  $DEVA/(\text{slope of linear fit})$  which provides the contribution of FS deviation in the determination of G which is essentially in the direction of Z. The second plot in Fig. 6.16, shown with  $\Delta$ 's, for similar geometry but with a lot of uncompensated motion is more illustrative of smear as predicted by a linear fit. Another important contributor to resolution is the amount of useable signal history. Useable is defined in the next sub-section. If the entire spatial history for a target is useable, then the effective synthetic aperture (DEFF) is identical to the actual aperture (DACT), where  $DACT = 1/(FSCALE*BEAM)$  with  $FSCALE = 2/\lambda$  and  $BEAM = \frac{\lambda}{D}$ .  $\lambda$  is wavelength and D is the physical aperture of the antenna. D might be 5 to 10 feet. Hence for X-band ( $\lambda = .1$  ft) DACT would be 2.5 ft to 5 ft. As is well

TABLE I. Azimuth Signal History

T	VX	VY	VZ	R	SIN $\theta$	SIN $\phi$	HDUT	PSRATF	FIFMP	FILMSP	FSPAT	G	H	Z
1.054	300.000	0.0	0.0	25001.	0.00973	0.10999	2.545	-1.125	73.402	209.99	0.24001	596.20	5000.48	245.00
2.034	300.000	0.0	0.0	25001.	0.00973	0.10999	2.271	-1.125	67.922	209.99	0.22002	610.70	5000.48	269.49
2.117	300.000	0.0	0.0	25001.	0.00973	0.20000	1.977	-1.125	62.000	209.99	0.20002	635.20	5000.51	293.99
2.147	300.000	0.0	0.0	25000.	0.00573	0.20000	1.683	-1.125	56.144	209.99	0.14722	659.69	5000.35	318.49
2.201	300.000	0.0	0.0	25000.	0.00473	0.20000	1.389	-1.125	50.285	209.99	0.14722	684.19	5000.25	342.99
2.302	300.000	0.0	0.0	25000.	0.00373	0.20000	1.095	-1.125	44.405	209.99	0.14002	708.69	5000.15	367.49
2.444	300.000	0.0	0.0	25000.	0.00273	0.20000	0.801	-1.125	38.526	209.99	0.12002	733.19	5000.05	391.98
2.524	300.000	0.0	0.0	25000.	0.00173	0.20000	0.507	-1.125	32.646	209.99	0.10002	757.69	5000.00	416.48
2.607	300.000	0.0	0.0	25000.	0.00073	0.20000	0.213	-1.125	26.768	209.99	0.08002	782.19	4999.97	440.97
2.689	300.000	0.0	0.0	25000.	-0.00027	0.20000	-0.041	-1.125	20.887	209.99	0.06003	806.69	4999.97	465.47
2.771	300.000	0.0	0.0	25000.	-0.00127	0.20000	-0.374	-1.125	15.007	209.99	0.05003	831.19	4999.98	489.97

DOPPLER HISTORY FOR TARGET 2:

T	VX	VY	VZ	R	SIN $\theta$	SIN $\phi$	HDUT	PSRATF	FIFMP	FILMSP	FSPAT	G	H	Z
1.205	300.000	0.0	0.0	25004.	0.01873	0.21730	5.483	-1.125	132.144	209.99	0.44050	370.52	5003.83	0.0
1.340	300.000	0.0	0.0	25003.	0.01773	0.21730	5.191	-1.125	126.310	209.99	0.42105	401.54	5003.45	22.40
1.415	300.000	0.0	0.0	25003.	0.01673	0.21730	4.898	-1.125	120.455	209.99	0.40153	424.44	5003.05	44.01
1.490	300.000	0.0	0.0	25003.	0.01573	0.21737	4.605	-1.125	114.599	209.99	0.38201	448.69	5002.70	67.37
1.565	300.000	0.0	0.0	25002.	0.01473	0.21737	4.312	-1.125	108.744	209.99	0.36249	469.33	5002.31	89.42
1.639	300.000	0.0	0.0	25002.	0.01373	0.21737	4.020	-1.125	102.888	209.99	0.34297	491.79	5002.06	112.28
1.714	300.000	0.0	0.0	25002.	0.01273	0.21737	3.727	-1.125	97.032	209.99	0.32345	514.24	5001.76	134.75
1.789	300.000	0.0	0.0	25001.	0.01173	0.21738	3.434	-1.125	91.176	209.99	0.30393	536.69	5001.49	157.16
1.864	300.000	0.0	0.0	25001.	0.01073	0.21738	3.141	-1.125	85.320	209.99	0.28441	559.14	5001.25	179.54
1.939	300.000	0.0	0.0	25001.	0.00973	0.21738	2.848	-1.125	79.463	209.99	0.26489	581.60	5001.03	202.09
2.014	300.000	0.0	0.0	25001.	0.00873	0.21738	2.555	-1.125	73.607	209.99	0.24537	604.05	5000.82	224.54
2.089	300.000	0.0	0.0	25001.	0.00773	0.21739	2.263	-1.125	67.750	209.99	0.22584	626.50	5000.64	247.00
2.164	300.000	0.0	0.0	25000.	0.00673	0.21739	1.970	-1.125	61.893	209.99	0.20632	648.95	5000.46	269.45
2.239	300.000	0.0	0.0	25000.	0.00573	0.21739	1.677	-1.125	56.036	209.99	0.18679	671.41	5000.35	291.90
2.314	300.000	0.0	0.0	25000.	0.00473	0.21739	1.384	-1.125	50.179	209.99	0.16727	693.86	5000.25	314.35
2.389	300.000	0.0	0.0	25000.	0.00373	0.21739	1.091	-1.125	44.321	209.99	0.14774	716.31	5000.14	336.81
2.464	300.000	0.0	0.0	25000.	0.00273	0.21739	0.798	-1.125	38.464	209.99	0.12822	738.76	5000.07	359.26
2.539	300.000	0.0	0.0	25000.	0.00173	0.21739	0.505	-1.125	32.607	209.99	0.10869	761.22	5000.02	381.71
2.614	300.000	0.0	0.0	25000.	0.00073	0.21739	0.213	-1.125	26.749	209.99	0.08917	783.67	5000.00	404.16
2.689	300.000	0.0	0.0	25000.	-0.00027	0.21739	-0.080	-1.125	20.892	209.99	0.06964	806.12	2999.99	426.61
2.764	300.000	0.0	0.0	25000.	-0.00127	0.21739	-0.373	-1.125	15.035	209.99	0.05012	828.57	5000.01	449.07

DOPPLER HISTORY FOR TARGET 3:

T	VX	VY	VZ	R	SIN $\theta$	SIN $\phi$	HDUT	PSRATF	FIFMP	FILMSP	FSPAT	G	H	Z
1.293	300.000	0.0	0.0	21003.	0.01873	0.23806	5.456	-1.125	131.620	209.99	0.43875	417.99	1003.45	0.0
1.401	300.000	0.0	0.0	21003.	0.01773	0.23806	5.145	-1.125	125.795	209.99	0.41933	438.59	1003.10	20.40
1.529	300.000	0.0	0.0	21003.	0.01673	0.23806	4.874	-1.125	119.969	209.99	0.39991	458.79	1002.76	40.40
1.597	300.000	0.0	0.0	21002.	0.01573	0.23807	4.582	-1.125	114.143	209.99	0.38049	479.18	1002.94	61.26
1.665	300.000	0.0	0.0	21002.	0.01473	0.23807	4.280	-1.125	108.317	209.99	0.36107	499.58	1002.11	81.40
1.733	300.000	0.0	0.0	21002.	0.01373	0.23807	4.000	-1.125	102.491	209.99	0.34165	519.98	1001.80	102.75
1.801	300.000	0.0	0.0	21002.	0.01273	0.23808	3.708	-1.125	96.664	209.99	0.32223	540.37	1001.54	124.20
1.869	300.000	0.0	0.0	21001.	0.01173	0.23808	3.417	-1.125	90.837	209.99	0.30280	560.77	1001.35	145.50
1.937	300.000	0.0	0.0	21001.	0.01073	0.23808	3.126	-1.125	85.010	209.99	0.28338	581.17	1001.15	166.80
2.005	300.000	0.0	0.0	21001.	0.00973	0.23808	2.834	-1.125	79.183	209.99	0.26395	601.57	1000.92	188.10
2.073	300.000	0.0	0.0	21001.	0.00873	0.23809	2.543	-1.125	73.356	209.99	0.24453	621.96	1000.74	209.40
2.141	300.000	0.0	0.0	21001.	0.00773	0.23809	2.252	-1.125	67.528	209.99	0.22510	642.36	1000.54	224.70
2.209	300.000	0.0	0.0	21000.	0.00673	0.23809	1.960	-1.125	61.701	209.99	0.20568	662.76	1000.44	240.00
2.277	300.000	0.0	0.0	21000.	0.00573	0.23809	1.669	-1.125	55.873	209.99	0.18625	683.16	1000.32	265.14
2.345	300.000	0.0	0.0	21000.	0.00473	0.23809	1.377	-1.125	50.045	209.99	0.16682	703.55	1000.21	285.55
2.413	300.000	0.0	0.0	21000.	0.00373	0.23809	1.086	-1.125	44.217	209.99	0.14740	723.95	1000.12	305.98



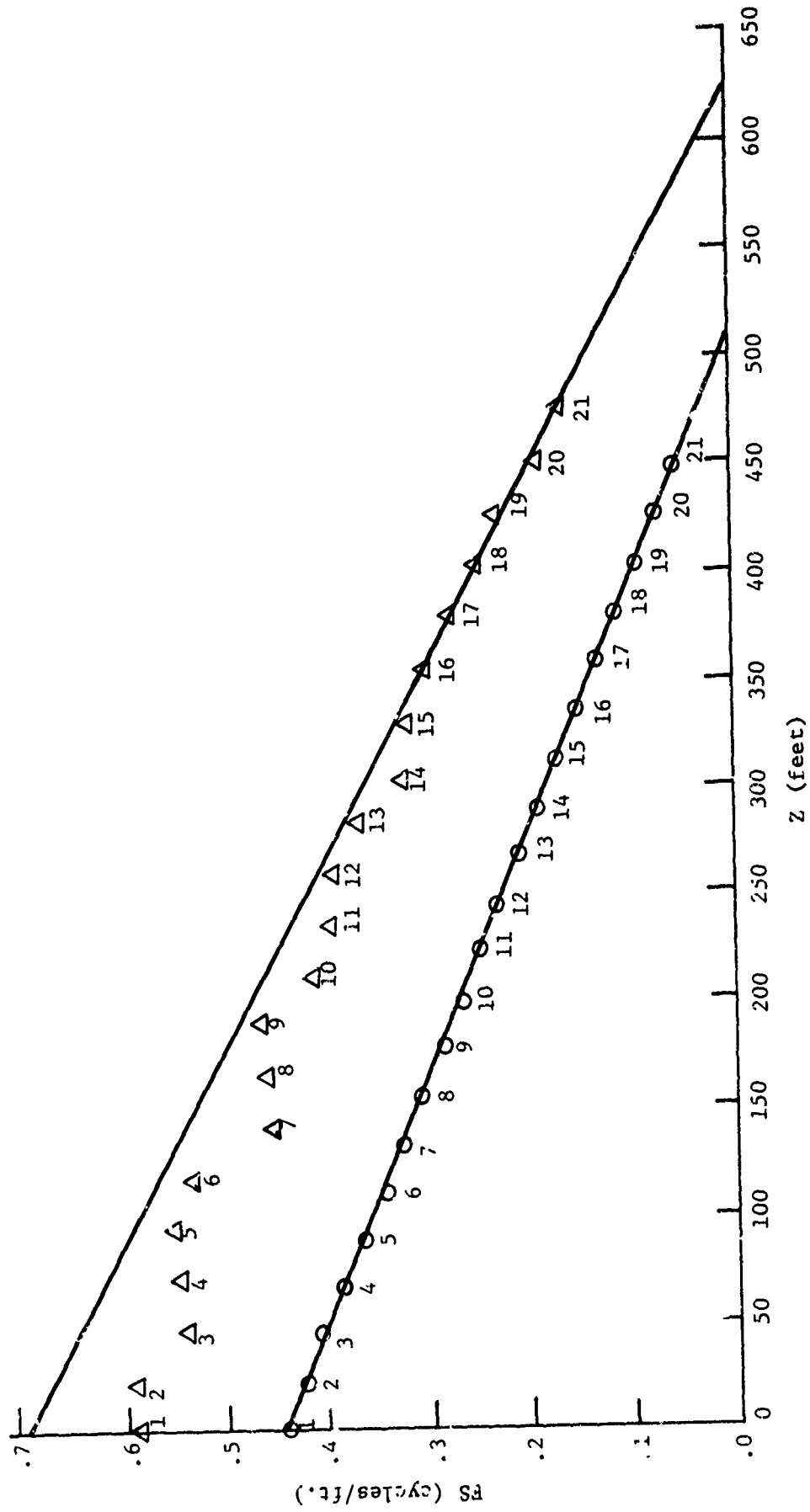


Figure 20. Sample Plots FS vs. Z

known,  $D/2$  is the theoretical best azimuth resolution. To illustrate the effect of useable information content, let 21 points of signal history represent the whole synthetic aperture. If, the largest useable history were 10 points, for example, then  $\frac{20}{9}$  is the degradation factor due to loss of information. In other words the effective aperture would be

$$DEFF = DACT * 20/9$$

or DEFF would take on a value of 11 to 22 feet. In our simulation, this contribution to smear would be summed (root sum of squares) with the contribution to smear given by the SMA. Thus azimuth resolution is computed as

$$\sqrt{(DEFF)^2 + (SMA)^2}$$

A similar linear fit for W vs G, W is range position and G is azimuth position, provides a smear or contribution (DEVR) to range resolution that results from range walk and uncompensated motion of aircraft or target. The other major contributor to range smear is chirp non-linearity (similar to FS non-linearity). After recording chirp, temporal frequencies relative to a range sampler, chirp frequencies appear as spatial distributions FSV. These FSV distributions are distributed in range. Hence, a linear fit of FSV vs. WC, where WC is the spatial distribution of a chirp pulse in range, will provide a deviation from a best fit straight line or a video deviation DEVV. After focusing (com-

pressing in range) the image location of the WC's becomes a W in the azimuth compression, and the DEVR becomes a contributor to range smear.

In MSTRIP, the short pulse simulation, an input RRMIN is used with DEVR to give range smear as

$$SMR = \frac{(DEVR)^2}{(1 + SLW^2)} + (RRMIN)^2$$

where SLW is the slope of the W vs. G fit. Since  $1 + (SLW)^2$  is the  $\csc^2$  of the slope angle, dividing by it provides the contribution of DEVR in the direction of W or the range direction.

#### 6.4.2 Optimization Choices

The second history in Fig. 20 ( $\Delta$ 's) is a good illustration of a signal history which can be optimized with respect to azimuth resolution. Optimization is performed in the following way. First, the doppler history for a selected target (the focus target) is screened relative to the minimum (FSMIN) and maximum (FSMAX) values of FS. Dopplers outside this range are not used. Secondly, each possible segment that contains at least three points and consists of a beginning point, an ending point, and all points in between, is checked for consistency in sign. Either all FS's are positive or all must be negative; otherwise this segment is not used. For each segment that remains, the azimuth resolution, for azimuth optimization, and, if RMS optimization is desired, the range resolution, for the focus target are computed. Table

IIF presents the azimuth resolution table for the target with  $\Delta$ -points in Fig. 20. Data for this figure were taken from FS and Z for target 2 in Table IIF. The smallest value in this table corresponds to the best possible azimuth resolution. From the table we obtain 9.678 as the minimum azimuth smear (best resolution). Tabular output is organized, so that each row corresponds to a fixed number of points in each segment. The first row, one entry, corresponds to the use of all 21 sample points; the second row, two entries, corresponds to segment (1, 20) and segment (2, 21), and so on for all possible segments. (If \*\*\*'s appear in an entry, the corresponding segment was excluded by the screening process.) Thus, in the table, an entry in the  $I^{\text{th}}$  row, from the top, and  $K^{\text{th}}$  column, from the left, is for the segment (N1, N2) where

$$N1 = K \text{ and } N2 = 21 - I + K$$

Hence entry 9.678 is for segment (15,21). It is noted that a row with greater than 13 entries is extended around onto the next line and an extra space is printed after an extended line.

If RMS resolution is desired, then an RMS resolution table is generated. RMS optimization is computed with rules similar to those for azimuth optimization. The only difference is in the table used for choosing the best resolution.

After optimization, each target history is processed

(azimuth, range, and RMS resolutions are computed) using the frequency band limits and focal lengths obtained during optimization. In addition, to frequency band limits (both positive or both negative), one further criteria must be met by each segment of doppler history. That is, the dopplers are required to be monotonically decreasing with increasing  $Z$ . Focal length at the focus target is directly proportional to the slope of FS vs.  $Z$ . This is azimuth focal length. It is assumed for subroutine PROCESS that either short pulse or de-chirp (range compressed) data is used as an input. Targets at different ranges than the focus target can be focused only at a longer (for greater range) or shorter (for near range) focal length that is proportional to range. Correcting the optimum focal length by the ratio of range at the focus target to the range of the target being processed produces the desired change. Doing so provides the essence of a tilted plane processor.

If chirp pulses (two dimensional signal film) are to be processed, then subroutine RNGPRC is used to de-chirp the video signal histories. Subsequent use of PROCESS proceeds as discussed above. Transparent to the user is the fact that RRMIN is computed in using RNGPRC and is assumed as an input parameter when only PROCESS is used. RRMIN is data initialized but can be changed by a Type II parameter input to any desired value.



### 6.4.3 Image Location

Images are located in azimuth and range. A focal point for image location is obtained by linearly fitting  $W$  vs.  $FS$  and  $G$  vs.  $FS$ .  $W$  is range location of signal points and  $G$  is azimuth location of signal points. These best fit straight lines are then used to extrapolate to  $FS = 0$ .  $FS = 0$  corresponds to the mean focal point. Thus,  $W_0 = W(FS = 0)$  and  $G_0 = G(FS = 0)$  are the linearly predicted coordinates of the image point.

Two important distortions in image location are due to squint angle and depression. Since the nominal squint and depression are known a priori, geometrical transformations can be performed to correct for these distortions. Corrections for squint can be accomplished in an optical processor. Both corrections can be achieved in a digital system. The correction for squint is

$$G_{01} = G_0 / |\cos \theta_c| + (W_0 + R_{MIN}) * \sin \theta_c$$

and

$$W_{01} = W_0 * |\cos \theta_c|$$

where  $\theta_c$  is the squint angle to center of beam,  $W_0$  and  $G_0$  are initial location of focused image, and  $R_{MIN}$  adjust  $W_0$  from range into swath to total range.  $G_0$  is already in absolute terms. The effect of a squint correction is shown in Fig. 21 where  $A$  is the input image,  $B$  is the initial output image,  $C$  is the

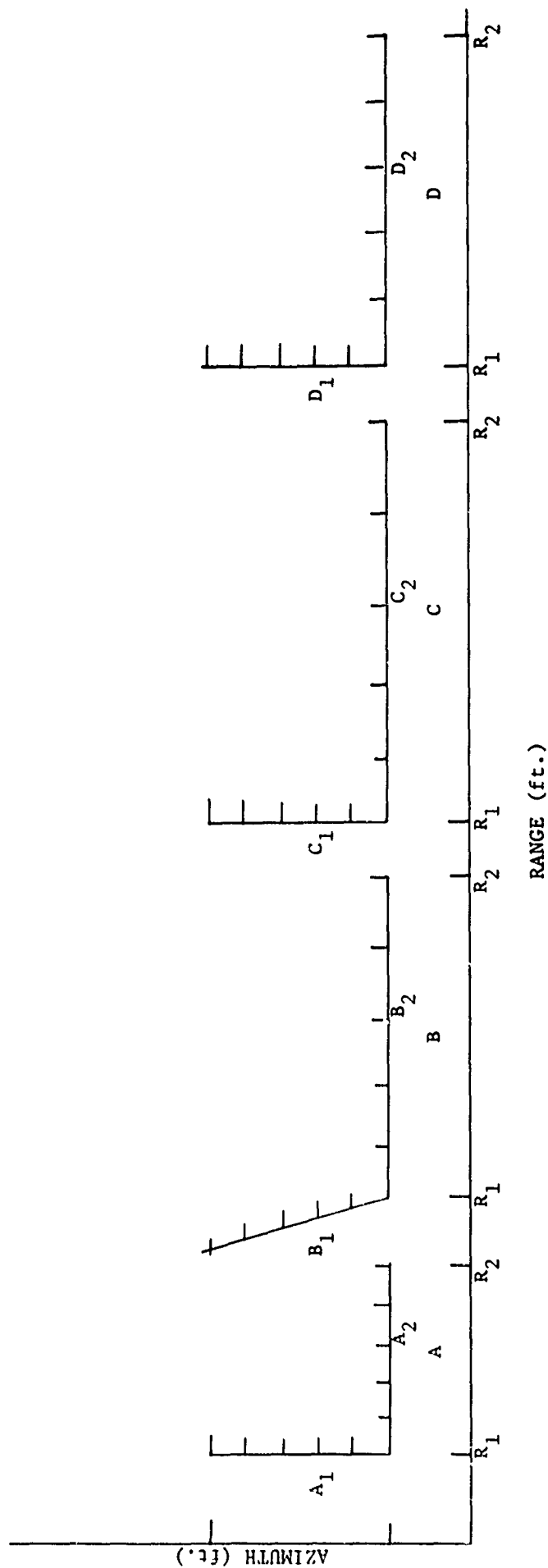


Figure 21. Corrections for Squint and Distortion.

image corrected for squint, and D is image C corrected for depression angle. The purpose of the first correction is to change B by erecting the image so that equal azimuth inputs tend to produce equal azimuth in the image. The second correction provides a scale change in the range direction which compensates for nonlinearities due to changes in depression. This latter change is effected by

$$U = G_{01}$$

and

$$V = W_{01}/\cos(\text{DEPC})$$

where DEPC is the nominal depression angle to center of beam at center range of strip swath.

#### 6.4.4 Geometrical Distortion

A measure of geometrical distortion is given by forming the ratio of the length of a line in the output image to length of the same line in the input image. For example, in Fig. 6.17,  $\overline{B_1B_2}/\overline{A_1A_2}$  is a measure of distortion. Obviously going to RSMOD  $\overline{C_1C_2}/\overline{A_1A_2}$  will improve this particular ratio. Similarly, distortion ratios relative to the D image (at least in the range direction) will be better than for C. Since target inputs to are point target, it is a simple calculation to provide every possible ratio for the distance between pairs of points with respect to B, C, and D images.

#### 6.4.5 Processor Subroutines

Imaging in the RSMOD simulation is accomplished by two subroutines. To compress or focus video history a range focusing subroutine, RNGPRC, is called into play. This subroutine calls on the linear fit subroutines, FIT and DEV, to obtain range smear, intermediate range and azimuth focussed location, and to provide a contribution of video non-linearity to azimuth smear. Use of RNGPRC is implied by the box in Fig. 10(b) which contains "Compress Range History to obtain one point on Azimuth History". From a programming sense RNGPRC fits, most naturally, inside the time iteration in SIGGEN. During the range compression for one pulse, video spatial frequencies are fitted to a best fit straight line with respect to range. Thus range smear is obtained. Dopplers for this same pulse are also fitted with respect to range to obtain a smear in azimuth due to non-linearity of doppler that results from chirp non-linearity and due to any non-linear sampling rates in range. Similarly the focused point in range, where video spatial frequency goes to zero, is also obtained. From the linear fit of doppler vs. range, the mean doppler to be associated with this range (at zero video) is easily computed.

After signal generation and/or range processing, the subroutine PROCES is called to obtain final images and smear as

described earlier. Figure 23 is a generalized flow diagram for this latter subroutine.

### 6.5 Output

There are numerous integer and logical switches that control output. For the purposes of this discussion, we illustrate a useful selection of outputs as shown in Table II and III. The order of outputs are fixed.

Considering individual parts of the output we have first the run number, RUN NO. 1 in this case, followed by a line headed with & PARAMS. This latter line indicates parameter values selected as TYPE II inputs for this run. Following the params line is a table of roll, pitch, yaw, xs, ys, zs, vxs, vys, and vzs which are target frame motions provided through the use of the subroutine SHIPMO. The table is 100 items long and corresponds to a 10 second period of logged ship motion. Underneath this table is a list of parameters used in developing the tabular entrees.

As labeled this motion history came from Buckley logs, coded 14A1. Also, the center item, item number 50, corresponds to a GMT (Greenwich Mean Time) of 14 hrs., 14 min and 53.0 seconds.

Table IIC continues the example output with three lines about doppler history. For each of the three targets, the number of useable parts (segments) and the largest part, with the beginning point and ending point, are given. Following these

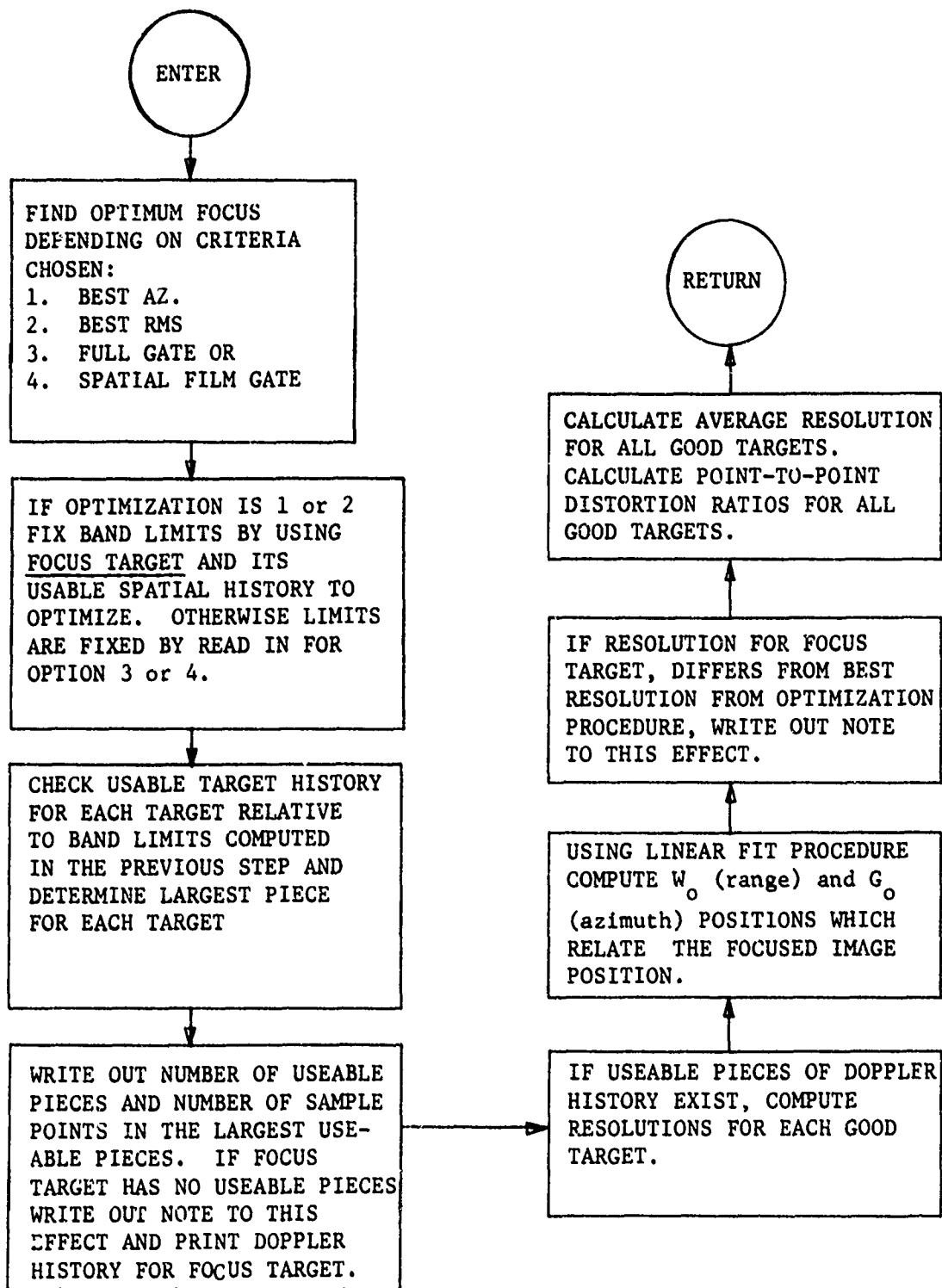


Figure 22. PROCES Generalized Flow Diagram.

BUICK LFY 14A1 14:14:53.0

TÄRLF2(1,1)

ROW	INDEX	ROLL	PITCH	YAW	XS	YS	ZS	VXS	VYS	VZS
1		-0.2401E-01	-0.5750E-02	0.0	1480.	-0.2245E 05	0.0	18.99	-0.0134	0.0
2		-0.3220E-01	-0.6109E-02	0.0	1482.	-0.2245E 05	0.0	18.99	-0.0134	0.0
3		-0.3453E-01	-0.6352E-02	0.0	1484.	-0.2245E 05	0.0	18.99	-0.0134	0.0
4		-0.3687E-01	-0.6595E-02	0.0	1485.	-0.2245E 05	0.0	18.99	-0.0134	0.0
5		-0.4007E-01	-0.7336E-02	0.0	1487.	-0.2245E 05	0.0	18.99	-0.0134	0.0
6		-0.5210E-01	-0.7479E-02	0.0	1489.	-0.2245E 05	0.0	18.99	-0.0134	0.0
7		-0.5550E-01	-0.7453E-02	0.0	1491.	-0.2245E 05	0.0	18.99	-0.0134	0.0
8		-0.5904E-01	-0.8020E-02	0.0	1493.	-0.2245E 05	0.0	18.99	-0.0134	0.0
9		-0.6423E-01	-0.8201E-02	0.0	1495.	-0.2245E 05	0.0	18.99	-0.0134	0.0
10		-0.6811E-01	-0.8232E-02	0.0	1497.	-0.2245E 05	0.0	18.99	-0.0134	0.0
11		-0.7365E-01	-0.7450E-02	0.0	1499.	-0.2245E 05	0.0	18.99	-0.0134	0.0
12		-0.7810E-01	-0.7473E-02	0.0	1501.	-0.2245E 05	0.0	18.99	-0.0134	0.0
13		-0.8044E-01	-0.7350E-02	0.0	1503.	-0.2245E 05	0.0	18.99	-0.0134	0.0
14		-0.8430E-01	-0.6752E-02	0.0	1504.	-0.2245E 05	0.0	18.99	-0.0134	0.0
15		-0.8740E-01	-0.6109E-02	0.0	1506.	-0.2245E 05	0.0	18.99	-0.0134	0.0
16		-0.9054E-01	-0.5593E-02	0.0	1508.	-0.2245E 05	0.0	18.99	-0.0134	0.0
17		-0.9268E-01	-0.5061E-02	0.0	1510.	-0.2245E 05	0.0	18.99	-0.0134	0.0
18		-0.9512E-01	-0.4712E-02	0.0	1512.	-0.2245E 05	0.0	18.99	-0.0134	0.0
19		-0.9721E-01	-0.4534E-02	0.0	1514.	-0.2245E 05	0.0	18.99	-0.0134	0.0
20		-0.9824E-01	-0.4187E-02	0.0	1516.	-0.2245E 05	0.0	18.99	-0.0134	0.0
21		-0.9904E-01	-0.3453E-02	0.0	1518.	-0.2245E 05	0.0	18.99	-0.0134	0.0
22		-0.1001	-0.3143E-02	0.0	1520.	-0.2245E 05	0.0	18.99	-0.0134	0.0
23		-0.1014	-0.2974E-02	0.0	1522.	-0.2245E 05	0.0	18.99	-0.0134	0.0
24		-0.1028	-0.1707E-02	0.0	1523.	-0.2245E 05	0.0	18.99	-0.0134	0.0
25		-0.1038	-0.0	0.0	1525.	-0.2245E 05	0.0	18.99	-0.0134	0.0
26		-0.1028	0.6941E-03	0.0	1527.	-0.2245E 05	0.0	18.99	-0.0134	0.0
27		-0.1014	0.1571E-02	0.0	1529.	-0.2245E 05	0.0	18.99	-0.0134	0.0
28		-0.1035	0.2044E-02	0.0	1531.	-0.2245E 05	0.0	18.99	-0.0134	0.0
29		-0.9824E-01	0.5142E-02	0.0	1533.	-0.2245E 05	0.0	18.99	-0.0134	0.0
30		-0.9590E-01	0.5840E-02	0.0	1535.	-0.2245E 05	0.0	18.99	-0.0134	0.0
31		-0.9352E-01	0.4534E-02	0.0	1537.	-0.2245E 05	0.0	18.99	-0.0134	0.0
32		-0.9124E-01	0.5234E-02	0.0	1539.	-0.2245E 05	0.0	18.99	-0.0134	0.0
33		-0.8901E-01	0.6099E-02	0.0	1541.	-0.2245E 05	0.0	18.99	-0.0134	0.0
34		-0.8681E-01	0.6964E-02	0.0	1542.	-0.2245E 05	0.0	18.99	-0.0134	0.0
35		-0.8133E-01	0.7479E-02	0.0	1544.	-0.2245E 05	0.0	18.99	-0.0134	0.0
36		-0.7603E-01	0.8523E-02	0.0	1546.	-0.2245E 05	0.0	18.99	-0.0134	0.0
37		-0.7202E-01	0.9250E-02	0.0	1548.	-0.2245E 05	0.0	18.99	-0.0134	0.0
38		-0.6754E-01	0.9944E-02	0.0	1550.	-0.2245E 05	0.0	18.99	-0.0134	0.0
39		-0.6142E-01	0.1075E-01	0.0	1552.	-0.2245E 05	0.0	18.99	-0.0134	0.0
40		-0.5515E-01	0.1052E-01	0.0	1554.	-0.2245E 05	0.0	18.99	-0.0134	0.0
41		-0.5051E-01	0.1130E-01	0.0	1556.	-0.2245E 05	0.0	18.99	-0.0134	0.0
42		-0.4294E-01	0.1157E-01	0.0	1558.	-0.2245E 05	0.0	18.99	-0.0134	0.0
43		-0.5683E-01	0.1222E-01	0.0	1560.	-0.2245E 05	0.0	18.99	-0.0134	0.0
44		-0.5229E-01	0.1270E-01	0.0	1561.	-0.2245E 05	0.0	18.99	-0.0134	0.0
45		-0.2401E-01	0.1324E-01	0.0	1563.	-0.2245E 05	0.0	18.99	-0.0134	0.0
46		-0.1835E-01	0.1340E-01	0.0	1565.	-0.2245E 05	0.0	18.99	-0.0134	0.0
47		-0.1223E-01	0.1370E-01	0.0	1567.	-0.2245E 05	0.0	18.99	-0.0134	0.0

-82-

TABLE IIB. Example Output, Page 2

48	-0.4538E-02	0.1194E-01	0.0	1549.	-0.2245E 05	0.0	18.99	-0.6134	0.0
49	0.1571E-02	0.1431E-01	0.0	1571.	-0.2245E 05	0.0	18.99	-0.6134	0.0
50	0.7479E-02	0.1464E-01	0.0	1573.	-0.2245E 05	0.0	18.99	-0.6134	0.0
51	0.1526E-01	0.1501E-01	0.0	1575.	-0.2245E 05	0.0	18.99	-0.6134	0.0
52	0.2147E-01	0.1534E-01	0.0	1577.	-0.2245E 05	0.0	18.99	-0.6134	0.0
53	0.2915E-01	0.1553E-01	0.0	1579.	-0.2245E 05	0.0	18.99	-0.6134	0.0
54	0.3524E-01	0.1571E-01	0.0	1580.	-0.2245E 05	0.0	18.99	-0.6134	0.0
55	0.4134E-01	0.1588E-01	0.0	1582.	-0.2245E 05	0.0	18.99	-0.6134	0.0
56	0.4747E-01	0.1571E-01	0.0	1584.	-0.2245E 05	0.0	18.99	-0.6134	0.0
57	0.5374E-01	0.1553E-01	0.0	1586.	-0.2245E 05	0.0	18.99	-0.6134	0.0
58	0.5984E-01	0.1534E-01	0.0	1588.	-0.2245E 05	0.0	18.99	-0.6134	0.0
59	0.5404E-01	0.1501E-01	0.0	1590.	-0.2245E 05	0.0	18.99	-0.6134	0.0
60	0.6211E-01	0.1464E-01	0.0	1592.	-0.2245E 05	0.0	18.99	-0.6134	0.0
61	0.7422E-01	0.1431E-01	0.0	1594.	-0.2245E 05	0.0	18.99	-0.6134	0.0
62	0.8133E-01	0.1374E-01	0.0	1596.	-0.2245E 05	0.0	18.99	-0.6134	0.0
63	0.8439E-01	0.1301E-01	0.0	1598.	-0.2245E 05	0.0	18.99	-0.6134	0.0
64	0.8901E-01	0.1344E-01	0.0	1599.	-0.2245E 05	0.0	18.99	-0.6134	0.0
65	0.9250E-01	0.1301E-01	0.0	1601.	-0.2245E 05	0.0	18.99	-0.6134	0.0
66	0.9469E-01	0.1274E-01	0.0	1603.	-0.2245E 05	0.0	18.99	-0.6134	0.0
67	0.9904E-01	0.1234E-01	0.0	1605.	-0.2245E 05	0.0	18.99	-0.6134	0.0
68	0.1624	0.1222E-01	0.0	1607.	-0.2245E 05	0.0	18.99	-0.6134	0.0
69	0.1754	0.1187E-01	0.0	1609.	-0.2245E 05	0.0	18.99	-0.6134	0.0
70	0.1873	0.1152E-01	0.0	1611.	-0.2245E 05	0.0	18.99	-0.6134	0.0
71	0.1089	0.1134E-01	0.0	1613.	-0.2245E 05	0.0	18.99	-0.6134	0.0
72	0.1100	0.1104E-01	0.0	1615.	-0.2245E 05	0.0	18.99	-0.6134	0.0
73	0.1112	0.1092E-01	0.0	1617.	-0.2245E 05	0.0	18.99	-0.6134	0.0
74	0.1122	0.1075E-01	0.0	1618.	-0.2245E 05	0.0	18.99	-0.6134	0.0
75	0.1134	0.1030E-01	0.0	1620.	-0.2245E 05	0.0	18.99	-0.6134	0.0
76	0.1145	0.9944E-02	0.0	1622.	-0.2245E 05	0.0	18.99	-0.6134	0.0
77	0.1134	0.9774E-02	0.0	1624.	-0.2245E 05	0.0	18.99	-0.6134	0.0
78	0.1121	0.9599E-02	0.0	1626.	-0.2245E 05	0.0	18.99	-0.6134	0.0
79	0.1112	0.9250E-02	0.0	1628.	-0.2245E 05	0.0	18.99	-0.6134	0.0
80	0.1100	0.9074E-02	0.0	1630.	-0.2245E 05	0.0	18.99	-0.6134	0.0
81	0.1087	0.8901E-02	0.0	1632.	-0.2245E 05	0.0	18.99	-0.6134	0.0
82	0.1073	0.8727E-02	0.0	1634.	-0.2245E 05	0.0	18.99	-0.6134	0.0
83	0.1058	0.8552E-02	0.0	1636.	-0.2245E 05	0.0	18.99	-0.6134	0.0
84	0.1019	0.8374E-02	0.0	1637.	-0.2245E 05	0.0	18.99	-0.6134	0.0
85	0.9424E-01	0.8203E-02	0.0	1639.	-0.2245E 05	0.0	18.99	-0.6134	0.0
86	0.9315E-01	0.8029E-02	0.0	1641.	-0.2245E 05	0.0	18.99	-0.6134	0.0
87	0.8744E-01	0.7854E-02	0.0	1643.	-0.2245E 05	0.0	18.99	-0.6134	0.0
88	0.8374E-01	0.7479E-02	0.0	1645.	-0.2245E 05	0.0	18.99	-0.6134	0.0
89	0.7810E-01	0.7505E-02	0.0	1647.	-0.2245E 05	0.0	18.99	-0.6134	0.0
90	0.7365E-01	0.7330E-02	0.0	1649.	-0.2245E 05	0.0	18.99	-0.6134	0.0
91	0.6754E-01	0.7156E-02	0.0	1651.	-0.2245E 05	0.0	18.99	-0.6134	0.0
92	0.5954E-01	0.6991E-02	0.0	1653.	-0.2245E 05	0.0	18.99	-0.6134	0.0
93	0.5374E-01	0.6497E-02	0.0	1655.	-0.2245E 05	0.0	18.99	-0.6134	0.0
94	0.4747E-01	0.6332E-02	0.0	1656.	-0.2245E 05	0.0	18.99	-0.6134	0.0
95	0.3997E-01	0.6254E-02	0.0	1658.	-0.2245E 05	0.0	18.99	-0.6134	0.0
96	0.3229E-01	0.6254E-02	0.0	1660.	-0.2245E 05	0.0	18.99	-0.6134	0.0
97	0.2501E-01	0.6100E-02	0.0	1662.	-0.2245E 05	0.0	18.99	-0.6134	0.0
98	0.1833E-01	0.5934E-02	0.0	1664.	-0.2245E 05	0.0	18.99	-0.6134	0.0
99	0.1042E-01	0.5750E-02	0.0	1666.	-0.2245E 05	0.0	18.99	-0.6134	0.0
100	0.3142E-02	0.5555E-02	0.0	1668.	-0.2245E 05	0.0	18.99	-0.6134	0.0

ITEM=

UNIT=FLPDRIVE=1,UNIT=1,DEPRSE=0.21914107, XUNIT= 1572.8577, YUNIT= -22449.046

N2= 50,DELTA= 0.19999993

N2P= 9A,TERU=-21229135,LABE= 1046514571, -757873176,CUDE= -235617807

END

RS=232

ALPHAS= 90.000000

SUM= 0.50000000

SUPERS= 91.649991

PGS= 22449.041

PANLE= 23000.004

ALT= 5000.0000

DEPRSD= 12.555860



TABLE IIC. Example Output, Page 3

REND

TARGET 1 DUPP=HTST. HAS NO USEABLE PARTS.

TARGET 2 DUPP=HTST. HAS 1 USEABLE PART(S). LARGEST PART: 15 THRU 21.

TARGET 3 DUPP=HTST. HAS 1 USEABLE PART(S). LARGEST PART: 5 THRU 12.

TARGET 1 FMREAM = 0.25000575E-02 FMRATE = -0.65793656E-03

TARGET 2 FMREAM = 0.39012522 FMRATE = -0.69218258E-03

TARGET 3 FMREAM = 0.19867287 FMRATE = -0.76305660E-03

[illegible]

BUCKLEY 10A1 1011453.0

**DOPPLER HISTORY FOR TARGET 1:**

T	VX	VY	VZ	R	SINHA	SINDEP	ROUT	PKATE	FIEMP	FILMSP	FSPAT	G	M	Z
3.732	300.000	0.0	0.0	23194.	0.01673	0.21499	1.561	-1.125	53.716	299.99	0.17906	1119.55	3194.10	0.0
3.712	300.000	0.0	0.0	23194.	0.01774	0.21504	0.875	-1.125	39.996	299.99	0.13313	1143.71	3198.10	24.16
3.693	300.000	0.0	0.0	23194.	0.01668	0.21505	0.582	-1.125	34.140	299.99	0.13340	1167.65	3193.70	48.31
3.674	300.000	0.0	0.0	23194.	0.01569	0.21510	0.808	-1.125	38.649	299.99	0.12883	1192.02	3193.75	72.47
4.058	300.000	0.0	0.0	23194.	0.01871	0.21514	0.217	-1.125	26.830	299.99	0.09449	1216.17	3193.72	96.62
4.135	300.000	0.0	0.0	23194.	0.01373	0.21520	-0.546	-1.125	15.171	299.99	0.05059	1240.33	3193.87	120.78
4.715	300.000	0.0	0.0	23194.	0.01274	0.21526	0.232	-1.125	27.132	299.99	0.07044	1264.44	3193.95	144.84
4.794	300.000	0.0	0.0	23194.	0.01148	0.21526	-0.041	-1.125	21.276	299.99	0.07092	1286.64	3193.67	169.09
4.374	300.000	0.0	0.0	23194.	0.01070	0.21530	-0.671	-1.125	4.077	299.99	0.03026	1312.80	3193.72	193.25
4.457	300.000	0.0	0.0	23194.	0.00971	0.21536	-1.267	-1.125	-2.850	299.99	-0.00950	1336.93	3193.93	217.40

TABLE IIE. Example Output, Page 5

T	VX	VY	VZ	R	SINHA	SINDEP	ROUT	PSRATE	FIFMP	FILMSP	FSPAT	G	N	Z
4.537	300.000	0.0	0.0	23194.	0.00473	0.21541	-1.047	-1.125	0.750	294.49	0.00250	1361.11	3194.04	241.56
4.614	300.000	0.0	0.0	23194.	0.00715	0.21547	-1.001	-1.125	-9.521	299.49	-0.03174	1385.26	3194.25	265.71
4.674	300.000	0.0	0.0	23194.	0.00668	0.21547	-1.004	-1.125	-15.379	299.49	-0.05127	1409.42	3194.07	269.87
4.779	300.000	0.0	0.0	23194.	0.00509	0.21553	-2.062	-1.125	-18.735	299.49	-0.06245	1433.59	3194.33	314.03
4.859	300.000	0.0	0.0	23195.	0.00411	0.21558	-1.915	-1.125	-15.795	299.49	-0.05265	1457.73	3194.50	334.18
4.940	300.000	0.0	0.0	23195.	0.00373	0.21563	-2.438	-1.125	-26.269	299.49	-0.08751	1481.89	3194.79	362.34
5.020	300.000	0.0	0.0	23195.	0.00274	0.21570	-2.808	-1.125	-24.814	299.49	-0.09072	1506.04	3195.08	366.49
5.101	300.000	0.0	0.0	23195.	0.00174	0.21575	-2.794	-1.125	-33.376	299.49	-0.11126	1530.20	3195.33	410.65
5.181	300.000	0.0	0.0	23195.	0.00069	0.21575	-3.046	-1.125	-39.233	299.49	-0.13078	1554.35	3195.29	434.61
5.262	300.000	0.0	0.0	23196.	-0.00029	0.21581	-3.254	-1.125	-42.574	299.49	-0.14192	1578.51	3195.65	458.96
5.342	300.000	0.0	0.0	23196.	-0.00127	0.21586	-3.157	-1.125	-40.652	299.49	-0.13551	1602.67	3195.95	483.12

DOPPLER HISTORY FOR TARGET 2:

T	VX	VY	VZ	R	SINHA	SINDEP	ROUT	PSRATE	FIFMP	FILMSP	FSPAT	G	N	Z
3.799	300.000	0.0	0.0	22811.	0.01473	0.21979	7.564	-1.125	173.780	299.49	0.57931	1139.64	2810.50	0.0
3.874	300.000	0.0	0.0	22810.	0.01774	0.21974	7.718	-1.125	176.866	299.49	0.58458	1163.42	2809.88	23.79
3.957	300.000	0.0	0.0	22809.	0.01674	0.21969	6.946	-1.125	161.409	299.49	0.53005	1187.20	2809.23	47.58
4.037	300.000	0.0	0.0	22809.	0.01584	0.21966	7.003	-1.125	162.553	299.49	0.54180	1210.98	2808.70	71.37
4.114	300.000	0.0	0.0	22808.	0.01473	0.21960	7.052	-1.125	163.530	299.49	0.55512	1234.77	2808.03	95.16
4.195	300.000	0.0	0.0	22808.	0.01373	0.21940	6.759	-1.125	157.676	299.49	0.55561	1258.55	2807.64	118.95
4.275	300.000	0.0	0.0	22807.	0.01274	0.21955	5.807	-1.125	134.642	299.49	0.44083	1282.33	2807.15	142.74
4.354	300.000	0.0	0.0	22807.	0.01174	0.21952	5.846	-1.125	136.173	299.49	0.45393	1306.11	2806.73	166.52
4.433	300.000	0.0	0.0	22806.	0.01074	0.21945	5.746	-1.125	137.427	299.49	0.45011	1329.90	2806.19	190.31
4.512	300.000	0.0	0.0	22806.	0.00974	0.21940	5.820	-1.125	122.890	299.49	0.44945	1353.68	2805.71	214.10
4.592	300.000	0.0	0.0	22805.	0.00873	0.21941	4.727	-1.125	117.033	299.49	0.39013	1377.46	2805.50	237.88
4.671	300.000	0.0	0.0	22805.	0.00774	0.21930	4.703	-1.125	116.603	299.49	0.38069	1401.24	2805.09	261.66
4.750	300.000	0.0	0.0	22805.	0.00674	0.21929	4.332	-1.125	109.140	299.49	0.36581	1425.03	2804.55	285.45
4.830	300.000	0.0	0.0	22804.	0.00574	0.21924	3.634	-1.125	95.273	299.49	0.31759	1448.61	2804.30	309.24
4.909	300.000	0.0	0.0	22804.	0.00480	0.21919	3.628	-1.125	95.046	299.49	0.31684	1472.59	2804.00	333.02
4.984	300.000	0.0	0.0	22804.	0.00373	0.21919	3.335	-1.125	89.191	299.49	0.29731	1496.37	2803.49	356.80
5.067	300.000	0.0	0.0	22804.	0.00274	0.21913	2.961	-1.125	81.715	299.49	0.27239	1520.16	2803.57	380.58
5.147	300.000	0.0	0.0	22803.	0.00174	0.21908	2.808	-1.125	74.663	299.49	0.24499	1543.94	2803.32	404.37
5.226	300.000	0.0	0.0	22803.	0.00074	0.21901	2.234	-1.125	67.183	299.49	0.22393	1567.72	2803.06	428.15
5.305	300.000	0.0	0.0	22803.	-0.00020	0.21896	1.593	-1.125	54.350	299.49	0.18117	1591.50	2802.89	451.93
5.384	300.000	0.0	0.0	22803.	-0.00127	0.21896	1.300	-1.125	48.491	299.49	0.16164	1615.29	2802.90	475.71

DOPPLER HISTORY FOR TARGET 3:

T	VX	VY	VZ	R	SINHA	SINDEP	ROUT	PSRATE	FIFMP	FILMSP	FSPAT	G	N	Z
3.765	300.000	0.0	0.0	23002.	0.01473	0.21737	4.538	-1.125	113.250	299.49	0.57751	1120.59	3002.27	0.0
3.845	300.000	0.0	0.0	23002.	0.01774	0.21737	4.268	-1.125	107.659	299.49	0.55454	1153.56	3001.93	23.97
3.925	300.000	0.0	0.0	23002.	0.01674	0.21738	3.998	-1.125	102.467	299.49	0.54157	1177.53	3001.62	47.94
4.005	300.000	0.0	0.0	23001.	0.01574	0.21738	3.729	-1.125	97.075	299.49	0.52360	1201.50	3001.33	71.91
4.085	300.000	0.0	0.0	23001.	0.01473	0.21738	3.439	-1.125	91.219	299.49	0.50406	1225.47	3000.98	95.88
4.165	300.000	0.0	0.0	23001.	0.01373	0.21734	3.167	-1.125	85.027	299.49	0.48610	1249.44	3000.73	119.85
4.245	300.000	0.0	0.0	23001.	0.01274	0.21739	2.897	-1.125	80.435	299.49	0.46813	1273.41	3000.50	143.82
4.325	300.000	0.0	0.0	23000.	0.01174	0.21739	2.627	-1.125	75.042	299.49	0.45015	1297.39	3000.30	167.79
4.405	300.000	0.0	0.0	23000.	0.01074	0.21739	2.355	-1.125	69.644	299.49	0.43217	1321.34	3000.12	191.78
4.485	300.000	0.0	0.0	23000.	0.00974	0.21739	2.085	-1.125	63.792	299.49	0.41465	1345.31	2999.87	215.73
4.564	300.000	0.0	0.0	23000.	0.00874	0.21739	1.795	-1.125	58.400	299.49	0.39461	1369.28	2999.74	239.70
4.644	300.000	0.0	0.0	23000.	0.00774	0.21739	1.525	-1.125	53.006	299.49	0.37669	1393.25	2999.62	263.67
4.724	300.000	0.0	0.0	23000.	0.00674	0.21740	1.256	-1.125	47.013	299.49	0.35872	1417.22	2999.53	287.64
4.804	300.000	0.0	0.0	22999.	0.00574	0.21740	0.986	-1.125	42.220	299.49	0.34074	1441.19	2999.45	311.61
4.884	300.000	0.0	0.0	22999.	0.00471	0.21740	0.693	-1.125	36.563	299.49	0.32121	1465.16	2999.33	335.56
4.964	300.000	0.0	0.0	22999.	0.00373	0.21740	0.424	-1.125	30.970	299.49	0.30324	1489.13	2999.31	359.55

TABLE HF. Example Output, Page 6-

[illegible]

BEST NP = 7.      BEST IA = 15

BEST-FOCUS LINLAR FIT: FSPAT= 0.6964 = (Z/ 892.3)

**RESULTING RESOLUTIONS:**

TARGET	1	2	3	AVG(RMS) ALL TGT
AZ. RES.	*****	9.678	18.705	14.892
RNG. RES.	*****	3.002	3.003	3.003
RMS RES.	*****	7.165	13.395	10.742

TARGET	AZ.	RES.	E(FS=0)	N(FS=0)	E1(FS=0)	W1(FS=0)	U(FS=0)	V(FS=0)
1								
2	9.68		1758.6	2801.5	1957.6	2801.4	1957.6	2810.0
3	18.70		1625.1	2947.6	1825.9	2997.5	1825.9	5070.9

TABLE HG. Example Output, Page 7

POINT-TO-POINT DISTORTION RATIOS (SIG. FILM):

TARGET	1	2
2	*****	
3	*****	1.186053

POINT-TO-POINT DISTORTION RATIOS (INTERMEDIATE):

TARGET	1	2
2	*****	
3	*****	1.191244

POINT-TO-POINT DISTORTION RATIOS (FINAL FILM):

TARGET	1	2
2	*****	
3	*****	1.201267

TABLE III. Example Output, Page 8

SCALE: 8.3 5.0 RUN NO. 1 SHIP=BUCKLEY 1441 TIME=10:14:53.0

2

89

1 A  
2 B  
3 C  
4 D  
5 E  
6 F  
7 G  
8 H  
9 I  
10 J  
11 K  
12 L  
13 M  
14 N  
15 O

89

3

0000

TABLE II(I). Example Output, Page 9.

SUMMARY OF PARAMETER CHANGES:

RUN NO. 1 2PARAMS FSTUL=1.,LNEMP=F,LNTAB=F,LNWT=F,LSQB=T,LSOTGT=T,A(2)=300.,

RUN NO. 4

TABLE IIIA. Example 2, Page 1

PARAMS BEAMSC=001, LB=AMT, L=NEWPEF,

TARGET 1 NOPP-HIST. HAS 1 USEABLE PART(S). LARGEST PART: 7 THRU 20 .

TARGET 2 NOPP-HIST. HAS 1 USEABLE PART(S). LARGEST PART: 7 THRU 21 .

TARGET 3 NOPP-HIST. HAS 1 USEABLE PART(S). LARGEST PART: / THRU 21 .

TARGET 1 FMREAN = 0.24401408 FMRATE = -0.79991698E-03

TARGET 2 FMREAN = 0.24536308 FMRATE = -0.86948204E-03

TARGET 3 FMREAN = 0.24452801 FMRATE = -0.95228571E-03



TABLE IIB. Example 2, Page 2.

T	RQDI	AMPLITUDE	R	SINTHA	SINDEP	RDNT	PSRTE	FTEMP	FILMSP	FSPAT	G	M	Z
1.953	0.0	0.7250408E-11	25001.	0.00874	0.19999	2.570	-11.574	242.880	299.99	0.94297	585.77	5000.88	1115.86
2.324	0.0	0.5604192E-11	25000.	0.00410	0.20000	1.232	-11.574	256.113	299.99	0.85374	697.30	5000.18	1227.36
2.494	0.0	0.2457773E-11	25000.	-0.00034	0.20000	-0.106	-11.574	279.544	299.99	0.74451	808.98	4999.97	1338.56
3.094	0.0	0.5115893E-12	25000.	-0.00042	0.20000	-1.405	-11.574	292.574	299.99	0.67528	920.37	5000.25	1450.35
3.840	0.0	0.2710047E-13	25001.	-0.00007	0.19999	-2.743	-11.574	175.809	299.99	0.58605	1031.90	5001.04	1561.83
4.812	0.0	0.1942004E-14	25002.	-0.01002	0.19998	-4.121	-11.574	149.045	299.99	0.50684	1143.44	5002.32	1673.32
6.103	0.0	0.3421593E-14	25004.	-0.01857	0.19997	-5.459	-11.574	122.266	299.99	0.40764	1254.97	5004.11	1784.80
7.555	0.0	0.1534465E-13	25005.	-0.02312	0.19995	-6.797	-11.574	95.534	299.99	0.31846	1366.50	5006.38	1896.28
9.027	0.0	0.1044560E-13	25007.	-0.02767	0.19993	-8.134	-11.574	68.790	299.99	0.22931	1478.03	5009.16	2007.76
5.290	0.0	0.1277335E-14	25012.	-0.03222	0.19990	-9.471	-11.574	82.056	299.99	0.2019	1589.57	5012.43	2119.25
5.471	0.0	0.1924292E-14	25016.	-0.03677	0.19987	-10.807	-11.574	15.333	299.99	0.05111	1701.10	5016.20	2230.74

DOPPLER HISTORY FOR TARGET 2:

T	RQDI	AMPLITUDE	R	SINTHA	SINDEP	RDNT	PSRTE	FTEMP	FILMSP	FSPAT	G	M	Z
-1.395	0.0	0.6889892E-18	23032.	0.05420	0.21709	15.872	-11.574	548.917	299.99	1.82979	-418.56	3032.25	0.0
-1.055	0.0	0.1933303E-14	23027.	0.04664	0.21714	14.504	-11.574	522.352	299.99	1.74124	-316.34	3027.06	102.35
-0.714	0.0	0.1480098E-17	23025.	0.04513	0.21718	13.215	-11.574	495.770	299.99	1.65263	-214.12	3022.34	204.68
-0.373	0.0	0.2007549E-13	23014.	0.04050	0.21722	11.885	-11.574	469.173	299.99	1.56397	-111.90	3018.05	306.99
-0.032	0.0	0.0471323E-12	23010.	0.03600	0.21726	10.554	-11.574	442.561	299.99	1.47520	-9.68	3014.23	409.28
0.308	0.0	0.5105444E-14	23011.	0.03150	0.21729	9.223	-11.574	415.937	299.99	1.38651	92.55	3010.87	511.55
0.640	0.0	0.3842045E-13	23008.	0.02695	0.21732	7.892	-11.574	389.302	299.99	1.29772	194.77	3007.05	613.81
0.980	0.0	0.7091451E-12	23005.	0.02240	0.21734	6.559	-11.574	362.658	299.99	1.20891	296.99	3005.48	716.05
1.331	0.0	0.8340257E-11	23002.	0.01785	0.21736	5.227	-11.574	336.006	299.99	1.12066	399.21	3003.48	818.28
1.672	0.0	0.7720146E-11	23002.	0.01330	0.21737	3.894	-11.574	309.348	299.99	1.03120	501.43	3001.93	920.49
2.012	0.0	0.1002119E-10	23001.	0.00870	0.21738	2.561	-11.574	282.685	299.99	0.94232	603.65	3000.82	1022.70
2.353	0.0	0.7750355E-11	23000.	0.00410	0.21739	1.227	-11.574	256.019	299.99	0.85345	705.68	3000.18	1124.89
2.694	0.0	0.5422240E-11	23000.	-0.00034	0.21739	-0.106	-11.574	229.352	299.99	0.76454	808.10	2999.99	1227.08
3.035	0.0	0.3225803E-12	23000.	-0.00042	0.21739	-1.439	-11.574	202.685	299.99	0.67564	910.32	3000.25	1329.27
3.375	0.0	0.5983788E-13	23001.	-0.00047	0.21738	-2.773	-11.574	176.019	299.99	0.58675	1012.54	3000.97	1431.44
3.716	0.0	0.2122171E-14	23002.	-0.01402	0.21737	-4.106	-11.574	149.057	299.99	0.49748	1114.76	3002.74	1533.62
4.057	0.0	0.0419435E-14	23004.	-0.01857	0.21736	-5.439	-11.574	122.266	299.99	0.40901	1216.98	3003.77	1635.79
4.398	0.0	0.2104505E-13	23004.	-0.02312	0.21734	-6.771	-11.574	95.534	299.99	0.32018	1319.21	3005.85	1737.97
4.738	0.0	0.1494465E-13	23008.	-0.02767	0.21731	-8.103	-11.574	68.790	299.99	0.23136	1421.43	3008.38	1840.14
5.079	0.0	0.1956833E-14	23011.	-0.03222	0.21728	-9.442	-11.574	42.773	299.99	0.14258	1523.65	3011.37	1942.32
5.420	0.0	0.6995055E-14	23015.	-0.03677	0.21725	-10.746	-11.574	16.150	299.99	0.05384	1625.87	3014.81	2044.51

DOPPLER HISTORY FOR TARGET 3:

T	RQDI	AMPLITUDE	R	SINTHA	SINDEP	RDNT	PSRTE	FTEMP	FILMSP	FSPAT	G	M	Z
-1.020	0.0	0.6232197E-18	21020.	0.05420	0.21777	15.794	-11.574	547.346	299.99	1.82456	-307.08	1029.14	0.0
-0.710	0.0	0.7765723E-15	21020.	0.04964	0.21782	14.472	-11.574	520.912	299.99	1.73644	-214.21	1024.47	92.99
-0.404	0.0	0.5463058E-14	21020.	0.04513	0.21787	13.149	-11.574	494.461	299.99	1.64827	-121.34	1020.19	185.96
-0.105	0.0	0.7347910E-14	21016.	0.04050	0.21791	11.826	-11.574	467.995	299.99	1.56004	-28.47	1016.33	278.90
0.115	0.0	0.1468470E-14	21013.	0.03604	0.21795	10.502	-11.574	441.515	299.99	1.47177	64.40	1012.87	371.83
0.420	0.0	0.5039474E-13	21010.	0.03150	0.21798	9.178	-11.574	415.023	299.99	1.38346	157.27	1009.82	464.75
0.734	0.0	0.3471894E-13	21007.	0.02695	0.21801	7.852	-11.574	388.357	299.99	1.29511	250.10	1007.18	557.65
1.043	0.0	0.2502608E-12	21005.	0.02240	0.21804	6.527	-11.574	362.007	299.99	1.20674	343.01	1004.96	646.54
1.353	0.0	0.1218776E-11	21003.	0.01785	0.21806	5.201	-11.574	335.448	299.99	1.11833	435.87	1003.14	743.41
1.763	0.0	0.2751903E-11	21002.	0.01330	0.21808	3.874	-11.574	308.962	299.99	1.02991	528.70	1001.73	836.28
2.172	0.0	0.3566303E-11	21001.	0.00870	0.21809	2.548	-11.574	282.431	299.99	0.94147	621.61	1000.75	929.13
2.582	0.0	0.2762431E-11	21000.	0.00410	0.21809	1.221	-11.574	255.898	299.99	0.85302	710.44	1000.16	1021.98
2.991	0.0	0.1230725E-11	21000.	-0.00034	0.21810	-0.105	-11.574	229.363	299.99	0.76457	807.35	999.99	1124.82
3.401	0.0	0.2630090E-12	21000.	-0.00042	0.21809	-1.432	-11.574	202.826	299.99	0.67612	909.22	1000.22	1227.08
3.810	0.0	0.1513157E-13	21001.	-0.00047	0.21809	-2.759	-11.574	176.205	299.99	0.58747	993.09	1000.87	1300.48
4.220	0.0	0.6476851E-14	21002.	-0.01402	0.21807	-4.085	-11.574	149.765	299.99	0.49923	1085.96	1001.94	1393.31

results of azimuth processing are two items, FMBEAM and FMRATE, for each target which are FS at mid beam and linear fit slope of FS vs Z. These particular values are computed for no motion situations in which the aircraft flies perfectly. FMBEAM and FMRATE are then used by the impulse response calculations to form a standard filter to compress the actual doppler history observed under the prescribed motion of a simulation.

A complete listing of Type II inputs is shown at the top of Table IID. In this particular listing, the value - 0.69902160E-76 corresponds to a core constant, computer dependent, and a storage location which is not being used. For this example table only, three targets are being used but fifteen locations are reserved for each target oriented parameter.

Then a complete history of dopplers for every target along with a number of interesting parameters is printed. The following definition hold:

T	- time from beginning of run
VX	- aircraft velocity x direction
VY	- aircraft velocity Y direction
VZ	- aircraft velocity Z direction
R	- instantaneous slant range between target point and phase center of radar
SINTHA	- sin of actual squint angle to target
SINDEP	- sin of depression angle to target
RDOT	- Range rate or beam velocity (positive is closing)
PSRATE	- Phase shifter rate in ft/sec
FTEMP	- Temporal frequency of doppler in cycles/sec after phase shifting and clutterlock correction
FILMSP	- film speed in feet/sec.
FSPAT	- spatial frequency in cycles/ft.
G	- Azimuth position in feet
W	- Range position in feet
Z	- Position along doppler trace in feet

Due to target motion we note that RDOT and hence FSPAT for target 1 changes sign and FSPAT is not monotonically decreasing. Also FSPAT for target 1 is much lower than for target 2, the focus target. As a consequence target number 1 has no useable parts as indicated in Table IIC.

Following the doppler history print out, in Table IIF, we have the azimuth resolution table for the focus target and a summary of the best fit straight line which results from azimuth focusing. The range and rms resolutions which correspond, along with average values, are also given. Then a table of target positions G and W (direct from signal films), G1 and G2 (compensated for squint - intermediate), and U and V (compensated for depression - final film) are presented. Distortion ratios for each of these three output locations are then shown on the next page of print out.

For a quick look and for perspective orientation in smear and final location, the G and W positions (or alternatively the G1 and W1) positions can be plotted as shown in Table IIH. A scale in feet per row and feet per column (character position in a row) and a heading of run number and target information heads this print out. Numerals are then used to plot input target location with letters, correspondences shown by the list on the right side, to show image locations. Multiple letters like BB indicate how much azimuth smear has occurred.

Finally, the last page of print out contains a summary by run number of the specific parameters, Type II, used in each run.

Table III shows an alternative in output. In this particular case, amplitude of target return and the roll rate history of the target were selected for output. Amplitude is in watts. No target motion was allowed for this table and as a consequence the entire synthetic aperture for each target makes up a useable part. For the param line, Table 4A, LNEWP = F will stop the program with \$END, LSIG = T will cause a new signal film to be generated, and LAMPR = F signifies that no new target patterns are to be read in. Actually LAMPR was set true with Type I input, then it is automatically set false before Type II inputs begin. Hence, LAMPR = F in the params line is redundant.

#### 6.6 Conclusions

With respect to the RSMOD model, all of the goals set out in SAR DIGITAL Simulation Program Plan have been reached. Compilation of the entire computer model is essentially complete. All but the final checking and linking together is done. With the exception of chirp, chirp processing and the MTF functions all RSMOD functions have been used to obtain inputs for the impulse response calculations.

There are two omissions in the presently coded program. First a function and a call statement are required to realize

the effect of a video amplifier. This omission can be easily fixed since the RF-Amplifier, which is coded, is almost identical to the video amplifier representation. Secondly, the signal recorder in the present version does not contain a transfer function to attenuate signal strengths according to the input of a characteristic function. For example, a characteristic function is required in an optical recorder representation whenever a signal level (volts) is transformed into light intensity on the face of a CRT or when this intensity is transformed by a film characteristic into a gray scale on the film. A mathematical representation of each of these functions, amplifier or characteristic function, is available but neither have been coded into the program. Each of the characteristic functions can be input as a table obtained from calibration experiments or from equipment specifications.

## 7. IMPULSE RESPONSE GENERATION

### 7.1 Introduction

A major item within the scope of the SAR Image Quality Analysis program is the development of a digital computer model of a SAR radar system which is to be utilized for determining the effects of radar parameter variation on image quality. The model has been constructed so as to determine the response of an airborne SAR system in the presence of realistic errors (e.g., imperfect motion compensation, transmitter chirp nonlinearities) under actual aerodynamic flight conditions characteristic of high performance aircraft. An assessment of image quality is to be obtained in part by an analysis of the response of this model to point target inputs (i.e., the impulse response). This section will describe the software module which has been developed to accept SAR simulation outputs and produce an actual point target image. At present, the model is one-dimensional and is capable of processing either in azimuth or range. Extensions to two-dimensional processing is straightforward and could be implemented.

### 7.2 Theory of Operation

The SAR model is designed to be a "high-fidelity" digital simulation of a side-looking, chirp-pulsed, synthetic aperture radar. In either the range or azimuth direction, and under the usual far-field assumptions, the signal pulse returned from a point target is essentially of the form

$$r(x) = a(x-x_0) \cos (\phi(x-x_0)) \quad (7-1)$$

where,

$$\phi(x) = \omega_0 x - \alpha x^2 \quad (7-2)$$

and  $\alpha$  is a parameter proportional to the linear FM rate of the pulse. For azimuth processing  $\alpha$  is proportional to  $1/\lambda R$  where  $\lambda$  is the radar wavelength and  $R$  is the point target range. For range processing,  $\alpha/2$  is equivalent to the FM rate of the chirp pulse. The term,  $\omega_0$ , is the mid-band frequency of the chirped pulse in the range processing case, or is the doppler offset caused by antenna squint in the azimuth case. The processing required in both cases is identical so that the software described in this section is applicable to processing of either azimuth or range data. The variable  $x$  in the above equations can refer to time, slant-range distance, or film spatial coordinates, depending upon the scale factor inherent in  $x$ . Presently the variable used in the impulse response programs refers to slant range distance. The constant,  $x_0$ , represents the target position. The amplitude term,  $a(x)$ , is a function of antenna pattern and target cross-section and presently is assumed to be a real quantity.

The processing of pulses of the form (7-1) into point target images can be accomplished by a matched filtering operation. That is, the signal in (7-1) is

input to a linear, time-invariant system whose impulse response is given by  $h(x) = \bar{r}(-x)$ , where to bar ( $\bar{\phantom{x}}$ ) indicates a complex conjugate operation.

The resulting image is represented as

$$g(x) = r(x) * h(x) = \int_{-\infty}^{\infty} r(\tau) h(x-\tau) d\tau. \quad (7-3)$$

The operation given in (7-3) is most often performed in an optical analog fashion, but may be performed digitally as in the present model. There is generally a finite aperture over which the convolution can take place, such that  $g(x)$  is more correctly given as

$$g(x) = \int_{-\infty}^{\infty} r(\tau) h(x-\tau) \text{rect} \left( \frac{x-\tau + x_0}{L} \right) d\tau \quad (7-4)$$

Under realistic operating conditions, system errors introduce undesirable perturbations into the ideal received signal as given in (7-1). Thus, instead of processing  $r(x)$  one must work with a signal represented as

$$r'(x) = a'(x-x_0) \cos (\phi'(x-x_0)) \quad (7-5)$$

which is at best only an approximation to the signal given in (7-1). It is an analysis of the resultant signal,



$$g'(x) = r'(x) * h(x) \quad (7-6)$$

that will produce an assessment of image quality. To generate  $g'(x)$  one must therefore: 1) simulate the SAR system in order to generate artificially  $r'(x)$ ; 2) generate analytically an appropriate  $h(x)$ ; and 3) perform the convolution operation. Each of these tasks will be discussed in detail in relation to the current SAR simulation program.

7.2.1 Received Signal Generation. The SAR simulation package (RSMOD) is structured so as to provide a set of equal-time samples of  $a'(x)$  and of  $\phi'(x)$ , where  $\phi'(x)$  represents the instantaneous frequency of the returned pulse. Due to the possible presence of motion errors there may no longer be a one-one correspondence between time and spatial coordinates. Therefore a spatial coordinate value is supplied with each equal-time sample of signal amplitude and frequency. Knowledge of the sample values and their spatial positions allows one to apply interpolation techniques to obtain equidistant amplitude - frequency samples. Only equidistant samples can be efficiently processed in the digital environment. In addition, the interpolation step gives one the opportunity to generate a sufficient number of samples to satisfy the Nyquist sampling criterion for the  $r'(x)$  pulse to be generated (# samples  $> 2 \cdot \text{TBP}$  of the pulse, where TBP equals the duration of the pulse times its bandwidth.) The

simulation program can supply far fewer samples of  $a'(x)$  and  $\phi'(x)$  than are required to represent  $r'(x)$ , since generally  $a'(x)$  and  $\phi'(x)$  vary slowly with respect to  $x$  compared to  $r'(x)$ , which can be a relatively high frequency pulse.

A Chebyshev interpolation scheme has been chosen for this application. Let  $f(x_1), f(x_2) \dots, f(x_n)$  be samples (not necessarily equidistant) of  $f(x)$ , where  $f(x)$  could represent either  $a'(x)$  or  $\phi'(x)$ . The problem is to determine the coefficients of the polynomial

$$p(x) = \sum_{i=1}^n c_i x^{i-1}, \quad (7-7)$$

such that

$$\sum_{i=1}^n (f(x_i) - p(x_i))^2 = \text{minimum} \quad (7-8)$$

Once the coefficients  $c_i, i=1, \dots, n$  are found one can produce as many equidistant samples of  $p(x)$  as desired simply by evaluating the polynomial.

A Chebyshev interpolation involves expansion of the polynomial  $p(x)$  in terms of its Chebyshev expansion. The Chebyshev expansion of  $p(x)$  gives a much better indication of the accuracy of the curve fit than the coefficient vector of the polynomial itself. If the specified degree of the polynomial is too

high, the last terms of the Chebyshev expansion will be uniformly small compared to lower degree coefficients. The degree may be reduced by the number of small trailing coefficients without unduly enlarging the overall error. This possibility is checked for automatically by the present interpolation program. The reader is referred to the IBM System/360 Scientific Subroutine Package Programmer's Manual for further details concerning the interpolation scheme. The subroutines APCH and APFS, are used by the subroutine SFIT to generate the Chebyshev coefficients. The subroutine named CNPS is used to evaluate the polynomial  $p(x)$  to obtain the new function values.

Following the interpolation procedure one has  $M$  equidistant samples of  $a'(x)$  and  $\phi'(x)$  with which to generate  $M$  samples of

$$r'(x) = a'(x) \cos (\phi'(x)). \quad (7-9)$$

That is, the values

$$a'(k\Delta x), \quad k = 1, \dots, M$$

and

$$\phi'(k\Delta x), \quad k = 1, \dots, M$$

are stored in computer memory for use in generating the received signal,  $r'(x)$ . Obviously one requires a method of generating samples of  $\phi'(x)$  given samples of  $\dot{\phi}'(x)$ . Recall the fundamental theorem of calculus. If  $f(x)$  is continuous for  $a \leq x \leq b$ , and if  $F(x)$  is any anti-derivative of  $f(x)$  on this interval (i.e.,  $\dot{F}(x) = f(x)$  for  $a \leq x \leq b$ ), then

$$\int_a^b f(x) dx = \left[ F(x) \right]_{x=a}^{x=b} = F(b) - F(a) \quad (7-10)$$

We can assume that  $\dot{\phi}'(x)$  is continuous over the interval of interest and that  $\phi'(x)$  is its anti-derivative on the interval (by definition). Therefore by the Fundamental Theorem,

$$\int_0^x \dot{\phi}'(y) dy = \phi'(x) - \phi'(0) \quad (7-11)$$

or rearranging,

$$\phi'(x) = \phi'(0) + \int_0^x \dot{\phi}'(y) dy. \quad (7-12)$$

In terms of digital quantities,

$$\phi'(k\Delta x) = A + \sum_{j=1}^k \dot{\phi}'(j\Delta x), \quad K = 1, \dots, M, \quad (7-13)$$

where  $A = \phi'(0)$ , or the phase of the signal immediately upon the target entering the beam. This constant is chosen such that the phase of the signal is zero at midbeam, and the reference signal (described later) is derived accordingly. Having produced  $\phi'(k\Delta x)$ ,  $k = 1, \dots, M$  and using  $a'(k\Delta x)$  from the interpolation procedure, the received signal samples are generated as

$$r'(k\Delta x) = a'(k\Delta x) \cos(\phi'(k\Delta x)), \quad k=1, \dots, M. \quad (7-14)$$

The values of  $r'(k\Delta x)$  are equivalent to samples taken at equidistant intervals (and satisfying the Nyquist criterion) in the film or signal plane.

7.2.2 Reference Function Generation. The reference function refers to the impulse response of the linear time-invariant system used to compress the received pulses. In the present case it is of the form

$$h(x) = \exp\{j(\omega_0 x + \alpha x^2)\}. \quad (7-15)$$

A complex reference function is used so that the carrier ( $\omega_0$ ) inherent in the real received signal can be easily removed and to overcome problems caused by conjugate images. In the computer,  $h(x)$  (or rather  $h(k\Delta x)$ ) may be generated analytically with knowledge of  $\omega_0$  and  $\alpha$ . Several options have

been programmed as methods of choosing  $\omega_0$  and  $\alpha$ . They are: 1) Using the theoretically "correct"  $\omega_0$  and  $\alpha$  for each target. These values are entered into the subroutine as arguments and can be supplied by the user, or alternatively, calculated by the SAR simulation program itself. 2) Resorting to an autofocus mode whereby  $\omega_0$  and  $\alpha$  are estimated using the received doppler frequencies. 3) Using a previously generated reference function. In this case, the reference function used for compressing the previous target is just re-used, thereby reducing the amount of processing time required. A user must be cautious if relying upon this third option in ensuring that the reference function is the correct one. For instance, if one is azimuth processing, then only a string of targets of constant range can be processed with the same reference function since  $\alpha$  is a function of range for azimuth processing.

Processing option number two above requires additional explanation. In this case an estimate must be made of  $\omega_0$  and  $\alpha$  using the received samples,  $\phi'(k\Delta x)$ . The estimated midbeam frequency  $\omega_0$  is simply set equal to the time sample of  $\phi'(x)$  which comes nearest to the midbeam position. An estimate of  $\alpha$ , denoted  $\hat{\alpha}$ , is generated using the 1st order Chebyshev coefficient derived in the interpolation process. The resultant FM rate,  $\frac{\hat{\alpha}}{2}$ , is equivalent to a least-squares estimate of the FM rate of the incoming pulse. In this manner the system tends to optimize the match between

$r'(x)$  and  $h(x)$ , thus optimizing the focus for each target it processes. Since the estimates  $\hat{\omega}_0$  and  $\hat{\alpha}$  are already by-products of the interpolation process the autofocus option requires no additional computation time over that required for the theoretically "correct" focus option.

7.2.3 Performing the Convolution. The convolution required to compress the SAR signals must be performed digitally. The form of the operation originally given by (7-3) is thus of the form

$$g(k\Delta x) = \sum_{i=-\infty}^{\infty} r'(i\Delta x)h((k-i)\Delta x), \quad (7-16)$$

where it is assumed that  $r'(k\Delta x)$  and  $h(k\Delta x)$  are both zero for  $k < 1$  and  $K > M$ . The number of computations involved in performing the discrete convolution of (7-16) can be significantly reduced by use of the Fast Fourier Transform (FFT) algorithm. The steps required in this process are listed as follows:

- 1) Pad at least M zeros onto the ends of the arrays containing  $r'(k\Delta x)$  and  $h(k\Delta x)$  to insure that an aperiodic convolution will take place.
- 2) Take the Discrete Fourier Transform (DFT) of the padded signals  $r'(k\Delta x)$  and  $h(k\Delta x)$  using the FFT algorithm to save computation steps. Denote the transformed data as  $R'(k\Delta f)$  and  $H(k\Delta f)$ , respectively.

3) Multiply  $R'(k\Delta f)$  by  $H(k\Delta f)$  on a point-by-point basis,

$k=1, \dots, M$ .

4) Compute the inverse DFT of the product  $R'(k\Delta f) \cdot H(k\Delta f)$ .

This yields the desired convolution output.

Step 1) above is required since multiplication of DFTs corresponds to convolution of periodic functions, not aperiodic ones. A convolution of periodic functions can also be regarded as a circular convolution in which values of the kernel that are shifted from one end of a period are circulated into the other end, thus introducing what has been termed interperiod interference. By the proper padding with zeros a periodic convolution can be used to compute an aperiodic convolution. This is done by adding to each cycle of both functions a string of zero values of sufficient width to provide a kind of "grace band" during which the interperiod interference assumes zero numerical value.

In performing step 2) some computation time can be saved due to the fact that  $r'(k\Delta x)$  is a real valued function. Transforming of a real array of length  $2M$  can be accomplished by transforming a complex array of length  $M$  and then rearranging the resulting array. The point-by-point multiplication of step 3) is then accomplished by multiplying the positive frequency terms of  $H(k\Delta f)$  by the terms of  $R'(k\Delta f)$  and setting the remaining terms of the product equal to zero. This procedure follows from tacitly



assuming that the spectrum of  $h(k\Delta x)$  contains no negative frequency energy. Thus the present algorithm assumes the sufficient azimuth offset case whereby non-positive frequencies are absent. This procedure can be easily modified to account for negative frequencies. The presence of the non-positive frequency spectrum would create conjugate images and D.C. term interference in the current processing operation. In any case, step 4) is a straightforward complex transform operation.

Ideal system performance occurs when the reference function is perfectly matched to the incoming pulse, as is the case when  $h(x) = \bar{r}(-x)$ . In this case  $H(k\Delta f) = \bar{R}(k\Delta f)$ , the conjugate of  $R(k\Delta f)$ . Therefore, for a given reference function, the ideal system response can be obtained by multiplying  $H(k\Delta f)$  by its conjugate and then inverse transforming the result. This procedure is included in the present system as a user option. If the user specifies the use of this option, the program derives the ideal system response for the reference function of every target response generated.

The data generated by the point target response software is utilized primarily in two ways; visual display and digital analysis. For a visual assessment Calcomp and computer printer plots are produced of signal frequency, signal phase, signal recording (zone plate section), reference phase, and target response. Target response may be displayed as an

amplitude plot, a logarithm of intensity plot, or an expanded log-intensity plot. Ideal target response can be generated and displayed in an identical fashion. Digital analysis of the point target response is to be performed via the Modulation Transfer Function (MTF). To this end the MTF is generated and returned to the calling program in an auxiliary array. The MTF is the modulus of the Fourier transform of the point target intensity response. After multiplication of  $R'(k\Delta f)$  and  $H(k\Delta f)$  one has DFT of amplitude response. Therefore, one must take an inverse FFT to get amplitude response, square the resultant data, and then perform one additional FFT.

All of the processing and display options mentioned above are controlled by the user (calling program) through the control parameters in the argument list. The impulse response software package (IRMOD) is in the form of a subroutine which may be called by the simulation package (RSMOD). In addition, through the use of special purpose interface programs, the impulse response package can be operated offline. The next section will describe the software in detail.

### 7.3 Target Response Software Description

Table IV lists and identifies the arguments passed to and/or received from subroutine PROCES, the primary subroutine making up IRMOD. Appendix A contains a detailed flow diagram of subroutine PROCES.

TABLE IV  
SUBROUTINE PROCES ARGUMENT LIST

ARGUMENT	FUNCTIONAL DESCRIPTION
XPOINT	A real*4 array containing the spatial positions of the doppler history samples.
FREQU	A real*4 array containing the doppler frequency of each of the doppler history samples.
AMPL	A real*4 array containing the amplitude of each of the doppler history samples.
NPTS	An integer*4 location containing the number of doppler history samples and hence the number of elements in each of the three doppler sample arrays. NPTS must be $\leq 21$ at present.
IPOW	An integer*4 location containing the power with which to attempt the Chebyshev curve fitting procedure. IPOW must be less than or equal to 10.
NPEXP	An integer*4 location containing an exponent of two and describing the number of samples to be generated within the digital processing aperture. The number of samples is equal to $2^{**}NPEXP$ .
IOCNL	An integer*4 location containing all option specifications in coded form. Currently the 13 least significant bits represent I/O and/or processing options. A one in a given bit location indicates that the associated option is to be in effect. The following is a list of control bit assignments, beginning with the least significant bit and progressing toward the most significant bit:

TABLE IV (Continued)

ARGUMENT	FUNCTIONAL DESCRIPTION
	<p>(LSB)</p> <ol style="list-style-type: none"> <li>1) set for obtaining a listing of all original doppler samples, and all Chebyshev interpolation coefficients.</li> <li>2) set if all computer printer plots are to be Calcomp plotted also</li> <li>3) set to obtain a plot of interpolated signal amplitude</li> <li>4) set to obtain a plot of interpolated signal frequencies. (doppler history)</li> <li>5) set to obtain a plot of the signal phase (the integral of frequency)</li> <li>6) set to obtain a plot of the signal itself (zone plate section)</li> <li>7) set to obtain a plot of the reference signal phase.</li> <li>8) set to obtain a plot of the point target amplitude response</li> <li>9) set to obtain a plot of the logarithm of target intensity response. (truncated below -40 db and normalized to 0 db)</li> <li>10) set to obtain an expanded plot of the return above -40 db. (Log intensity)</li> </ol>

TABLE IV (Continued)

ARGUMENT	FUNCTIONAL DESCRIPTION
	<p>11) set to compute and obtain a plot of the ideal target amplitude response.</p> <p>12) set to obtain a plot of the logarithm of the ideal target intensity response.</p> <p>13) set to obtain an expanded plot of the ideal target log-intensity response.</p> <p>14) unused</p> <p>.</p> <p>.</p> <p>.</p> <p>LFOCUS =3 implies that the reference function generated for the previously processed target is to be used.</p>
FMBEAM	A real*4 location containing the user specified midbeam frequency to be used in reference function generation if the theoretically "correct" focus option is to be used. (i. e., if LFOCUS=1)
FMRATE	A real*4 location containing the user specified linear FM rate to be used in reference function generation if the theoretically "correct" focus option is to be used. (i. e., if LFOCUS=1)
RESP	A real*4 array area which, <u>upon return</u> , will contain the MTF of the point target response. The array must be of length 2**(NPEXP+1).

TABLE IV (Continued)

ARGUMENT	FUNCTIONAL DESCRIPTION
IER	An integer*4 location which, <u>upon return</u> , will contain an error indication. (i.e., if IER=2 the compression of the signal history is unsuccessful.)

Allowing the reader to use Table IV and the Appendix as guides this section will give an in-depth description of subroutine PROCES, the primary routine in IRMOD. The remaining subroutines are general purpose routines that are largely self-explanatory and will not be described further herein.

Upon entry into PROCES a set of program constants are initialized to correspond with the user specified digital aperture size (via NPEXP). Then the program checks to insure that the number of doppler history samples (NPTS) does not exceed 21, and that the specified power of the Chebyshev curve fit does not exceed 10. If either of these conditions occur an appropriate error message is printed and control is returned to the calling program with the error indicator set (IER=2). The next step is to decode the I/O control parameter. This is done by extracting each of the 13 bits used in IOCNTL and storing each bit for later reference in the 13 elements of the array IPLT. Next the Chebyshev curve fit power is stored temporarily in locations LPOW and MPOW. Thus, the value of the curve fit power for either the amplitude or frequency interpolation procedure can be modified later if the accuracy of the fit warrants it, without modifying the location (IPOW) passed to the routine by the user.

The program next performs the Chebyshev curve fitting procedure on the doppler frequency samples supplied by the calling program. The curve fit is done by subroutine SFIT, which returns the actual power of the fit, the Chebyshev coefficients, data scale and shift factors, and an error indicator. The scale and shift parameters (XD and XO) are used to modify the doppler sample positional data (XPOINT) such that the curve fit takes place on the new interpolated values. If the curve fit was unsuccessful (e.g., the required minimum error was not obtained) the error parameter will have the value "2" upon return and the subroutine PROCES will print an appropriate error message and return to the calling program.

Before performing a curve fit to the amplitude data the program checks to see if the amplitudes associated with the doppler history samples are uniform. If the amplitudes are all equal then the completed curve fitting procedure is bypassed and a logical variable named AMPCHK is set to true. Otherwise, a call to SFIT is made as in the frequency fit case and AMPCHK is set to false. The power of the amplitude fit and the associated coefficients are stored in separate locations than those used for the frequency curve fit. If the amplitude samples are all equal, their value is retained in location SAVE for later reference.



Next, the linear FM rate of the reference function is defaulted to that predicted by the 1st order Chebyshev (frequency fit) coefficient. Then, if LFOCUS=1 (theoretical focus) has been specified, the linear FM rate is reset to that value specified by the user via the argument FMRATE (see Table IV). (Note that the variable ALPHA represents one-half the FM rate.) The same procedure is followed for the reference function midbeam frequency, FMB. The midbeam frequency is first defaulted to the frequency of the time sample which occurs nearest the midbeam position, and, if LFOCUS=1 is reset to that value specified by the user via the subroutine argument list. Thus, the two parameters which specify the reference function, the linear FM rate and the midbeam frequency, are assigned according to the user specified focus option.

The program next enters a do-loop in which the interpolated equally spaced samples of frequency and amplitude are evaluated, the frequency is integrated to produce instantaneous phase, and the reference function values are generated -- all within the same loop. In addition, the values of the equally spaced sample positions are generated by adding the sample spacing to the previously generated sample position. Once the new sample position is known each time through the loop, that position is converted to the range -1, +1 using the scale and shift factors previously returned from SFIT (i.e., XD and XO). Using this converted positional value,

the frequency and, if required, the amplitude of each new sample are generated by calls to subroutine CNPS. (If logical variable AMPCHK=.TRUE., then the call to CNPS can be replaced by assigning the constant amplitude previously found for all samples.) The integration of the frequencies to obtain phase is accomplished by simply adding the new sample frequency to a total every time through the loop. This method is a reasonably accurate numerical integration technique since the doppler frequency curve is highly over-sampled with respect to its frequency content. If the user has specified that the previously generated reference function is to be used, (i.e., LFOCUS=3), the portion of the do-loop used for evaluating the instantaneous reference phase and the resultant complex reference function value is bypassed, thereby saving computation time and allowing the resident reference values to remain unaltered.

An additional do-loop is required to offset the signal phase such that the phase at midbeam is zero. Prior to the integration procedure one has no knowledge of the value of the integral at midbeam and thus must await the completion of the integration process to determine the required phase offset. The additional do-loop is used to subtract the required phase offset and to generate the resultant real signal values (zone plate samples).

The next section of the program prints the Chebyshev coefficients and lists the original doppler history samples if the print option has

been specified. A statement causing all interpolated quantities to be printed has been overridden at the time of this writing, due to the huge amount of data generated in high time-bandwidth product circumstances. Following the print section is a portion of the program responsible for generation of the printer and Calcomp plots of signal amplitude, doppler frequency, signal phase, zone plate section, and reference phase which have been requested by the user as I/O options.

The program is now prepared to perform the convolution required for target signature compression. To insure an aperiodic convolution zeros are padded onto the arrays containing the signal and reference function. (If LFOCUS=3 is specified, all references to the reference function are ignored.) Subroutine RHARM is used to Fourier transform the real valued signal. Subroutine HARM is used to transform the complex reference function array. The resultant two transforms are multiplied point by point, except that all negative frequencies are set to zero. (Setting the negative frequencies to zero insures complex processing and prohibits aliasing due to conjugate images being formed.) Taking the inverse transform results in the amplitude response of the simulated SAR to the point target excitation. The modulus of each point in this array is taken to produce a real response. Following this step the response is plotted either directly as an amplitude response, or as

a log-intensity plot, and/or as an expanded log intensity plot, as specified by the user.

The section of the subroutine PROCES which will generate the MTF and return it in a calling-program supplied array will follow next in the final version of PROCES. The exact interface requirements for the image quality assessment routines are not complete at this writing and thus the MTF code is not final. Basically the process will be to square the amplitude response and then take an additional FFT. The MTF is the modulus of the resulting transform.

The final portion of subroutine PROCES is dedicated to generating and plotting of the ideal system response (i.e., perfectly matched filter). If the user requests this option, the program proceeds to take the modulus of the reference function transform, filter out all negative frequencies to remove the conjugate image and then square all terms. An inverse transform (via HARM) results in the equivalent output of a perfectly matched filter. Plots are made of this ideal response according to user specifications. After this is complete control is returned to the calling program.

#### 7.4 Processing Examples

Examples of point target processing will be given in this section to illustrate the plot options currently offered and to demonstrate the ability of the overall model to determine the response of an airborne

SAR system in the presence of realistic errors and/or radar parameter variations. Preliminary plotting examples of each signal of interest to the user will be shown. Then, the results of simulated system flights will be reviewed which show the effects of motion-errors and antenna amplitude weighting patterns upon system response.

Plot Options - For any given target compression, the user has the option of obtaining any or all of eleven signal plots as listed below:

1. Signal amplitude vs. spatial position
2. Signal frequency vs. spatial position
3. Signal phase vs. spatial position
4. One-dimensional zone plate reconstruction
5. Reference function phase
6. Point target amplitude response
7. Point target log-intensity response (db)
8. Expanded log-intensity response (db)
9. Ideal system amplitude response
10. Log-intensity ideal system response (db)
11. Expanded log-intensity response (db)

Figure 23 is an example of a signal amplitude plot. The horizontal axis, which represents spatial position, is labeled in terms of slant range feet. Since the storage medium in the digital system is an imaginary

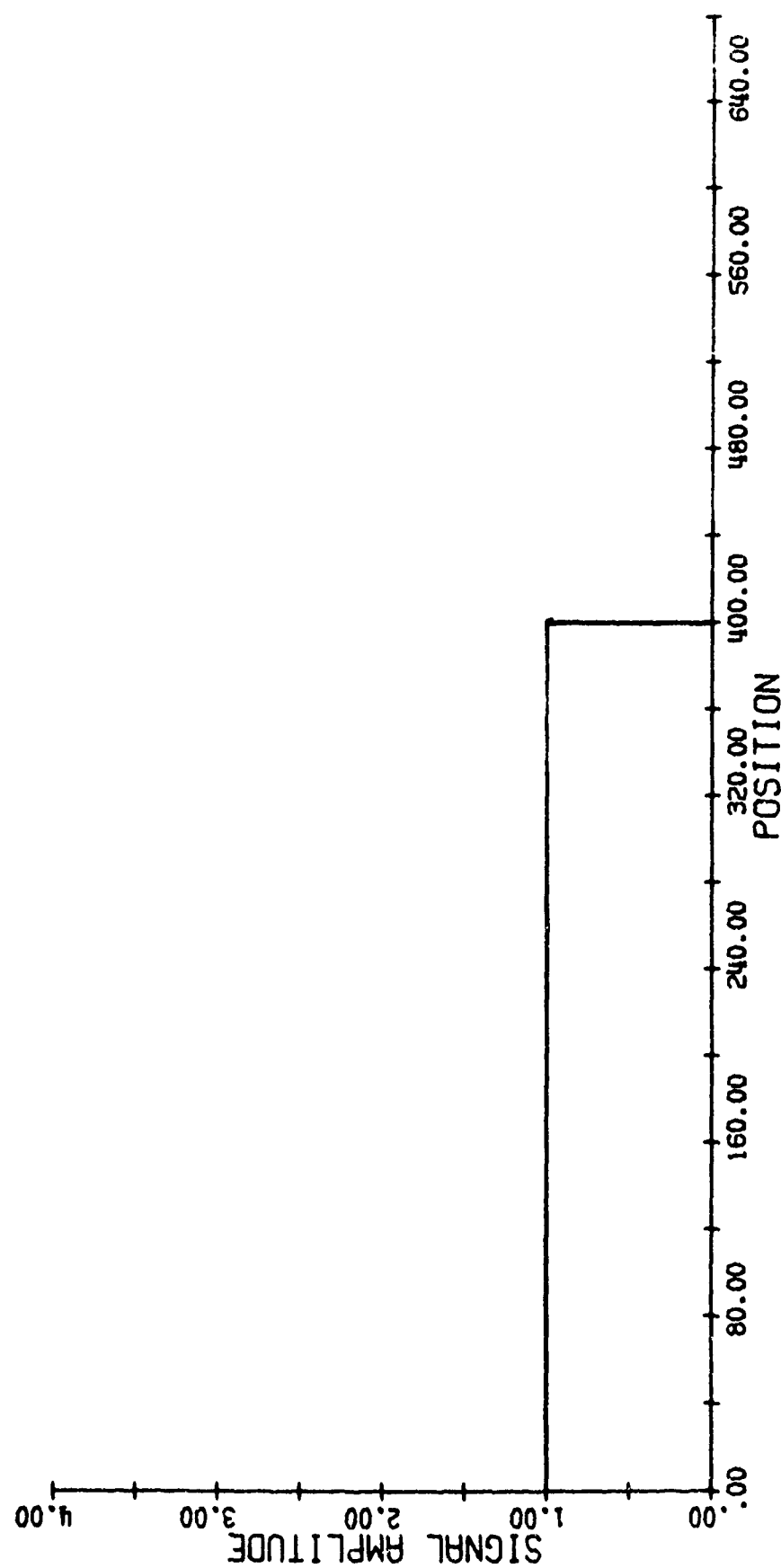


Figure 23. Signal Pulse Amplitude as a Function of Film Position

entity, it can be made as large as desired - in this case large enough such that the scale factor between storage distances and slant range distances is unity. The example shown in Fig. 23 represents the case where the beamwidth at the target range was 400 feet with unity gain over than interval. The target radar cross section also did not change with aspect angle such that a constant amplitude linear FM pulse is returned and recorded in memory.

Figure 24 represents an interpolated doppler history as produced by the model. Note that the frequency modulation is basically linear except for some perturbations near the end of the history due to target motion while in the beam. Note that in this example the beamwidth at the target range was 200 feet. The instantaneous signal phase resulting from integrating the frequency history of Fig. 24 is shown in Fig. 25. . Note that the phase has been automatically offset such that it is identically zero at the midbeam position. The frequency perturbations resulting from target motion cause the instantaneous phase to be only approximately quadratic. The signal pulse is formed by merely taking the cosine of the instantaneous signal phase. The resultant pulse may be thought of as a one-dimensional zone plate. The pulse associated with the instantaneous phase of Fig. 25 appears in Fig. 26. .

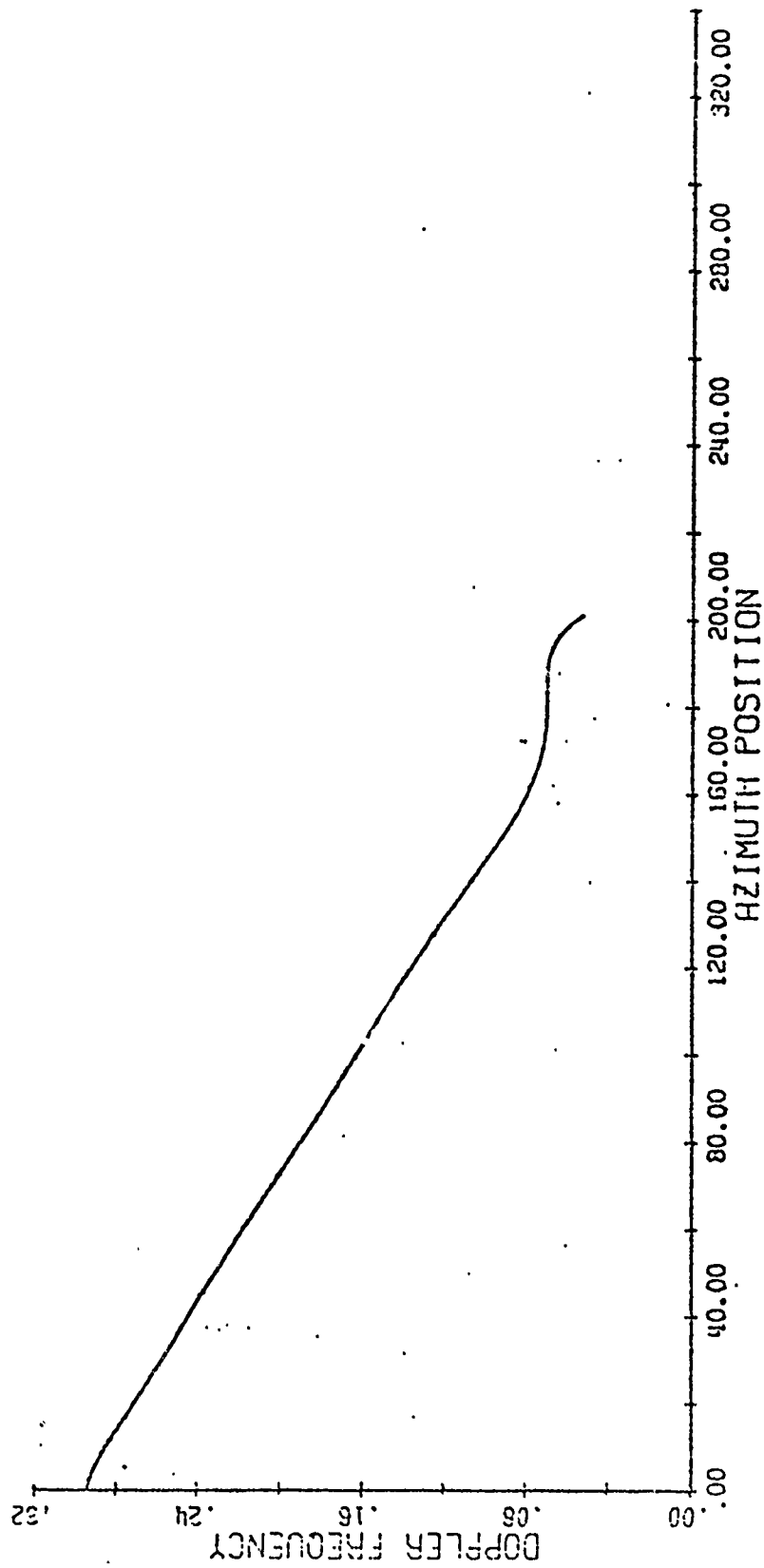


Figure 24. Doppler Frequency of Return as a Function of Azimuth Position. Nonlinearities are Due to Target Motion.



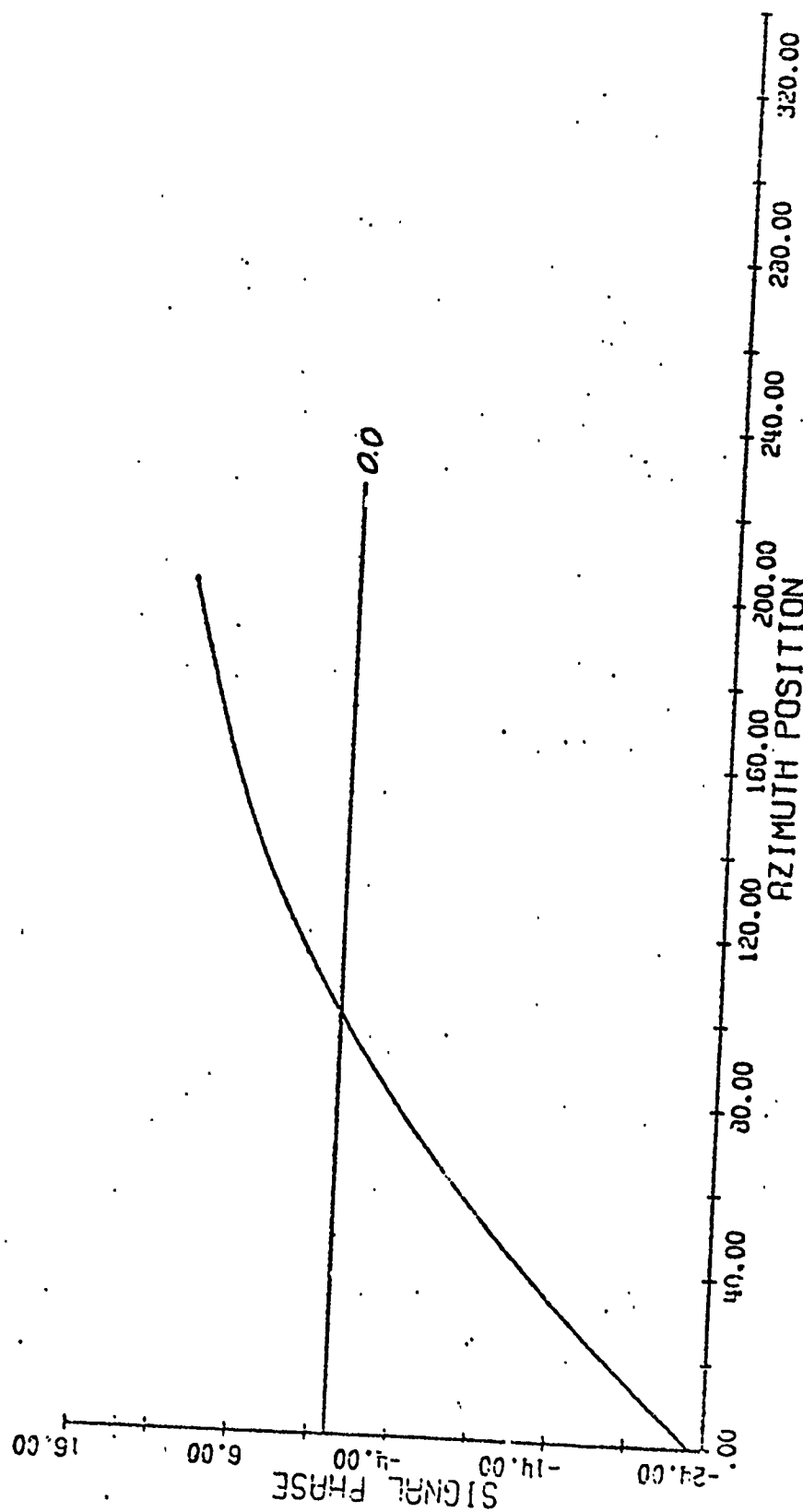


Figure 25. Signal Phase as a Function of Azimuth Position

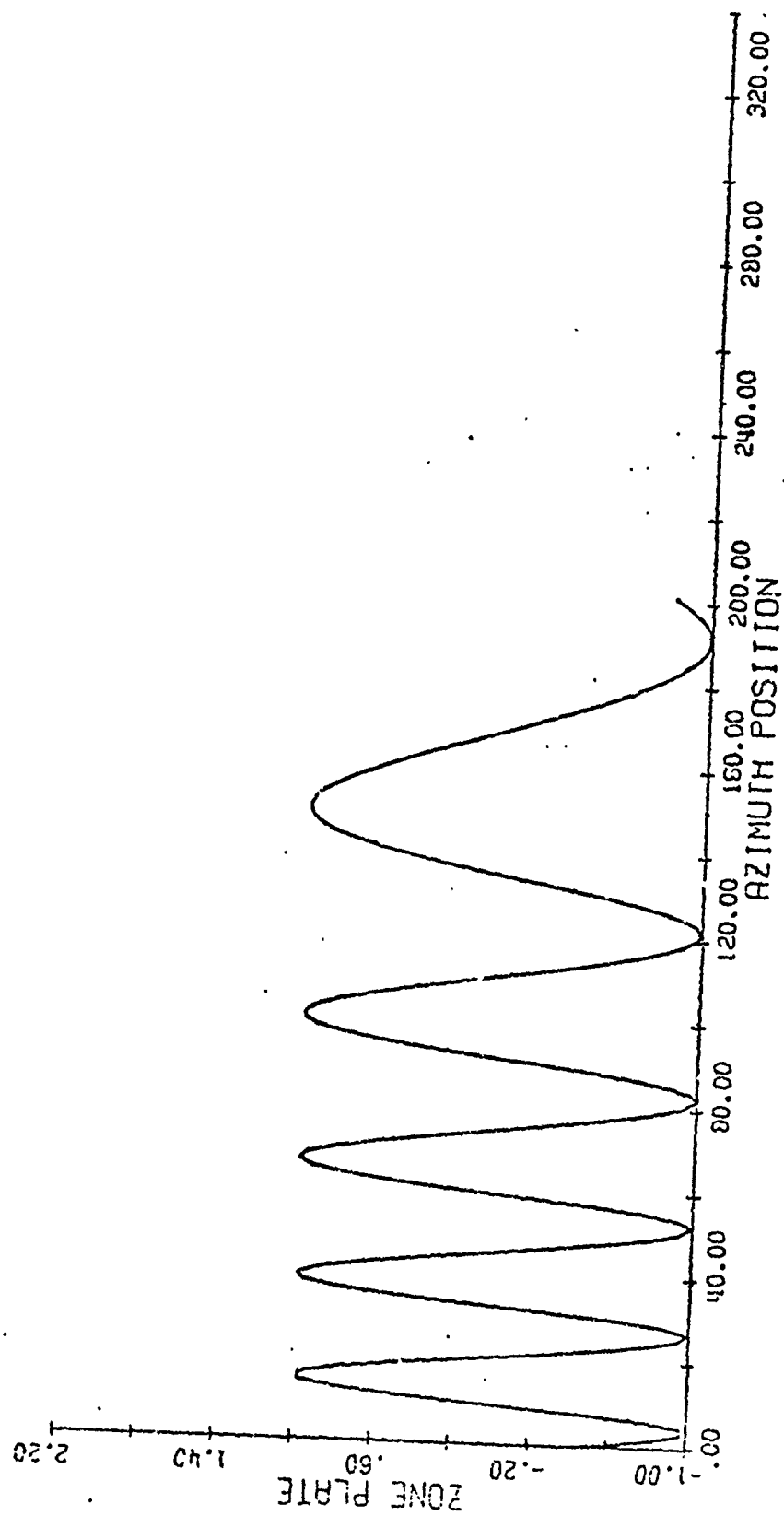


Figure 26. One-Dimensional Zone Plate Section Constructed Using Signal Phase.

The instantaneous phase of the reference function is analytically constructed as a quadratic as was described in the preceding section on theory of operation. The user may request that the reference phase be plotted. An example is the phase plot of Fig. 27, which is the reference phase associated with the signal phase of Fig. 25.

Convolution of the signal pulse and the reference function produces the desired point target response. Generally the resulting response has a  $(\sin x)/x$  appearance but may be non-symmetric and altered appreciably depending upon the system errors being modeled. Amplitude log-intensity, or expanded log-intensity plots may be requested by the user. For example, the amplitude of the target response associated with the signal pulse of Fig. 26 is plotted in Fig. 28.. Note the non-symmetry and offset from zero caused by the target motion. (Perfectly focused targets should be centered on the zero position.) For simulation of low resolution targets (low time-bandwidth product) the sidelobes of the response can be clearly seen in the normal amplitude or log-intensity plots ( $\text{log-intensity} = 10 \log_{10}$  of amplitude squared) but for high resolution targets the plots must be expanded in order to see the sidelobe shapes and levels clearly. As an example, consider the three plots appearing in Fig. 29. This illustration shows the three plot options as applied to a high resolution simulation. The top plot is an amplitude display

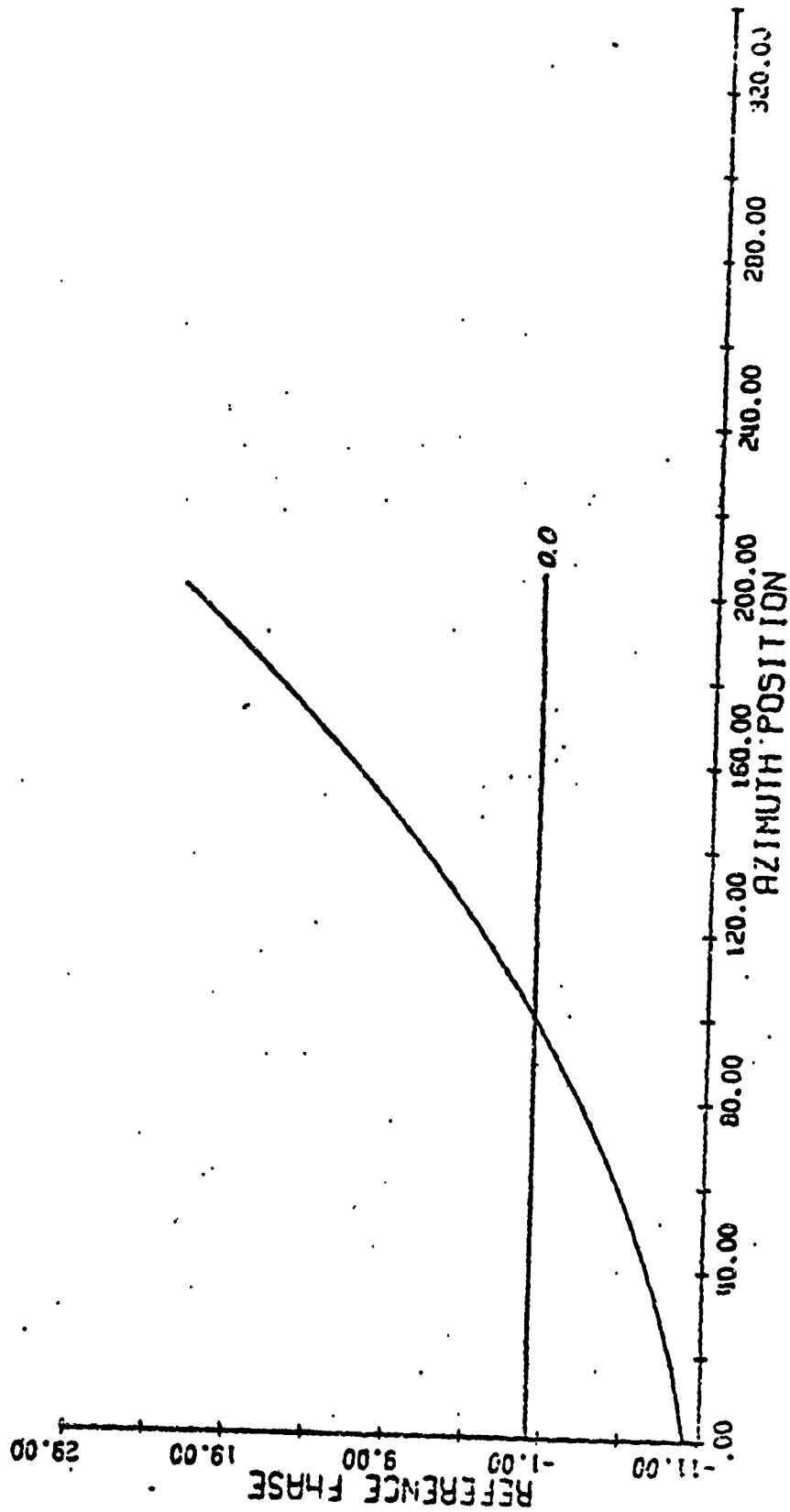


Figure 27. Quadratic Reference Phase as a Function of Azimuth Position.

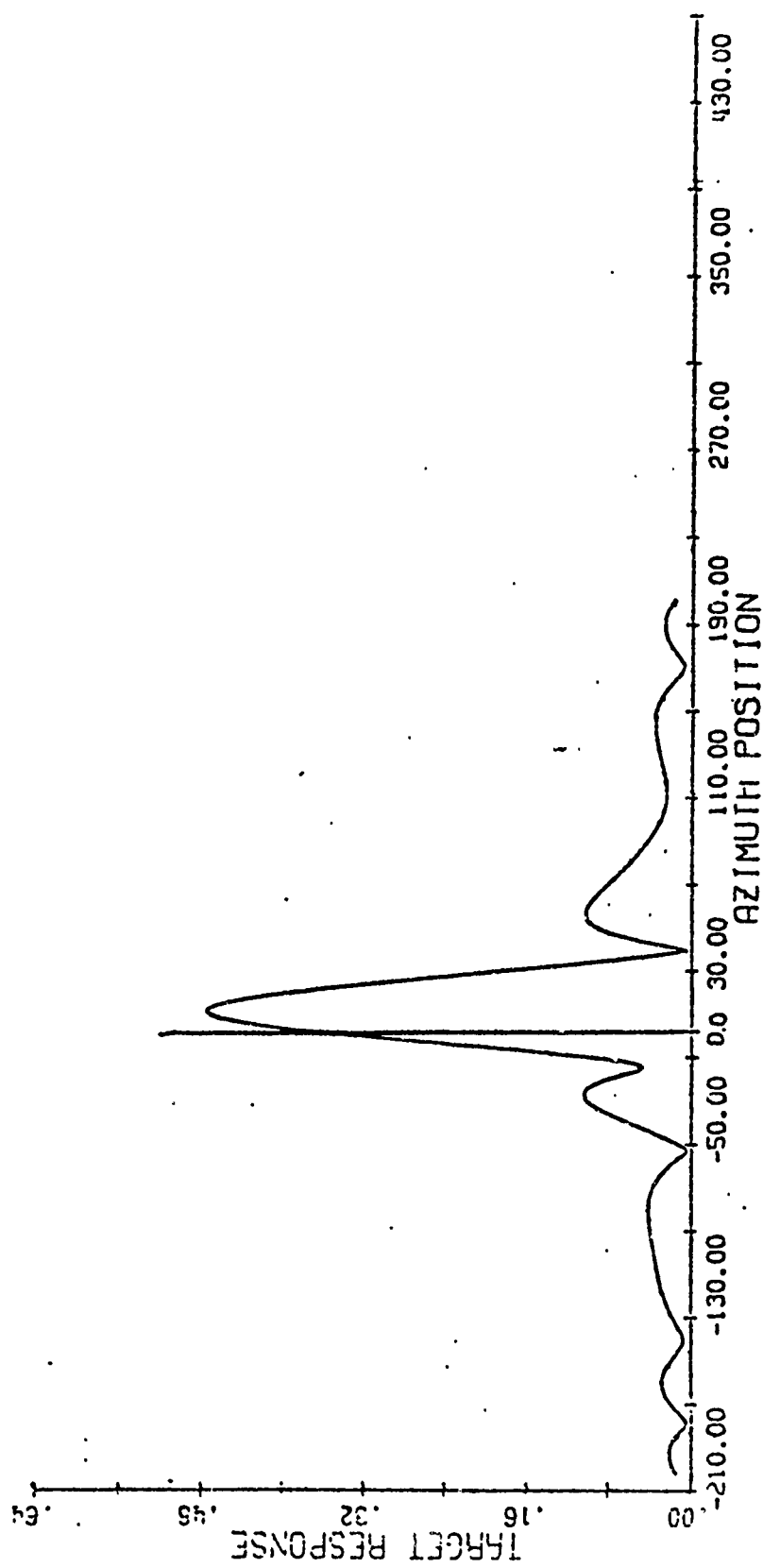


Figure 28. Point Target Response (0.0 Azimuth Position Represents True Target Location.)

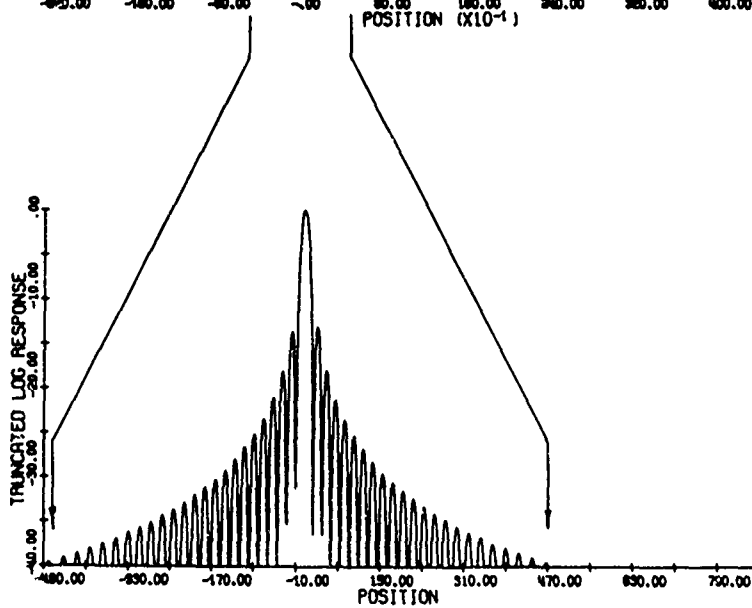
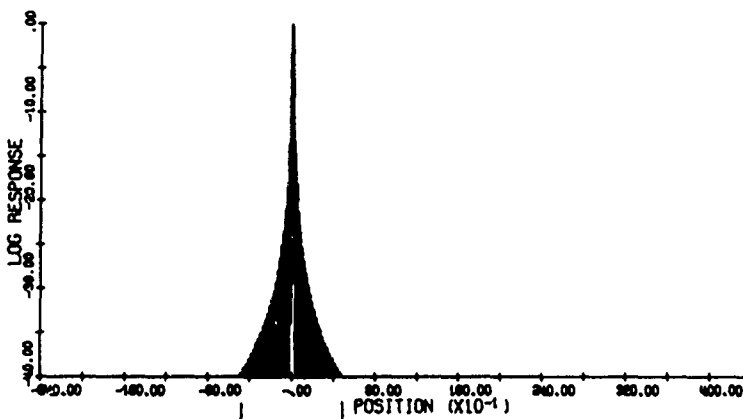
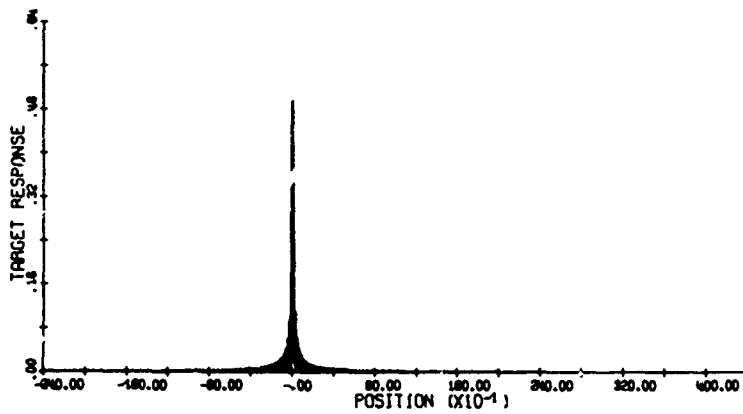


Figure 29. An Example of the Three Plot Options Associated with the Point Target Response

of point target response. The middle plot is simply  $10 \log_{10}$  of amplitude squared with all portions less than -40 db set to -40 db. Note that even in the log plot the sidelobes are still not clearly distinguishable. The bottom plot represents an expanded log plot (labeled "Truncated Log Response") in which those portions of the response greater than -40 db are expanded over the full plot width. The sidelobe levels and shapes become clearly discernable in the expanded plot. A note of caution is in order concerning the expanded log plots. Since only the portion of the response above -40 db is expanded over the plot range, the expansion factor (hence the x-axis scale factor) is thus a function of the response itself. Therefore, in comparing the expanded log plots of two or more point targets, one must pay special attention to the x-axis labeling such that the varying scale factor is taken into consideration.

The same three plot options mentioned above for the actual target response are also available for the idealized system response which the software is capable of generating as a byproduct of the signal compression. Characteristics of the ideal response is that it is always centered at and symmetric about the zero location. The idealized system response associated with the actual target response of Fig. 28 is shown as an amplitude response in Fig. 30.

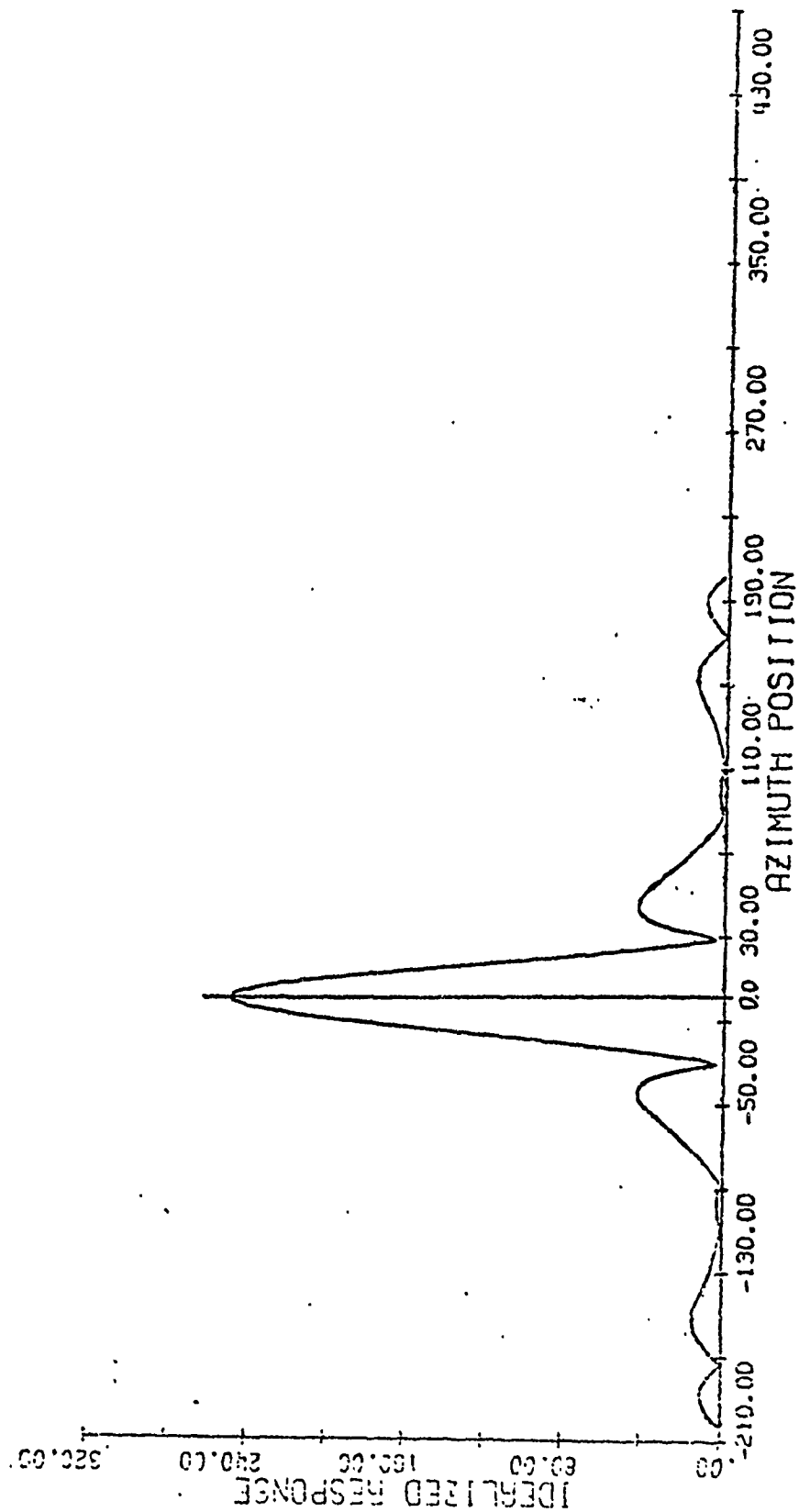


Figure 30. Idealized System Impulse Response

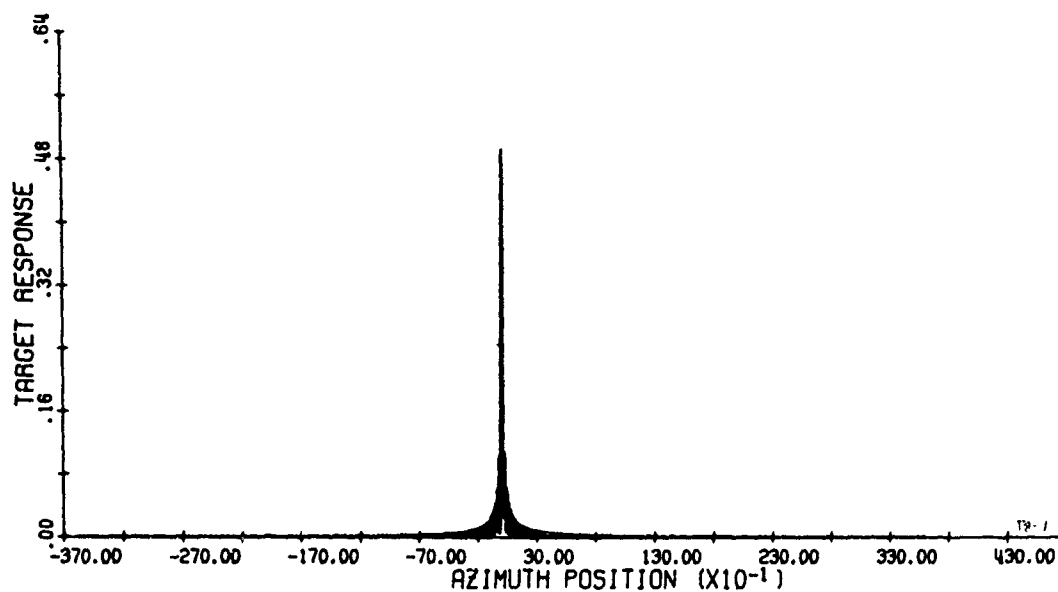


7.4.1 Demonstration of Motion Errors. A simulated flight was made to demonstrate that the model could indeed determine the effects of imperfect motion compensation. Two passes were made past an array made up of three targets; one each at far range, mid-range, and near range. On the first pass, the aircraft was modeled as flying a perfectly straight line at a constant velocity of 600 ft/sec at an altitude of approximately 40,000 feet. The second pass was made identical in every respect, except that a constant vertical acceleration of  $3.22 \text{ ft/sec}^2$  (0.1 g) was applied to the aircraft. During this second pass the simulated motion compensation system was instructed to correct for motion using the mid-range point as a reference.

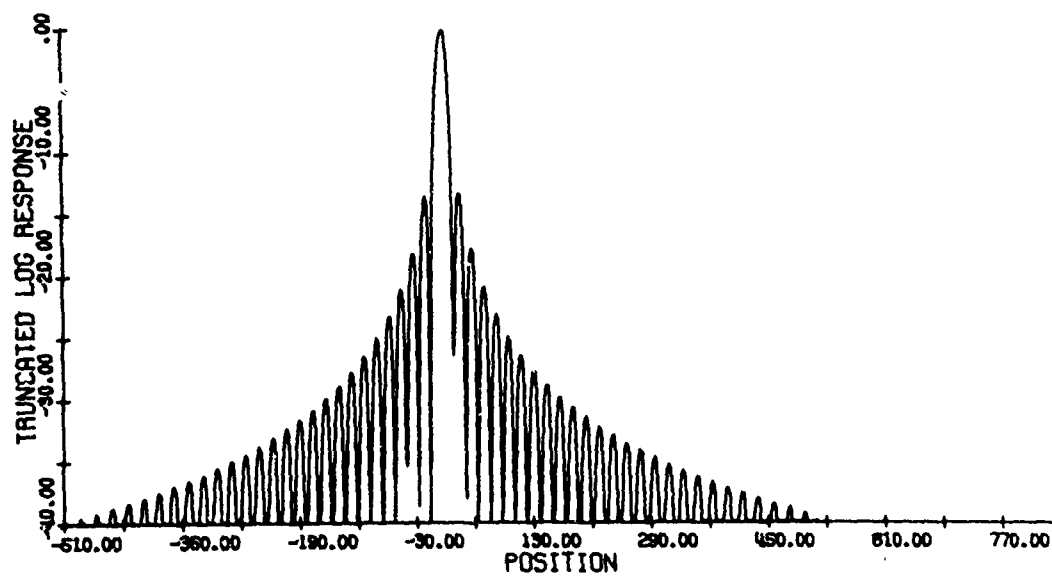
The beamwidth specified for this example was 0.02 radians. The mid-range target was at a ground range of 25 NM with the far and near range targets placed at plus and minus 5 NM from mid-range, respectively. The antenna was squinted forward 0.01 radians to provide an azimuth offset. Only azimuth processing was performed for this example. Under these conditions, the time-bandwidth product of the resulting doppler histories (azimuth TBP) was something over 1,000. To insure no aliasing problems 4096 digital signal samples were used. (Whereas, the number of samples required to satisfy the Nyquist criterion is twice the TBP.)

The no-motion azimuth responses for the far, mid, and near range targets are shown as amplitude and expanded log-intensity plots in Figs. 31, 32, and 33, respectively. In this example, unity signal amplitude was assigned to all signal returns, thereby ignoring the effects of antenna pattern and propagation attenuation. Thus, the magnitude of the far, mid, and near range responses are all identical. Note that for the no motion case the responses are for the most part symmetric, and all are situated at the zero spatial position, indicating that no target image position shift has occurred. For this example, the autofocus option was chosen as the focusing method.

The target responses for the case of a constant 0.1 g vertical aircraft acceleration are shown in Figs. 34, 35, and 36. Note that there is no significant change in the shape of target response for mid-range (Fig. 35) from that demonstrated for no motion error. This phenomena is as expected since the on-board motion compensation system was instructed to correct for motion with respect to the mid-range position. The compensation method specified was to correct for up-beam velocity and the compensation was to be ideal. That is, the aircraft navigation system was given the ability to exactly measure extraneous aircraft accelerations. Had the system been more realistically specified then the mid-range

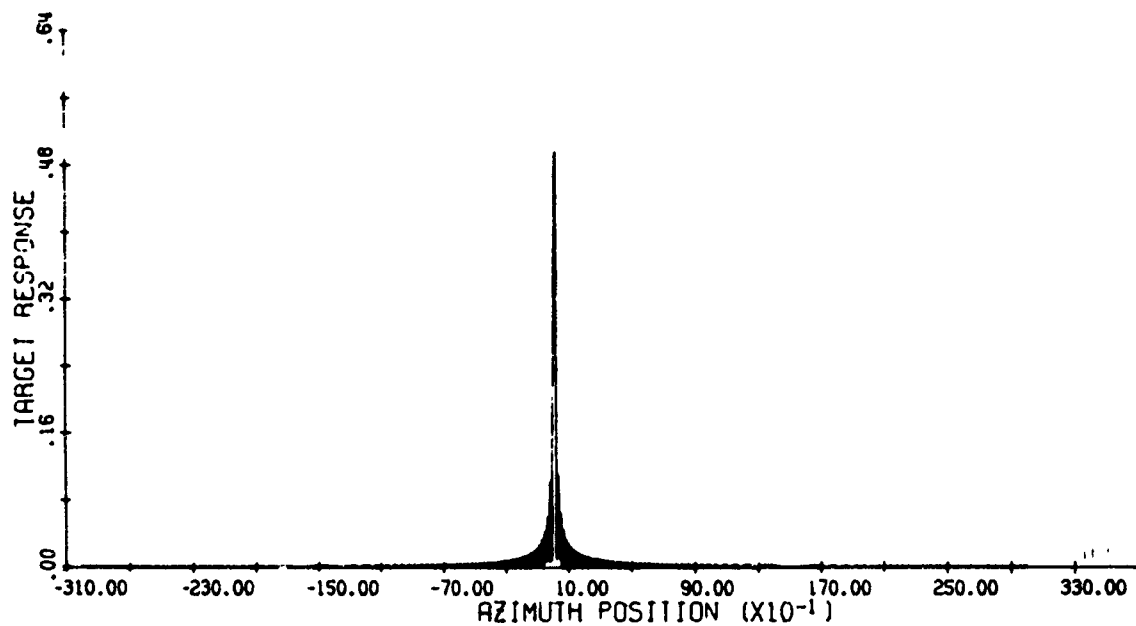


(a) Amplitude Response

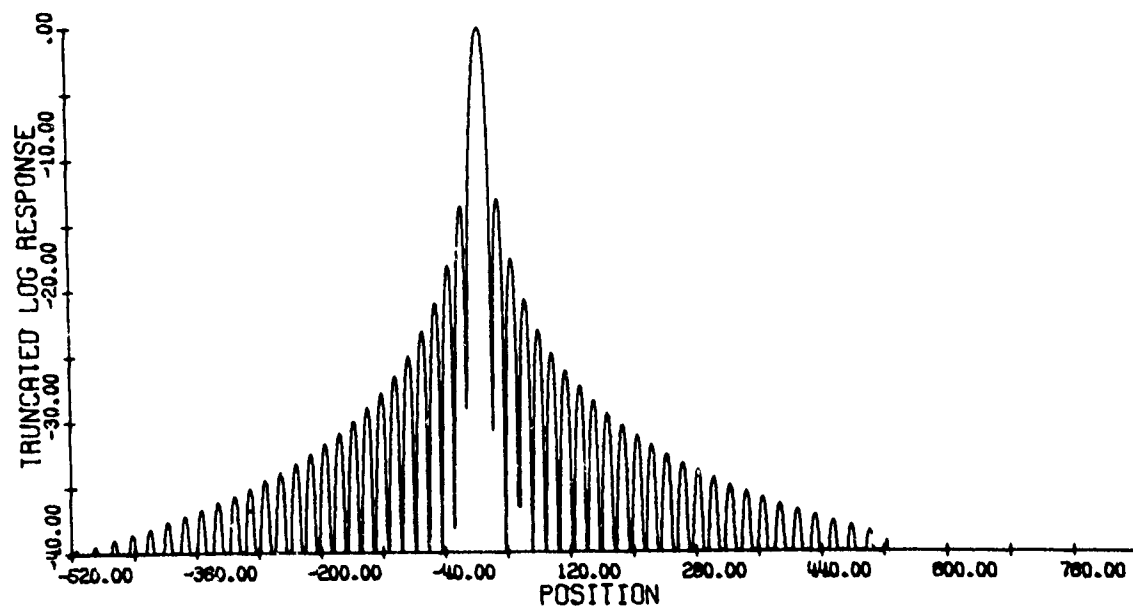


(b) Expanded Log-Intensity Response

Figure 31. Far Range, No Motion Point Target Response.

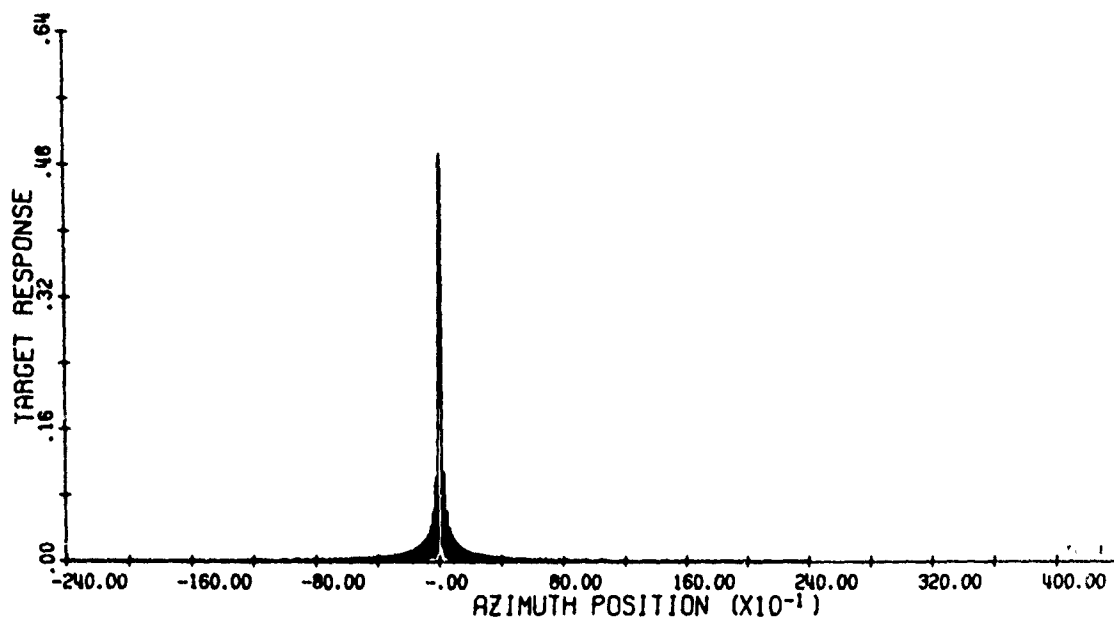


(a) Amplitude Response

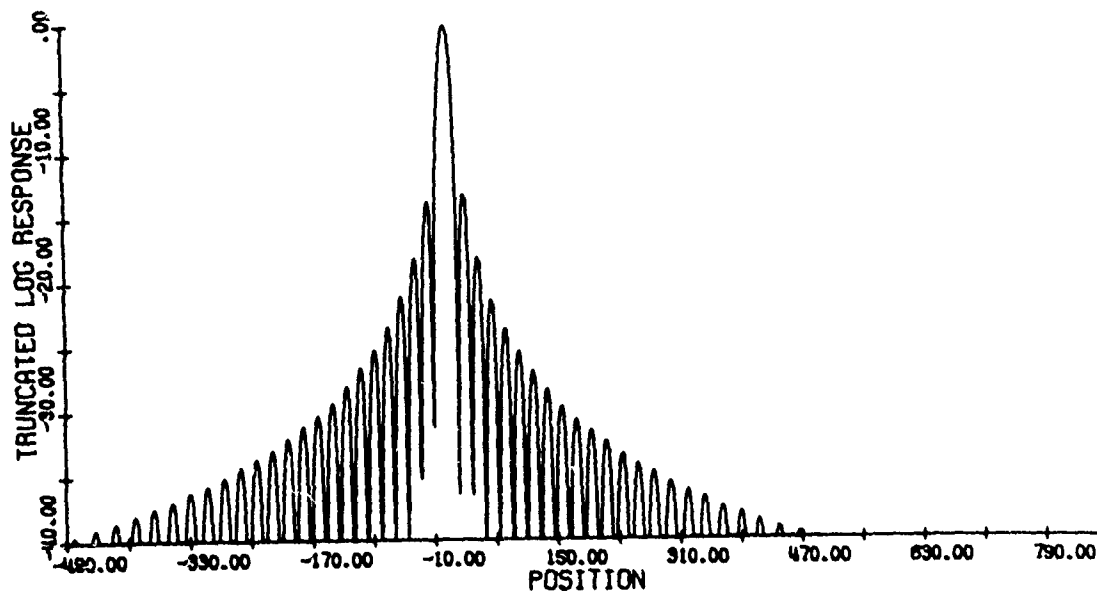


(b) Expanded Log-Intensity Response

Figure 32. Mid Range, No Motion Point Target Response.

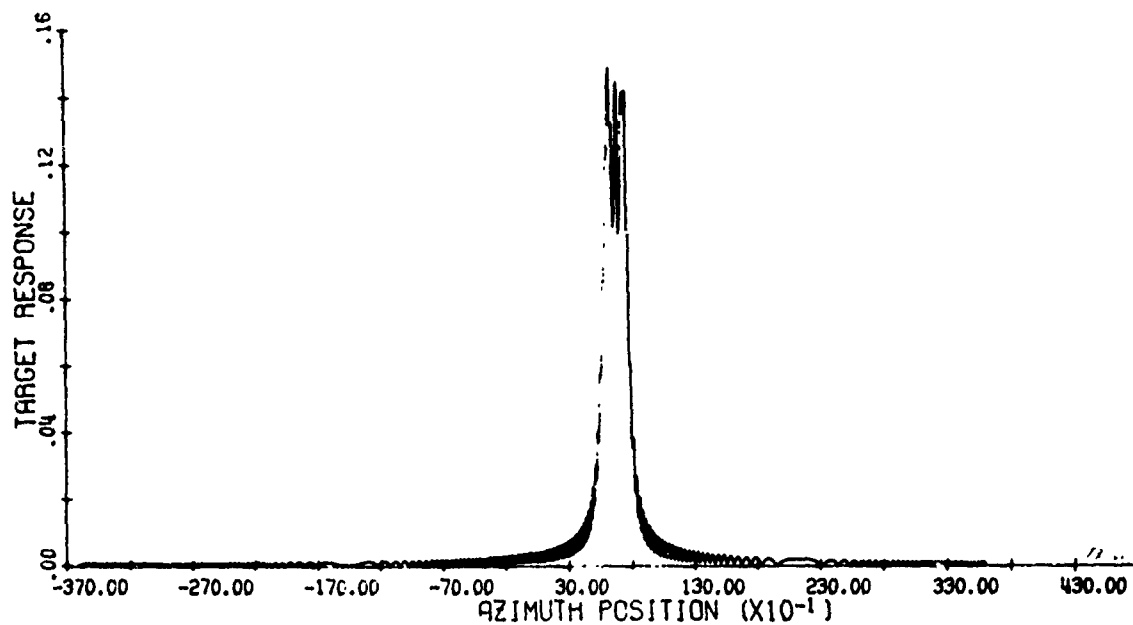


(a) Amplitude Response

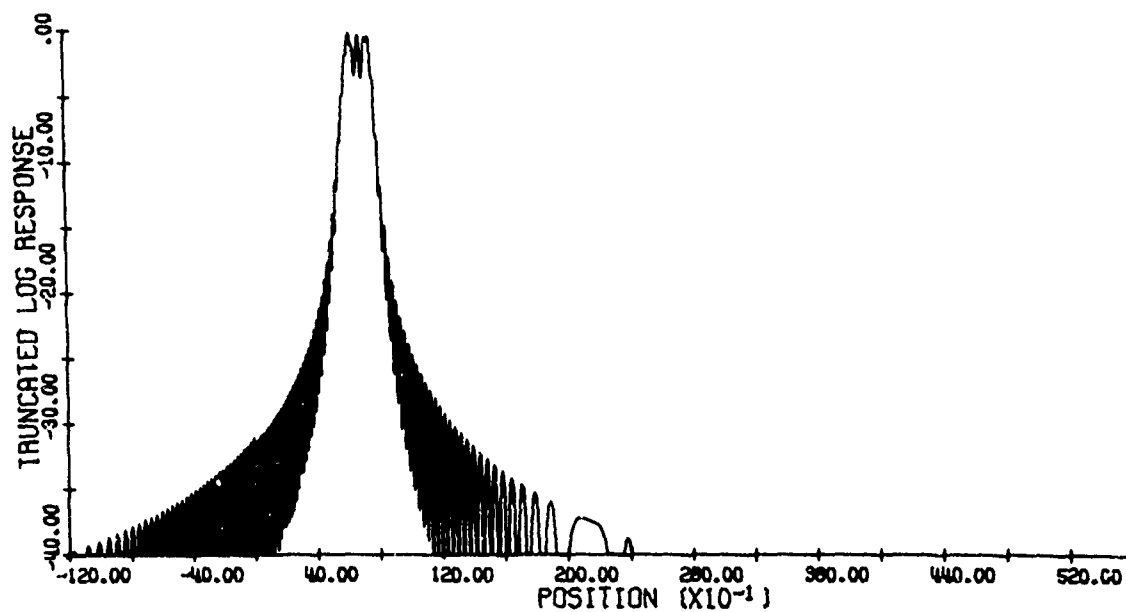


(b) Expanded Log-Intensity Response

Figure 33. Near Range, No Motion Point Target Response

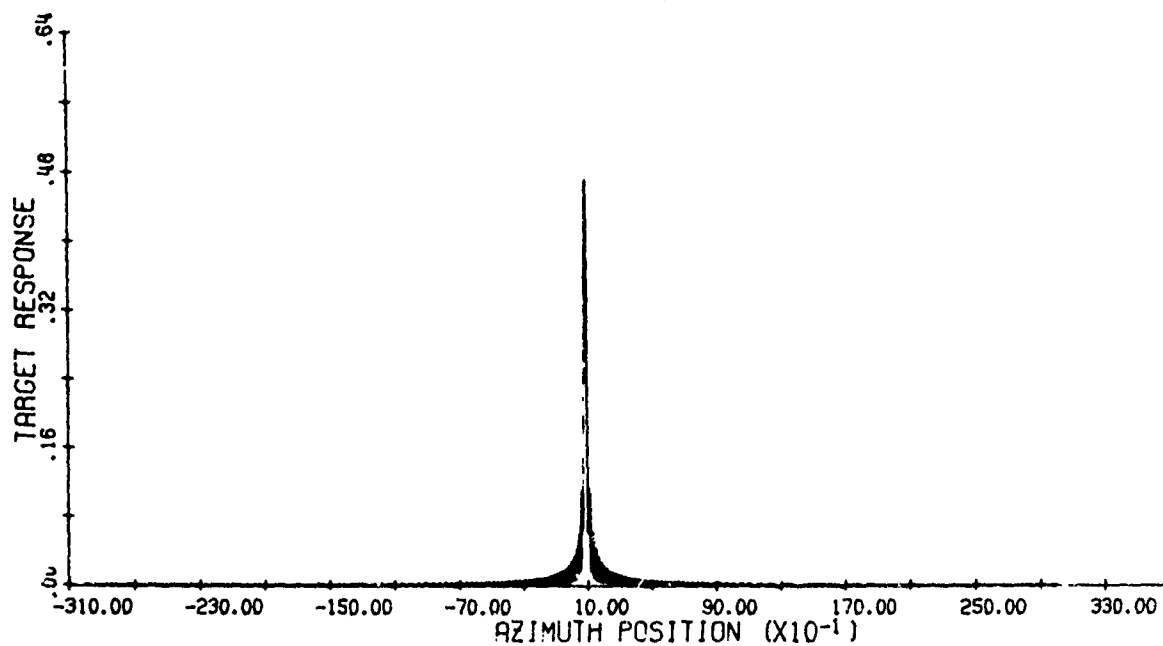


(a) Amplitude Response

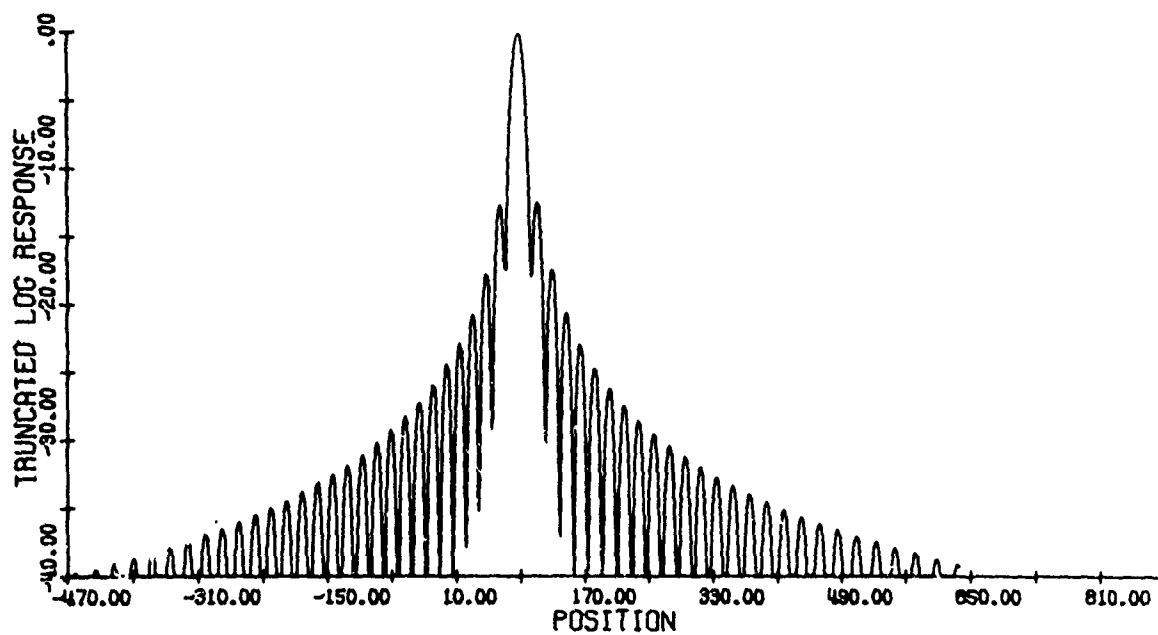


(b) Expanded Log-Intensity Response

Figure 34. Far Range Point Target Response with Motion Error.

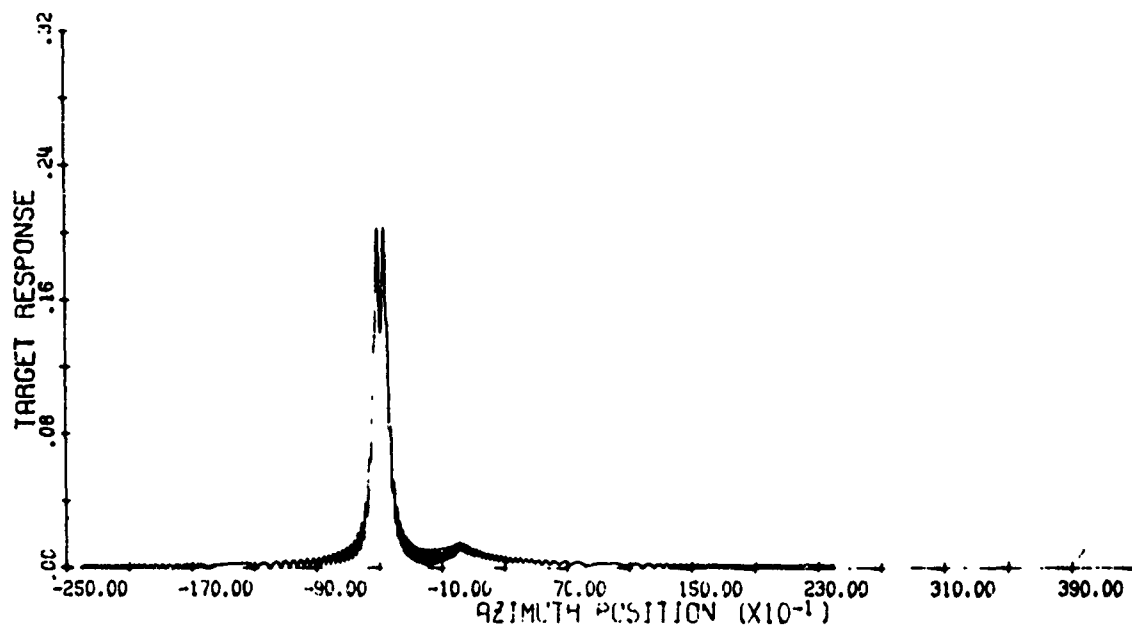


(a) Amplitude Response

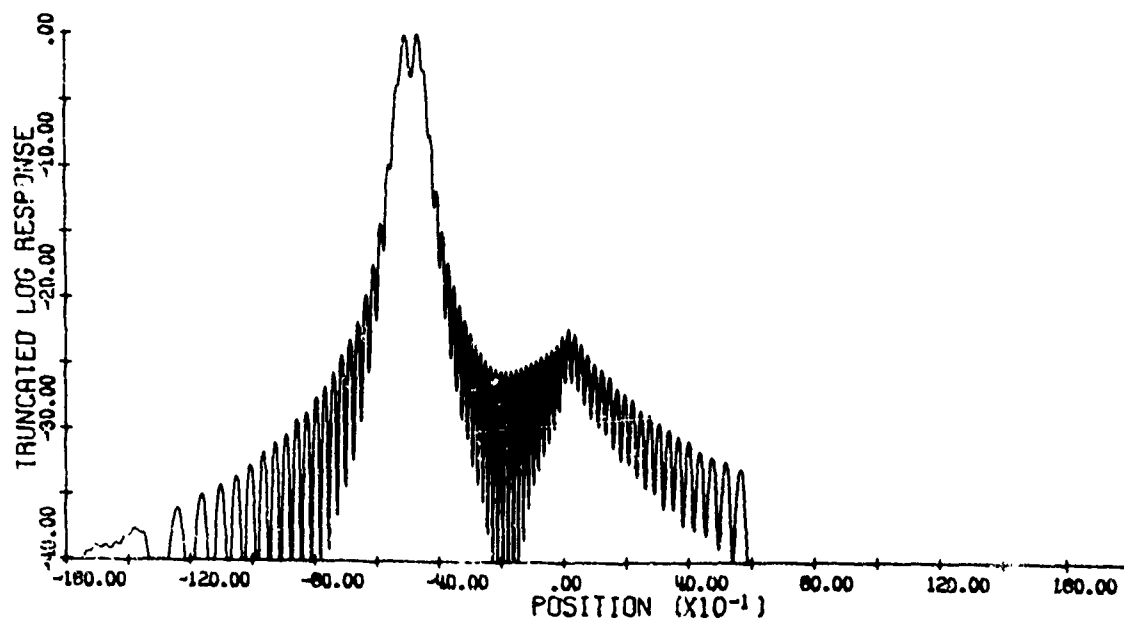


(b) Expanded Log-Intensity Response

Figure 35. Mid Range Point Target Response with Motion Error.



(a) Amplitude Response



(b) Expanded Log-Intensity Response

Figure 36. Near Range Point Target Response with Motion Error.



target response may have shown some smearing effects. The translation of the mid-range response from the expected zero position is due to the present implementation of electronic frequency offset. The electronic offset has been instructed to add a frequency shift sufficient to make the last in-beam time sample of doppler frequency have a value of 0.05 cycles per foot or above. In the present case, this implied that the resultant doppler histories had the correct FM rate, but an additional frequency offset. Thus, the azimuth position of the target response undergoes an apparent shift.

The joint effects of aircraft motion and system attempts at motion compensation are evident in Figs. 34 and 36 corresponding to far and near range targets, respectively. Due to extraneous aircraft motion the linear FM rate and mid-beam frequencies of the targets are no longer correctly matched to the reference function associated with each range. (To process the targets under the influence of motion, the reference functions derived in the no-motion case were retained and used again for the associated targets in the motion error examples.) Thus, the target responses at far and near range become smeared, asymmetrical, and displaced from the expected location. The motion compensation system modeled in this run is such that perfect compensation is possible only at a specified range. Elsewhere in the range swath non-perfect compensation is the result.

The purpose of this motion compensation example was to provide test runs of the system software and to demonstrate that aircraft motion within our model does manifest itself in the resulting target responses. No attempt was made to examine in detail the responses under these conditions and the effect of such responses upon image quality. Such an examination is not within the scope of the current program.

#### 7.4.2 Demonstration of Amplitude Weighting Effects - Antenna.

Three additional simulated flights were made to test the system's ability to demonstrate the effects of antenna pattern and amplitude weighting upon the azimuth response of point targets.

Two flights were made past an array of three targets situated at far, mid, and near-range. The two flights were identical in every respect except that antenna amplitude weighting was applied on the second pass. In this example, the vehicle was flying 300 ft/sec at an altitude of 5,000 ft and the beamwidth was 0.02 radians. The far, mid, and near-range targets were situated at slant range distances of 25K, 23K, and 21K feet, respectively. The swath width was approximately 6K feet. Figures 37 and 38 illustrate the amplitude weighting associated with pass one and two, respectively. The weighting displayed in Fig. 38 is of the  $(\sin x)/x$  form out to the -3 db point (approximately  $-\frac{\pi}{2} \leq x \leq \frac{\pi}{2}$ ).

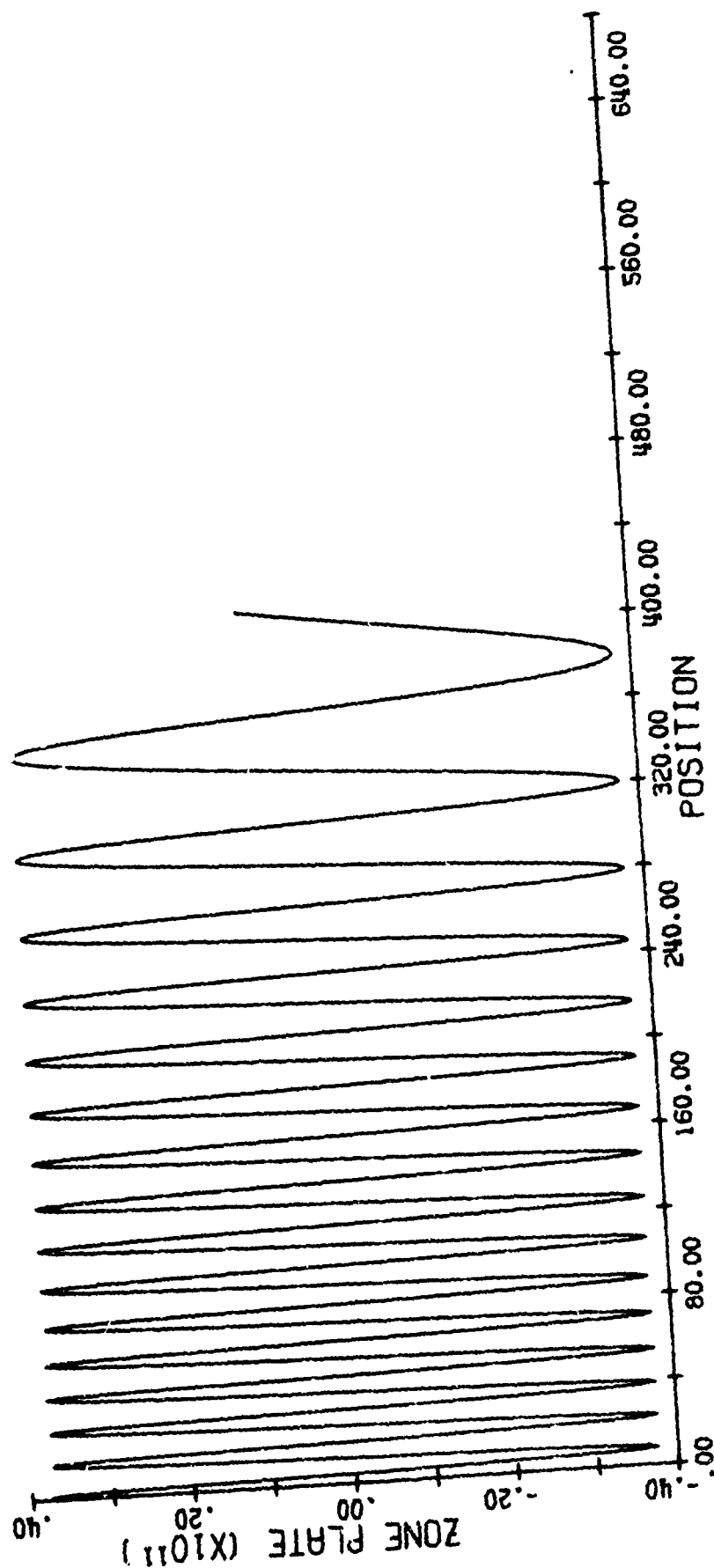


Figure 37. Uniform Amplitude Weighting for Returned Signal Pulse.

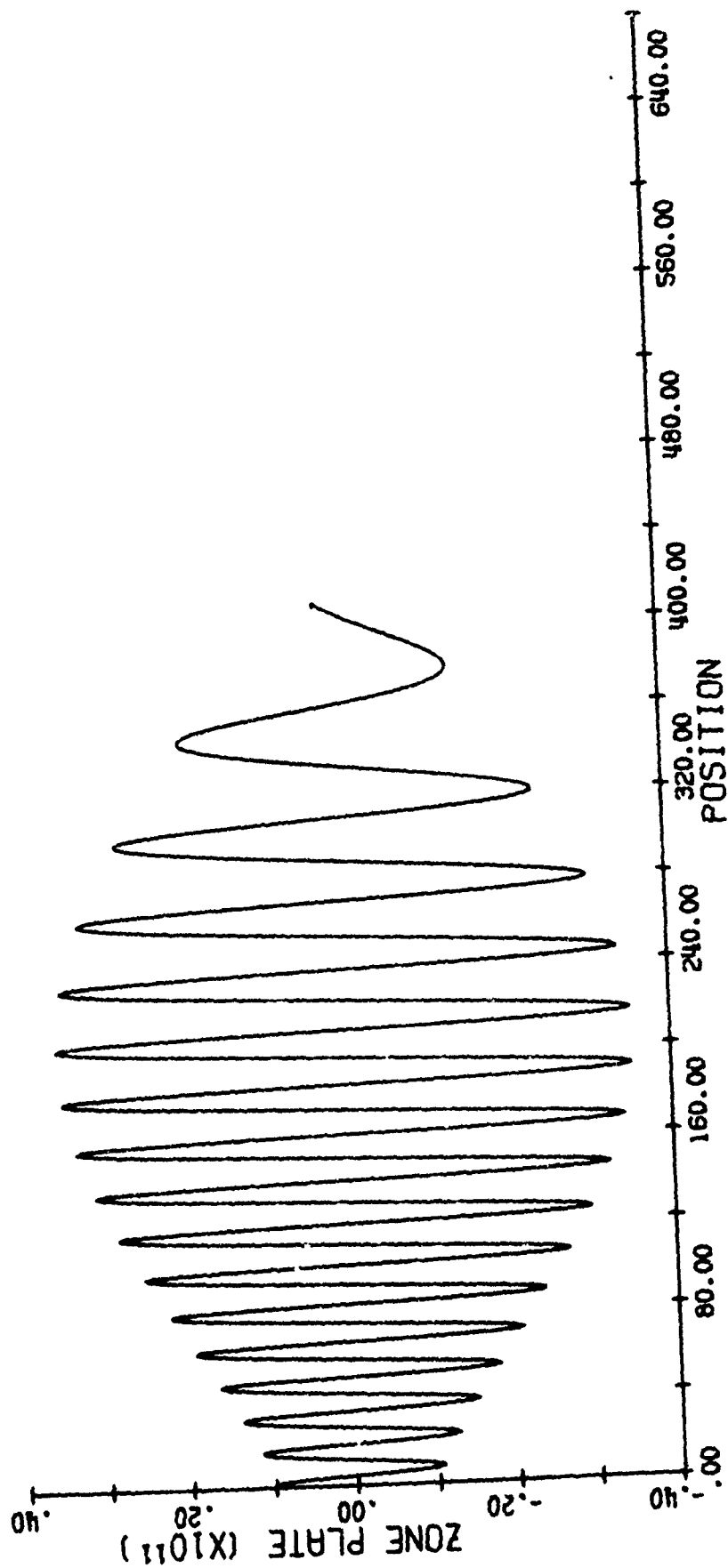
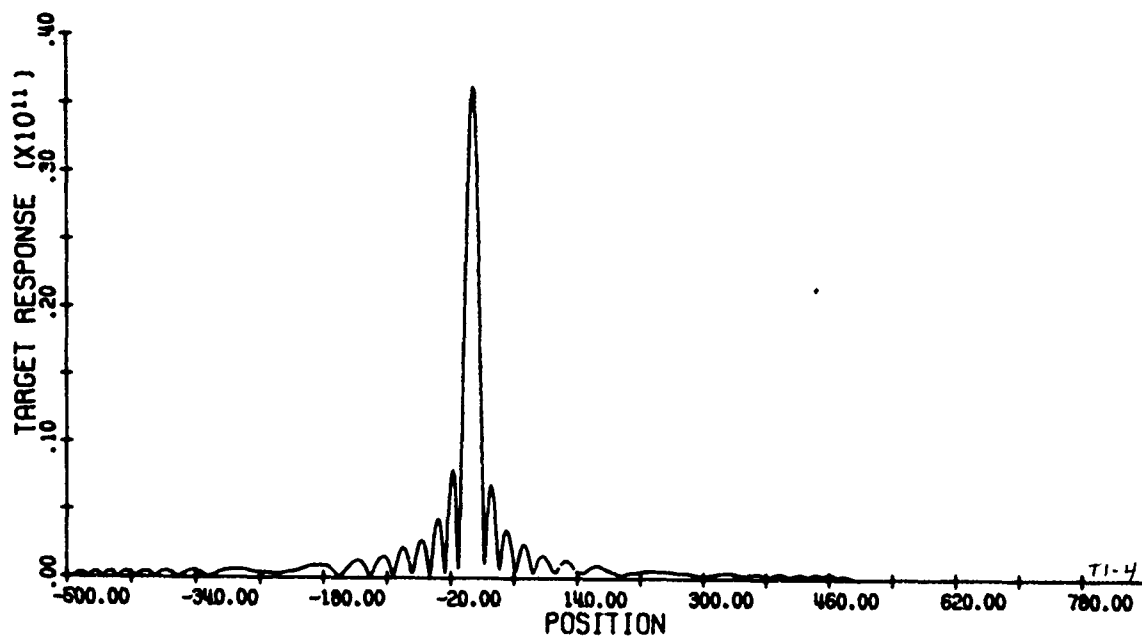


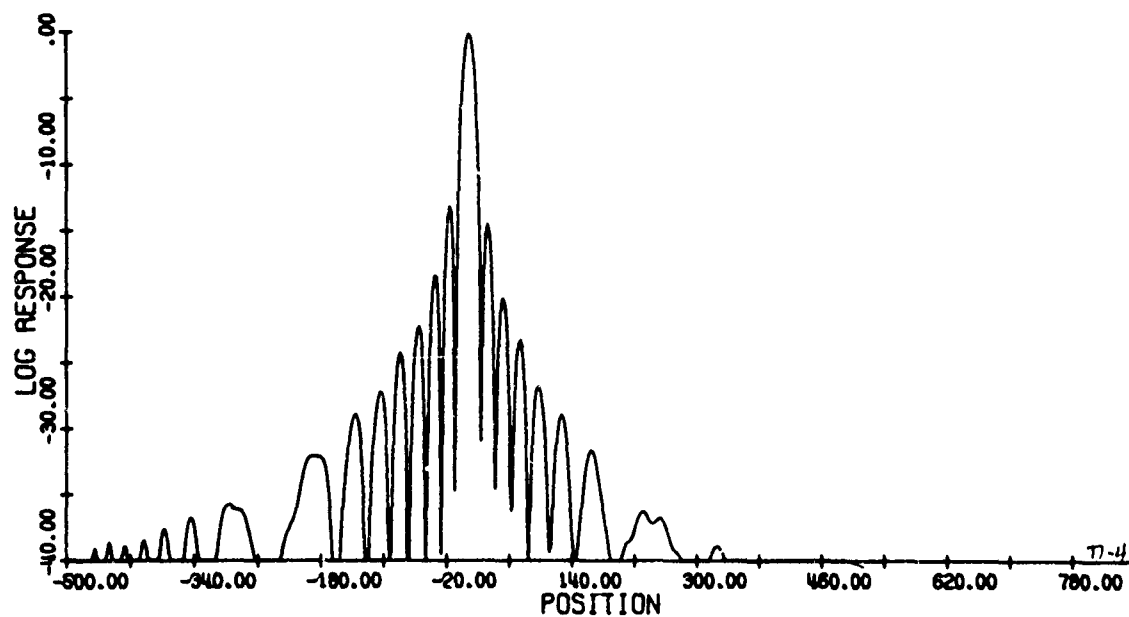
Figure 38.  $\sin x/x$  Amplitude Weighting (out to -3 db) for Returned Signal Pulse.

The target responses associated with the uniform weighting situation are shown in Fig. 39, 40, and 41 for the far, mid, and near-range targets respectively. The important items to notice are the sidelobe levels and relative response of the three targets. As expected for the uniform weighting case, the sidelobes are down approximately 13 db for all three targets. In this example, the theoretically "correct" reference function was used. A slight mis-match between signal and ideal reference due to range walk and other higher order effects causes a slight amount of asymmetry in the target response. (The gross asymmetries in the tails of the response (below -30 db) are most likely due to finite aperture effects.) The variation in relative peak amplitudes of the three responses is due to the amplitude weighting in the range direction assigned to the antenna. This range direction amplitude weighting is specified by the user via a table of values in IQMOD (the simulation section). Thus the antenna pattern for the first flight had uniform weighting in the azimuth direction across the beam-width but a nonuniform pattern in the range direction and hence the variation in the amplitude of returns.

The target responses in Figs. 42, 43, and 44 are the result of applying the weighting shown in Fig. 39 to the far, mid, and near-range target returns. As before there is a relative amplitude variance

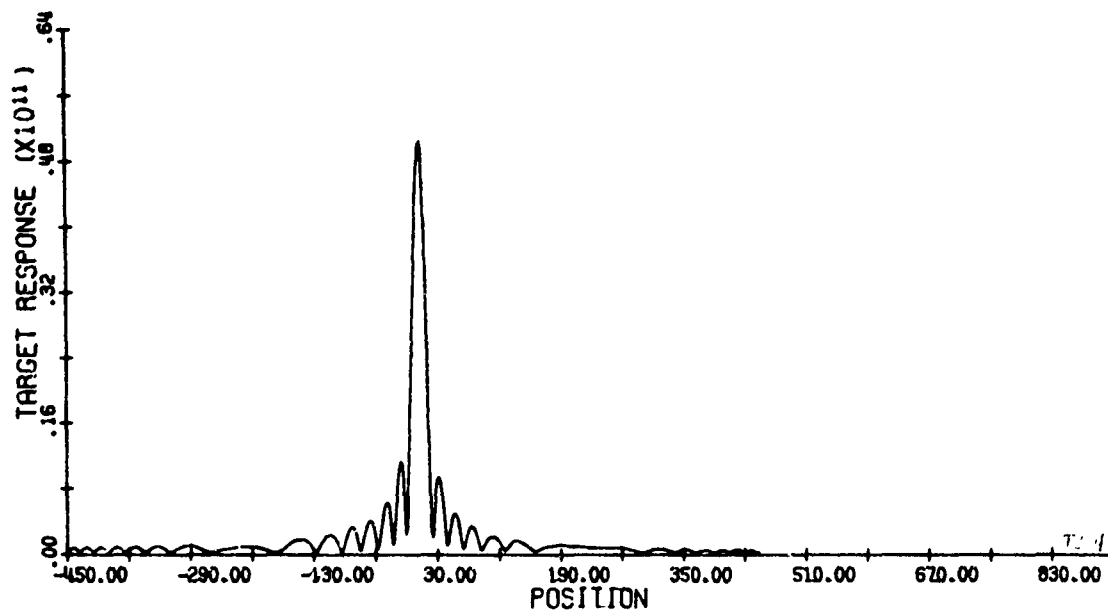


(a) Amplitude Response

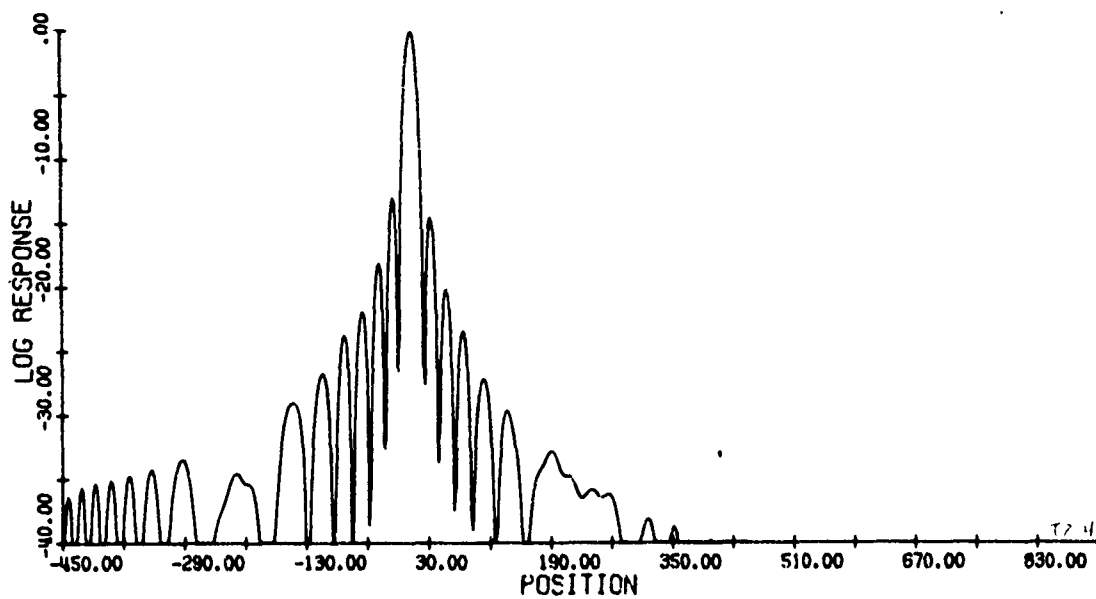


(b) Log-Intensity Response

Figure 39. Uniform Amplitude Weighting Far Range Response.

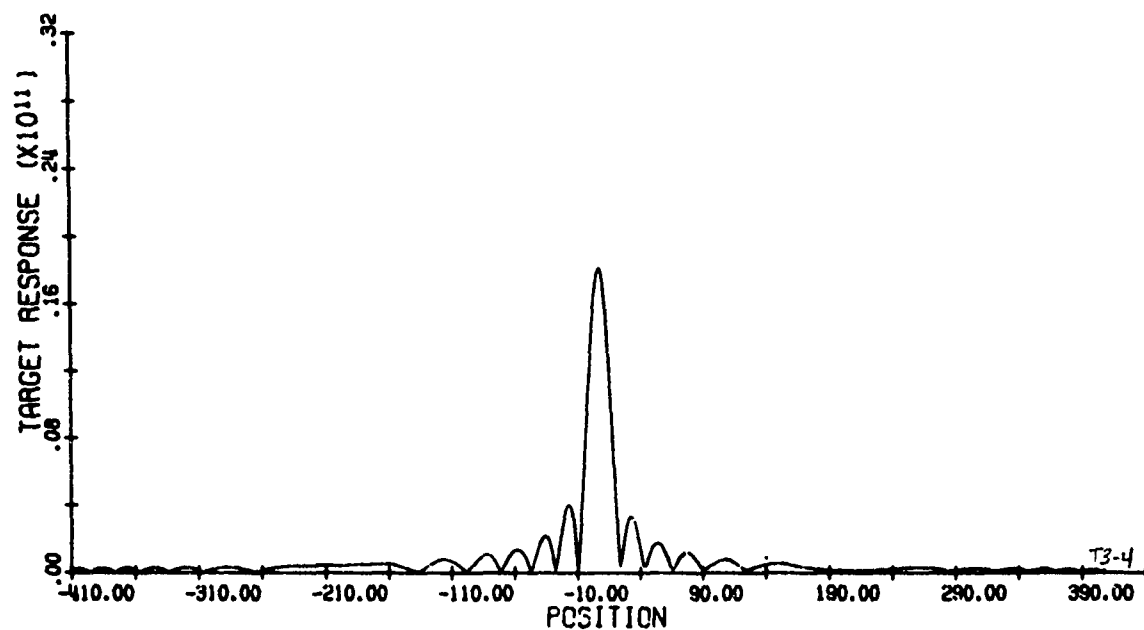


(a) Amplitude Response

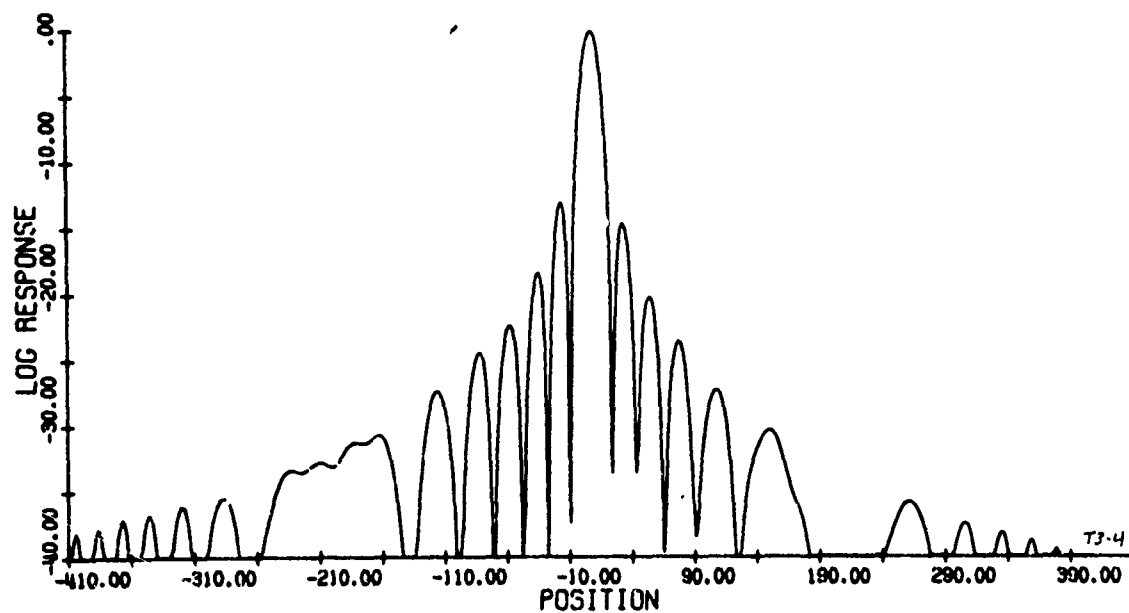


(b) Log-Intensity Response

Figure 40. Uniform Amplitude Weighting Mid Range Response.



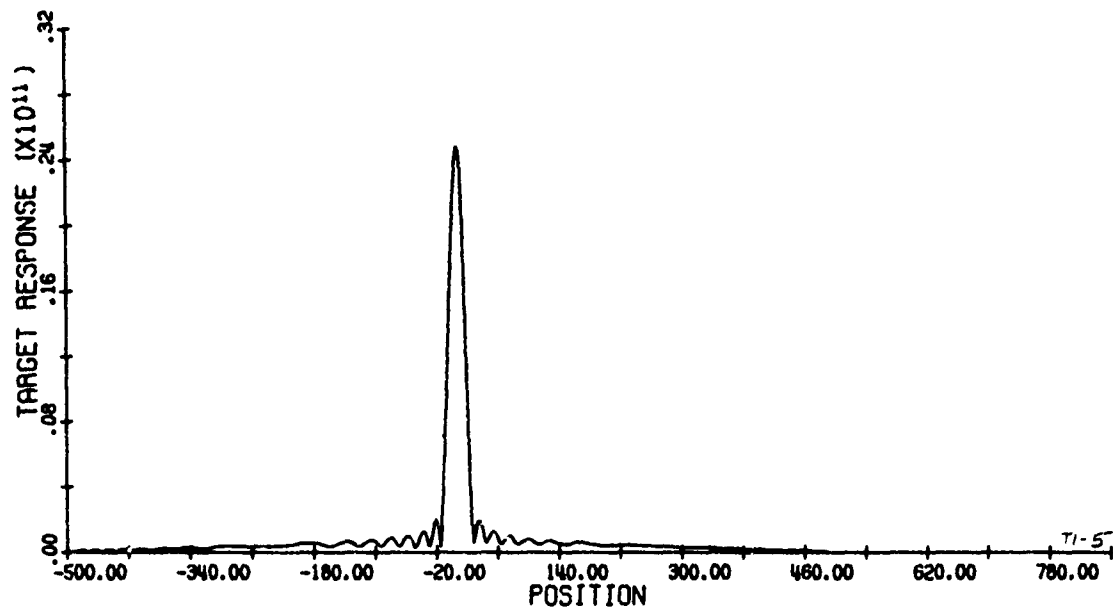
(a) Amplitude Response



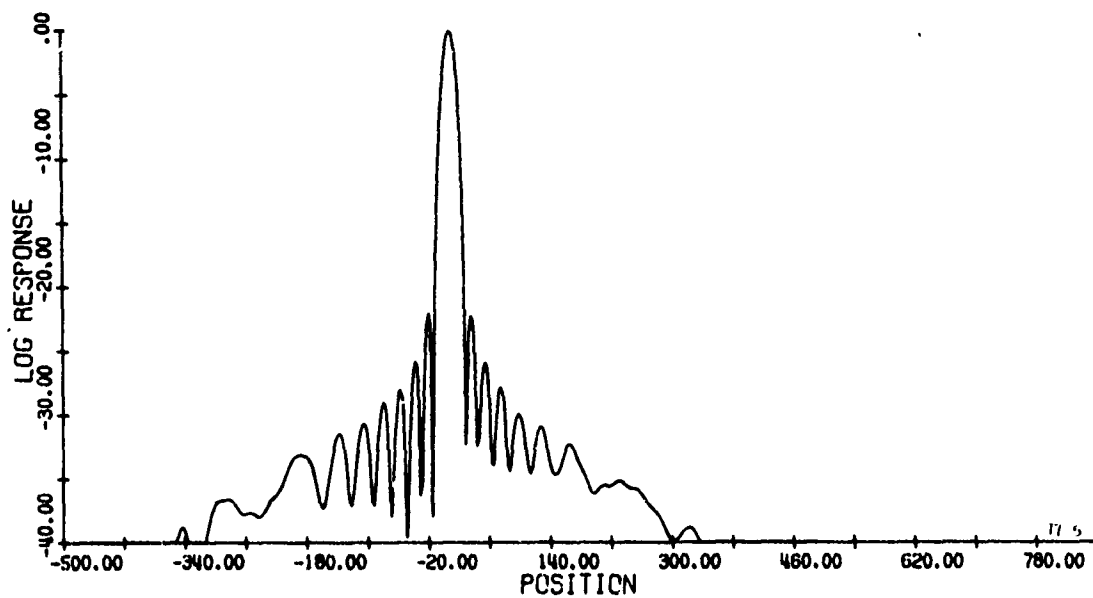
(b) Log-Intensity Response

Figure 41. Uniform Amplitude Weighting Near Range Response



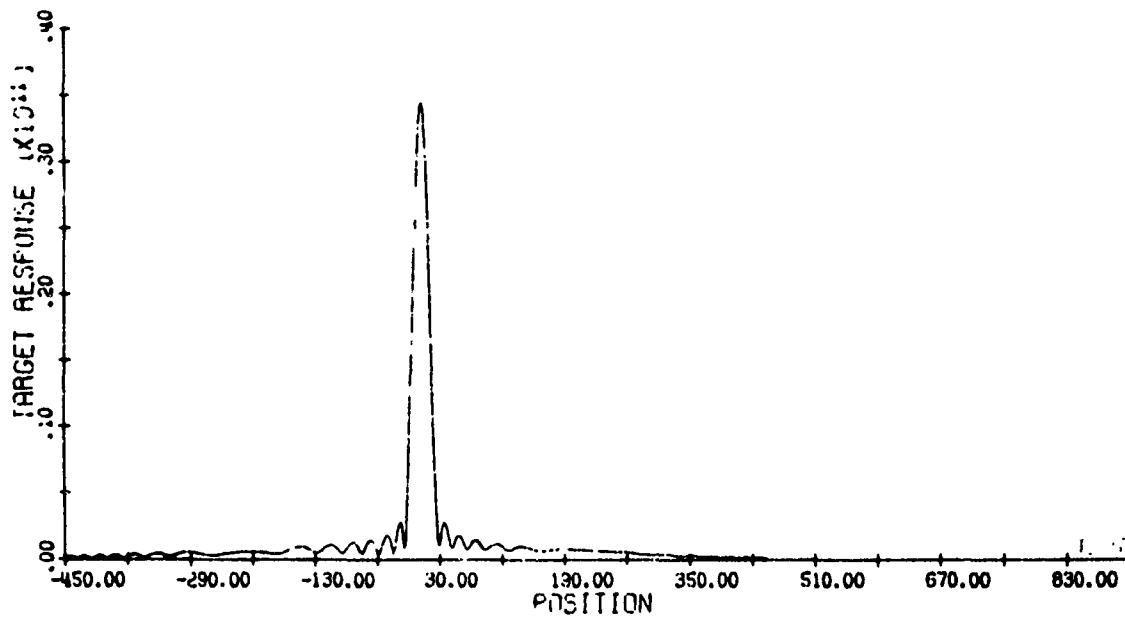


(a) Amplitude Response

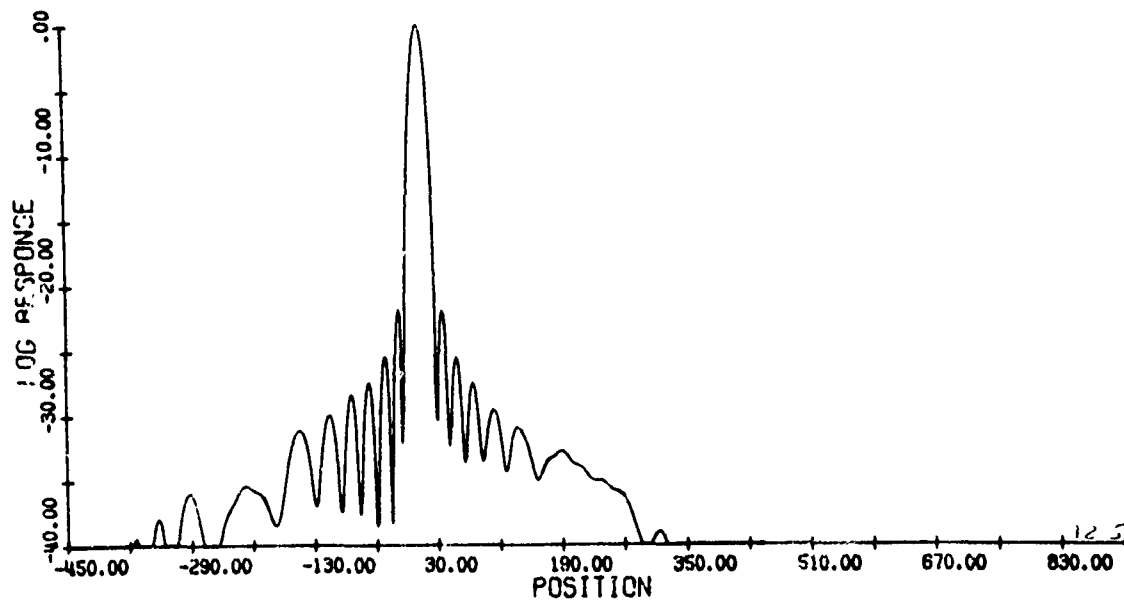


(b) Log-Intensity Response

Figure 42. Non-Uniform Weighting Far Range Response

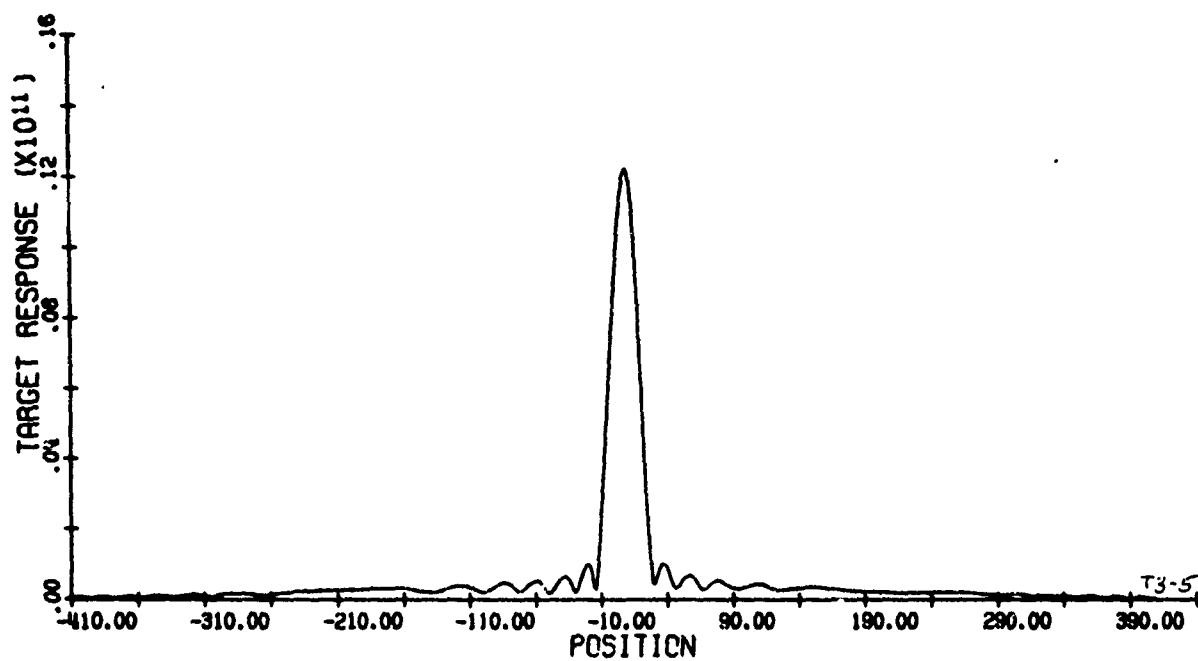


(a) Amplitude Response

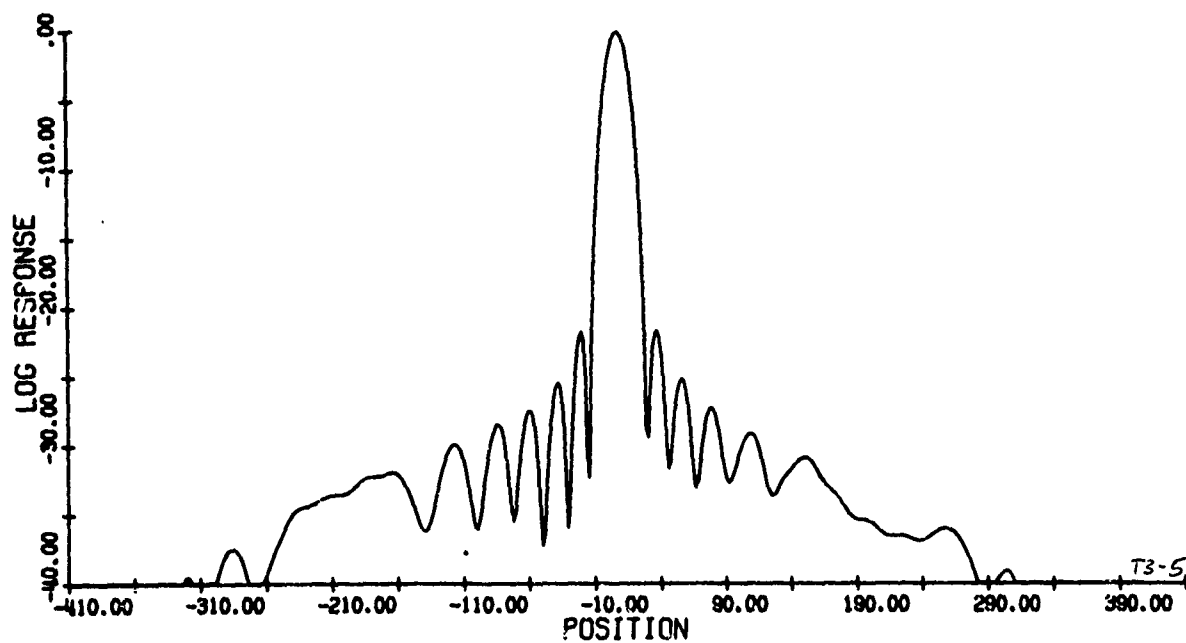


(b) Log-Intensity Response

Figure 43. Non-Uniform Weighting Mid Range Response



(a) Amplitude Response



(b) Log-Intensity Response

Figure 44. Non-Uniform Weighting Near Range Response.

between the three responses which is due to the antenna pattern in the range direction. The effect of the amplitude weighting in the azimuth direction is shown in the response sidelobes. They are now approximately 23 db down as compared to 13 db down with unity weighting. As expected the point target responses are basically the same as for the uniform amplitude case except that the sidelobe levels have been reduced. In addition, one notices a slight broadening of the mainlobe as a result of the amplitude weighting.

One additional flight was made to demonstrate the flexibility with which the antenna weighting can be applied. In this final example, the antenna pattern was broadened to include three sidelobes of the  $(\sin x)/x$  pattern as shown in the linear FM pulse of Fig. 45. To be able to process the required time-bandwidth product associated with a full antenna pattern signal, the -3 db beamwidth had to be halved from the previous example. Therefore, the responses associated with the signal pulse of Fig. 45 should not be compared with any previous responses. This example is included solely to demonstrate the flexibility of generating arbitrary antenna patterns. The far, mid, and near-range responses are shown in Figs. 46, 47 and 48 respectively. The flat-top on the mainlobe of each target response is indicative of the mainlobe broadening which generally occurs with antenna weighting schemes.

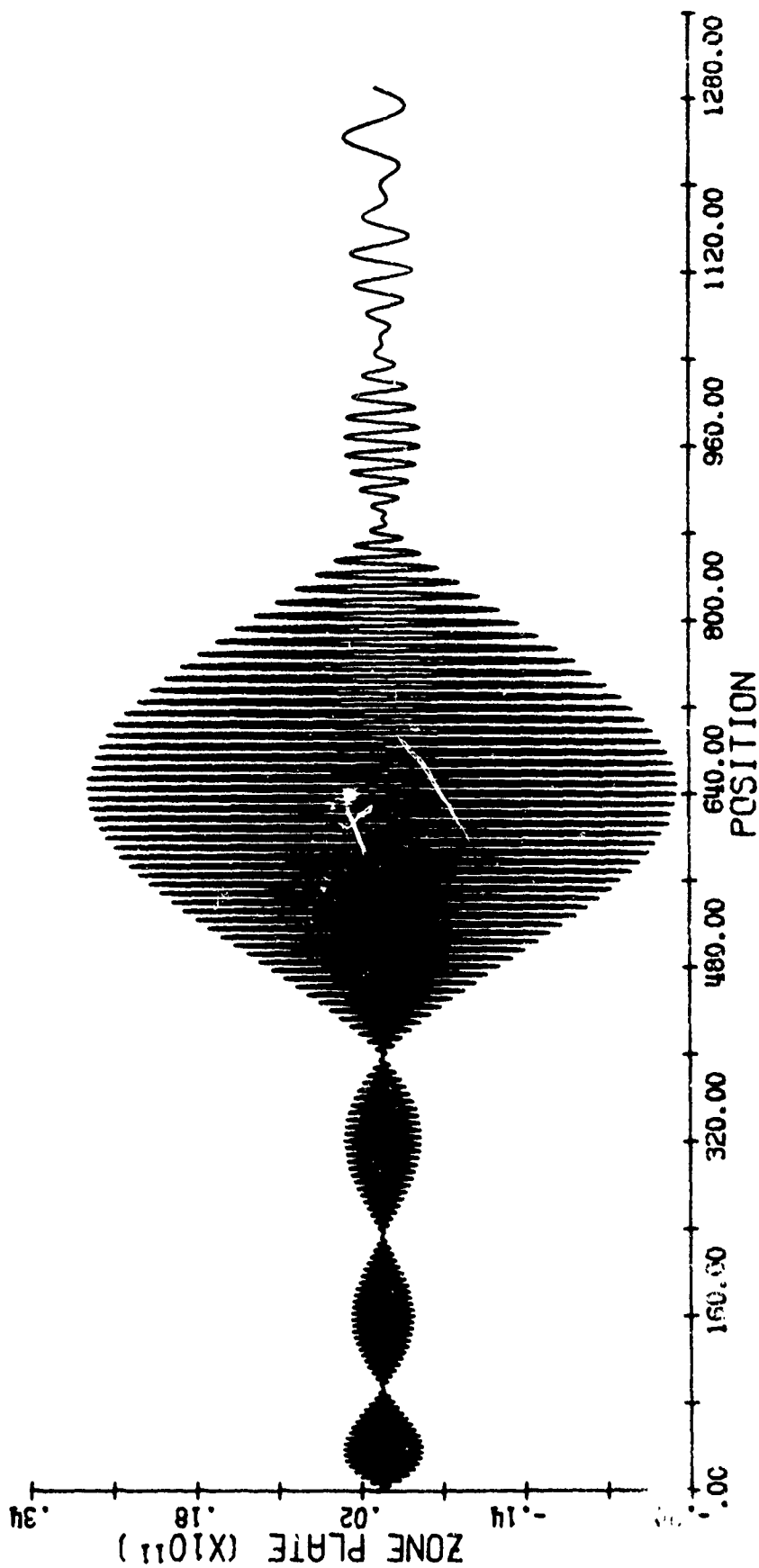
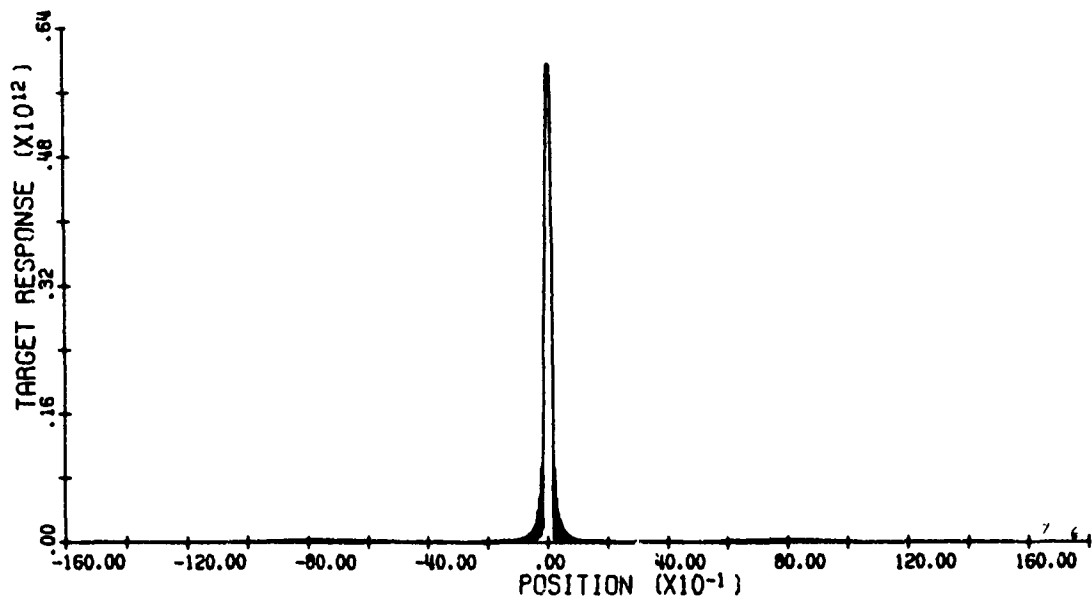
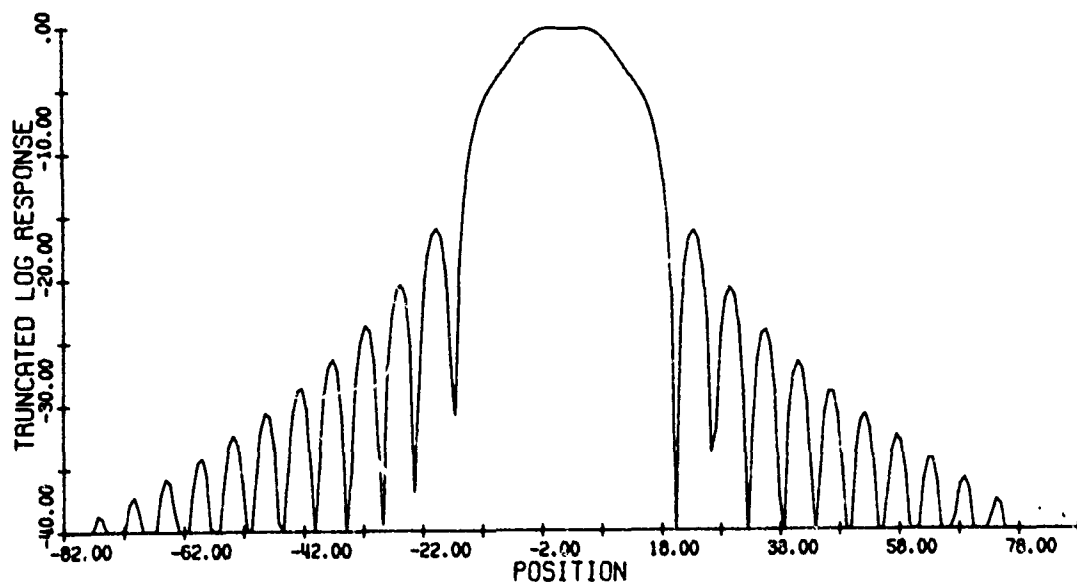


Figure 45. Three Sidelobe Sin x/x Antenna Weighted Doppler History.

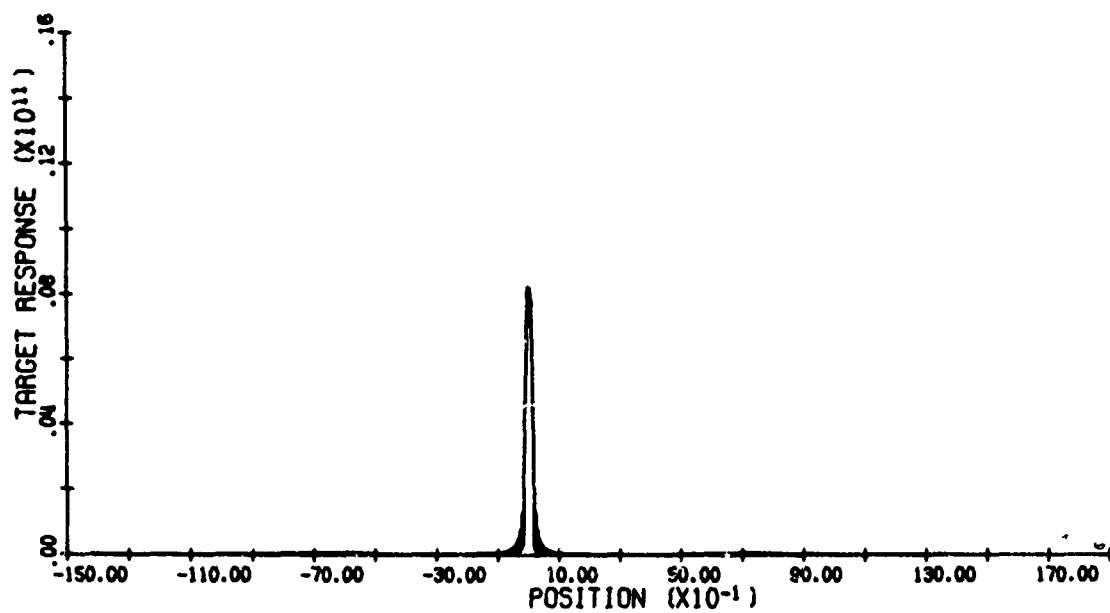


(a) Amplitude Response

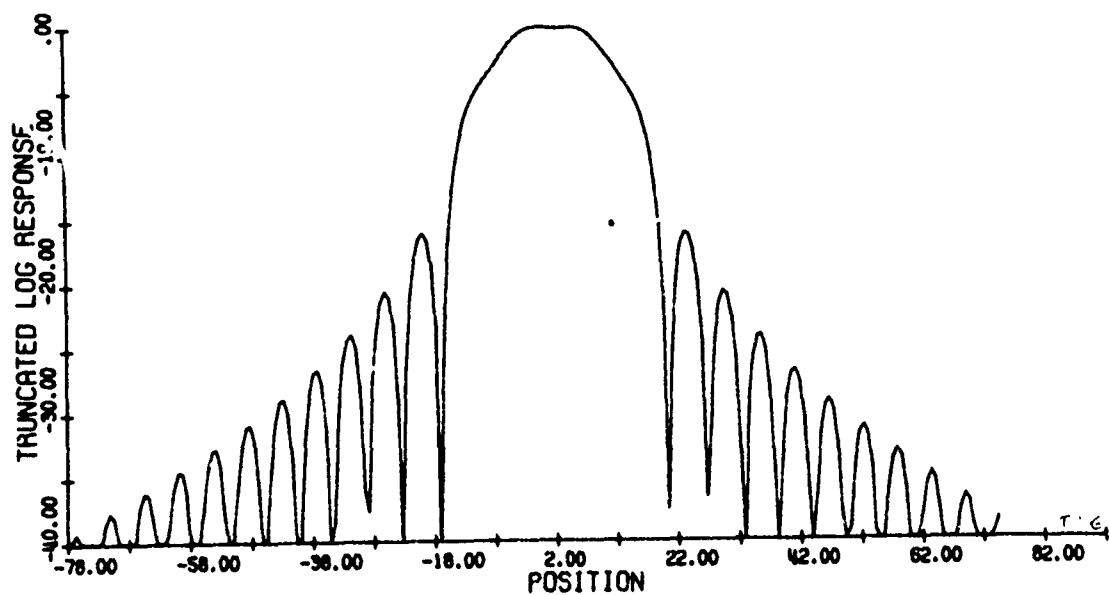


(b) Expanded Log-Intensity Response

Figure 46. Far Range Target Response

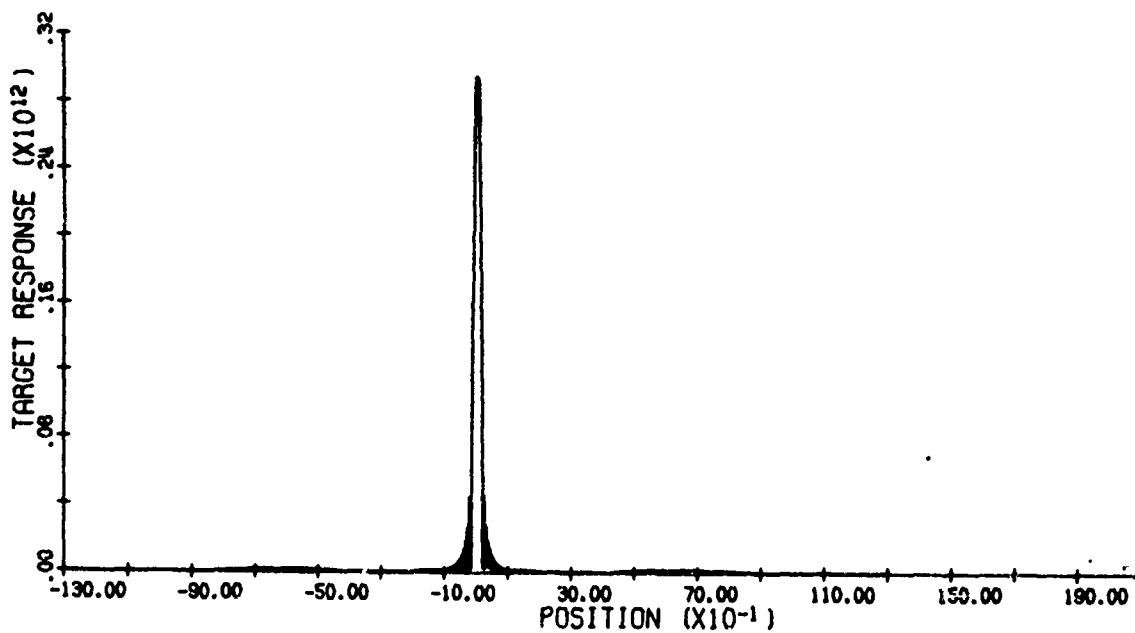


(a) Amplitude Response

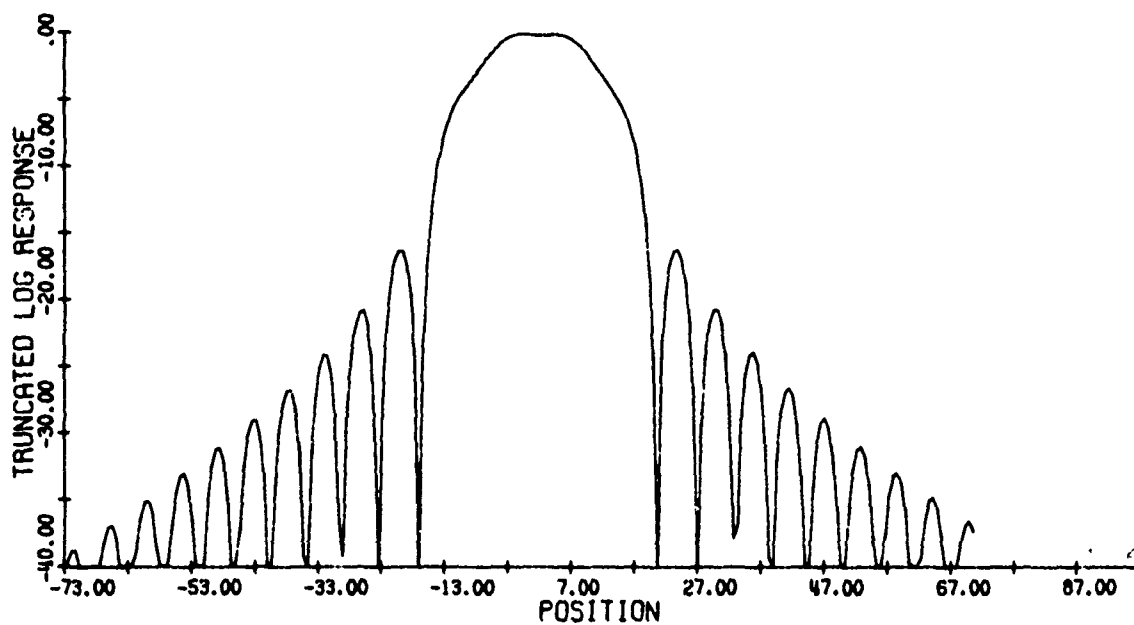


(b) Expanded Log-Intensity Response

Figure 47. Mid Range Target Response



(a) Amplitude Response



(b) Expanded Log-Intensity Response

Figure 48. Near Range Target Response



The sidelobes of the responses associated with this antenna pattern are down about 17 db.

### 7.5 Summary

The impulse response capability has been included in the model to provide quantitative input to the image quality analysis effort to be described in the next section. The previous examples have been included to demonstrate the flexibility and power of the technique. It should be noted that we have constructed a one dimensional routine equally applicable in range or azimuth for the explicit purpose of providing detailed quantitative data for SAR system image quality analysis.

## APPENDIX

### Flow Diagrams for the Impulse Response Software

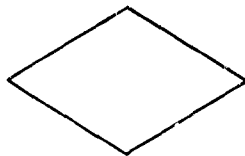
This appendix contains flow diagrams and listings for the software module described in the section of this report entitled, "Impulse Response Generation." The theory of operation, a narrative description, and some processing examples are all contained within that section.

#### Impulse Response Flow Diagram

The symbolism in the following diagrams is defined as follows:



- an off-page connector



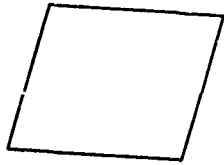
- a decision or branch point



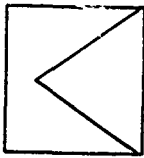
- processing or operation block



- a subroutine call (usually accompanied by an explanatory note)



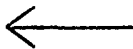
- an input or output operation



- represents a do-loop



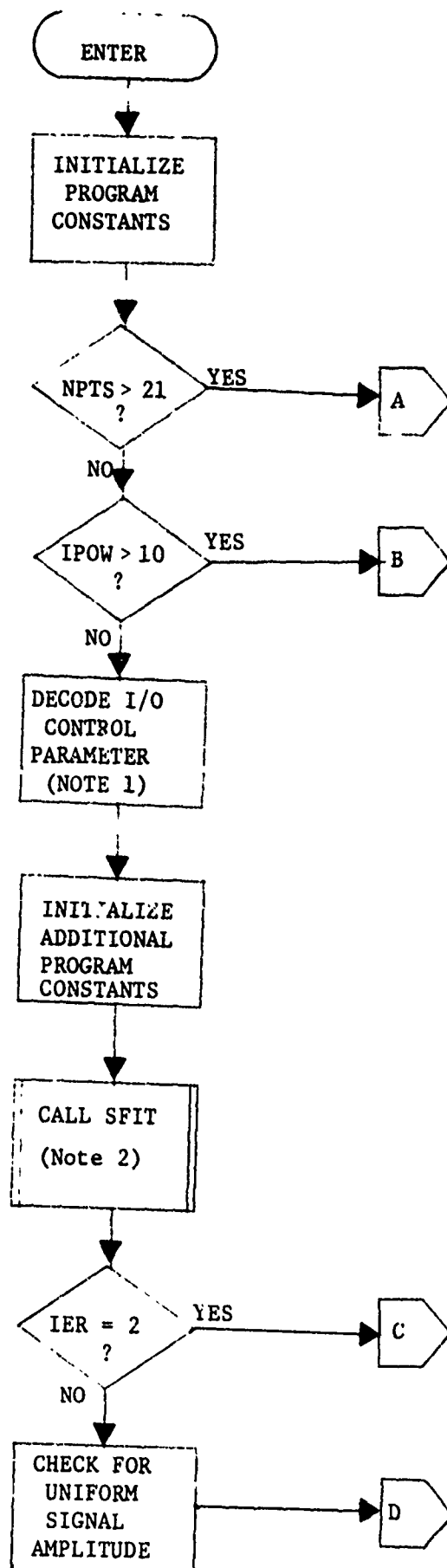
- entry point and return points



- assignment indicator

### Software Module Listings

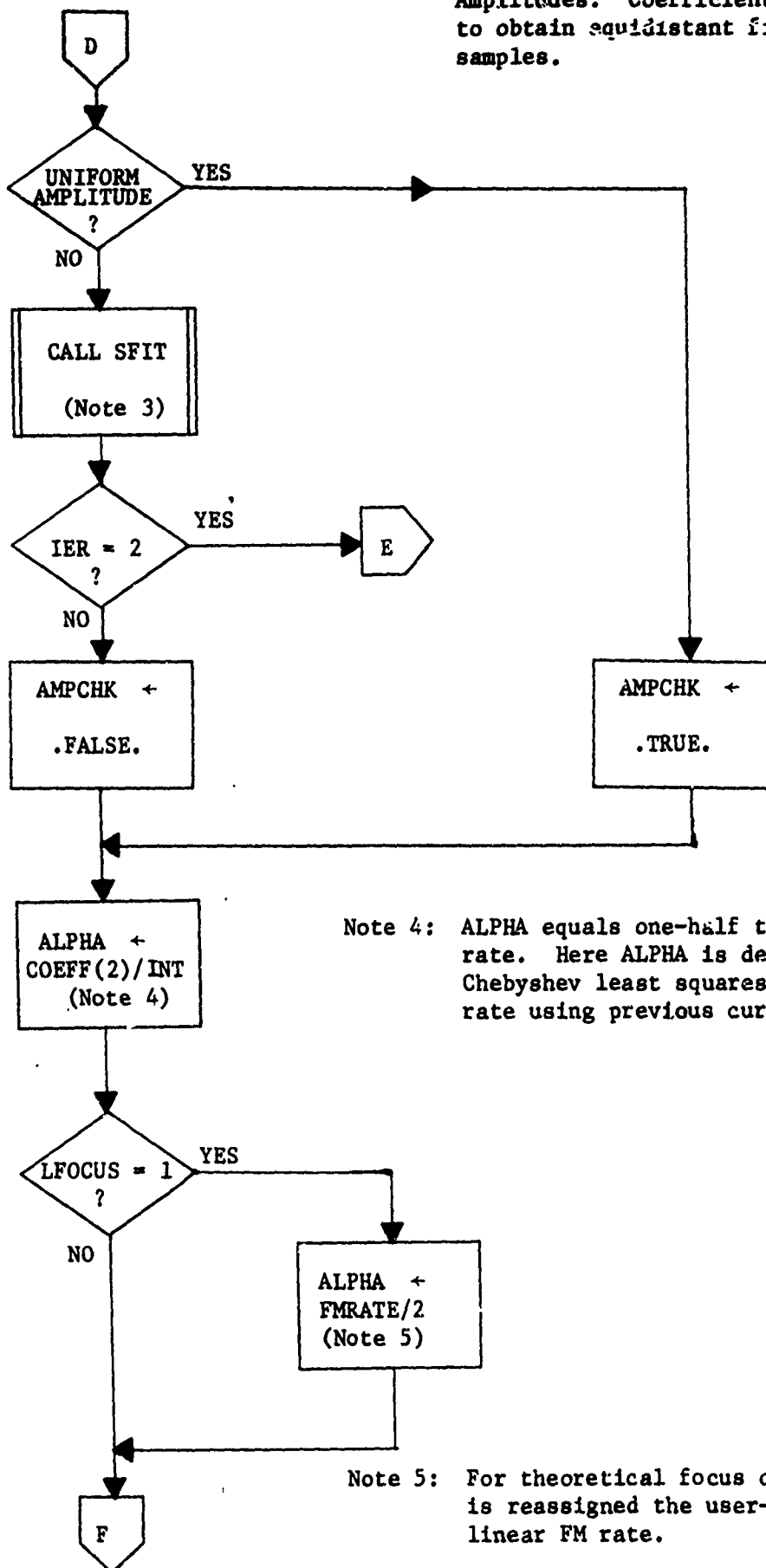
The listings of the Fortran source code associated with the impulse response module (IRMOD) follow the flow diagram.



Note 1: I/O control parameter controls the printing and plotting of all optional I/O data

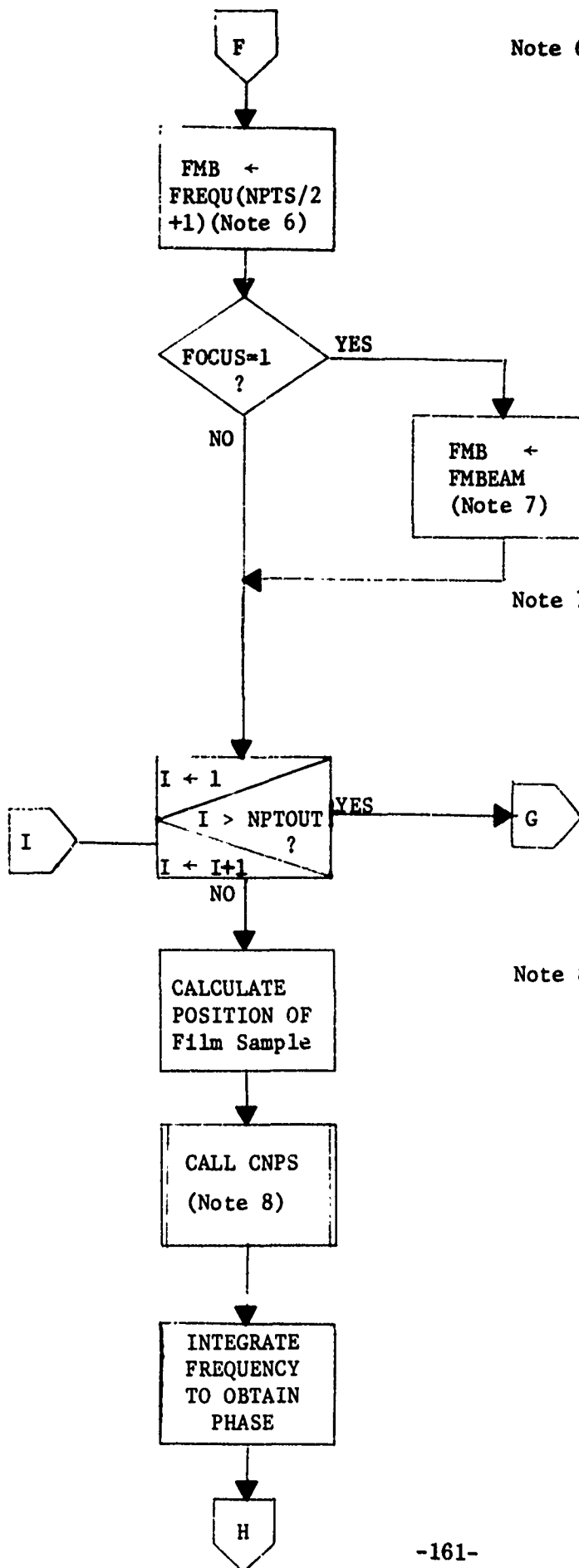
Note 2: Chebyshev curve fit to signal Doppler frequencies. Coefficients used later to obtain equidistant film-space samples.

Note 3: Chebyshev curve fit to signal Amplitudes. Coefficients used later to obtain equidistant film-space samples.



Note 4: ALPHA equals one-half the linear FM rate. Here ALPHA is defaulting to Chebyshev least squares linear FM rate using previous curve fit coefficients.

Note 5: For theoretical focus option ALPHA is reassigned the user-supplier linear FM rate.

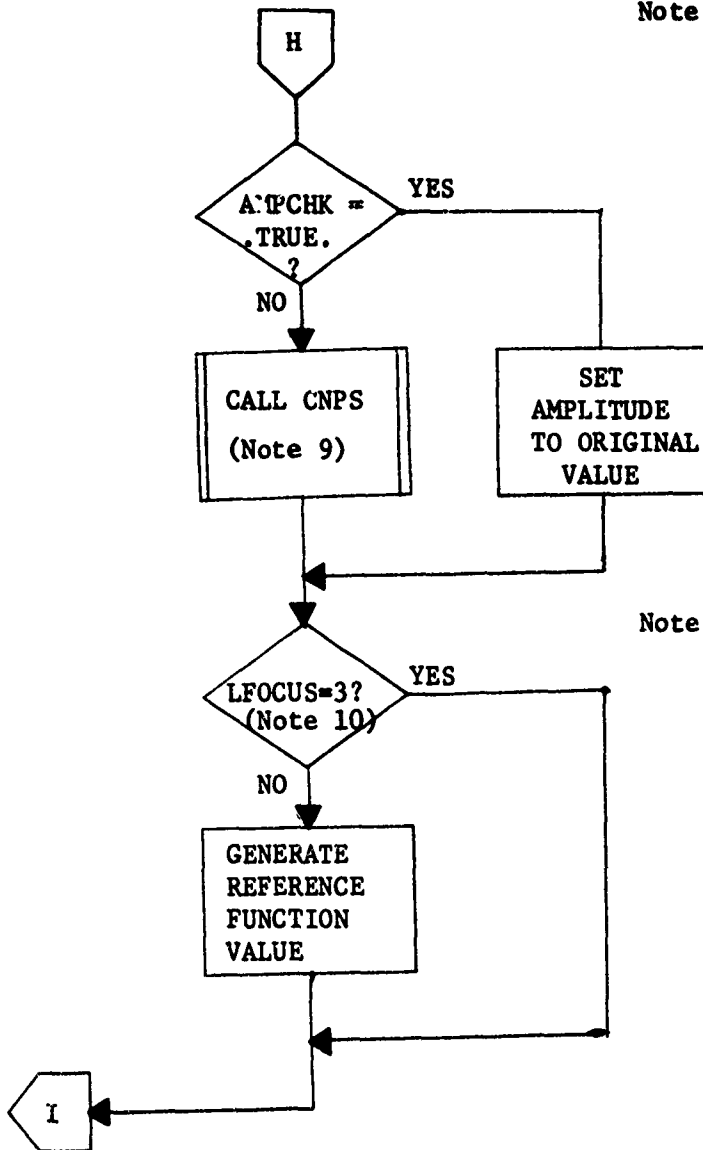


Note 6: The mid beam doppler frequency defaults to that actually observed during target flyby.

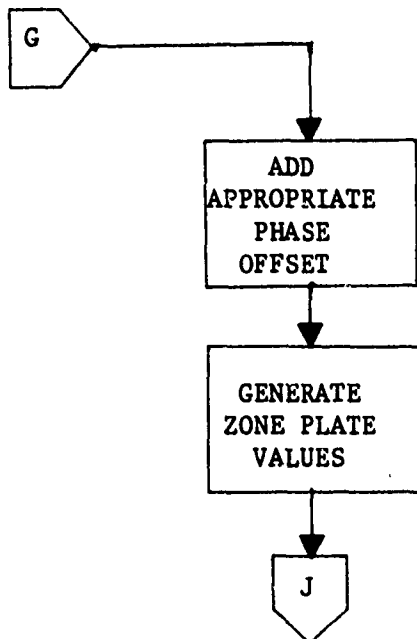
Note 7: For theoretical focus option the midbeam frequency is reassigned to the user supplied value.

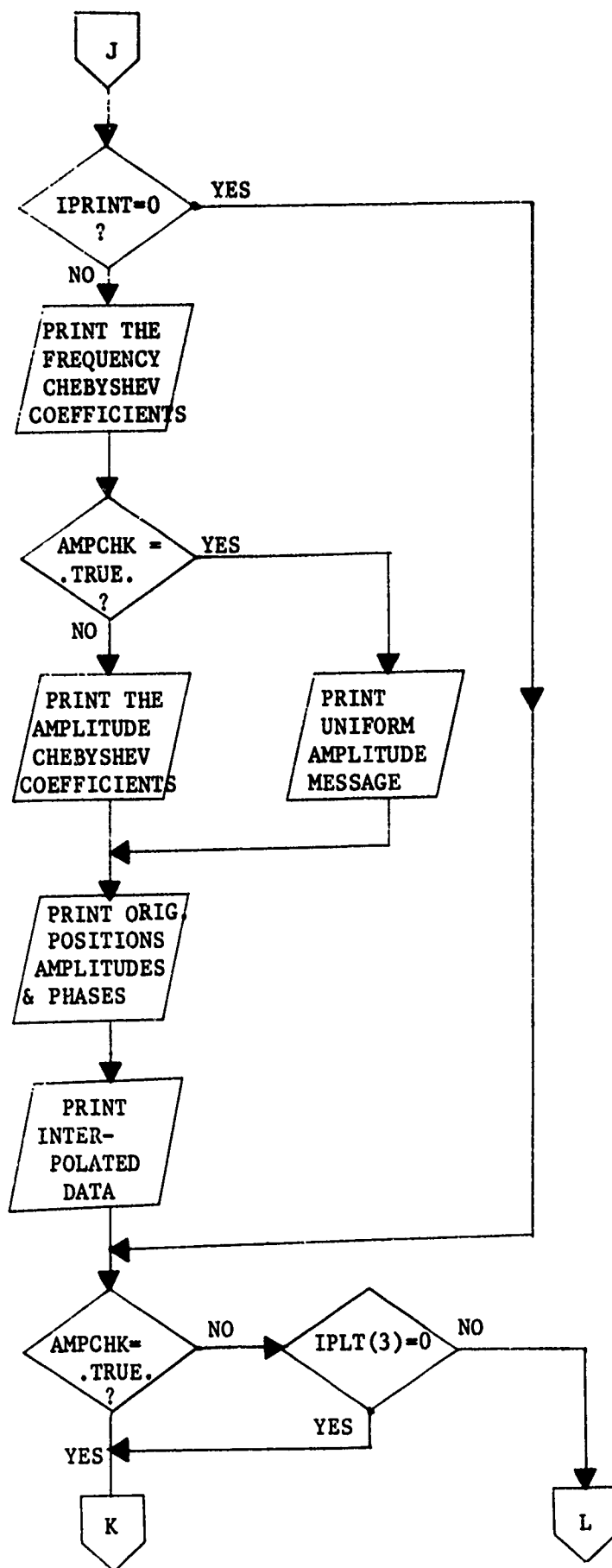
Note 8: CNPS uses sample position and Chebyshev coefficients to determine instantaneous doppler frequency at that point.

Note 9: CNPS uses sample position and Chebyshev coefficients to determine instantaneous signal amplitude at that point.

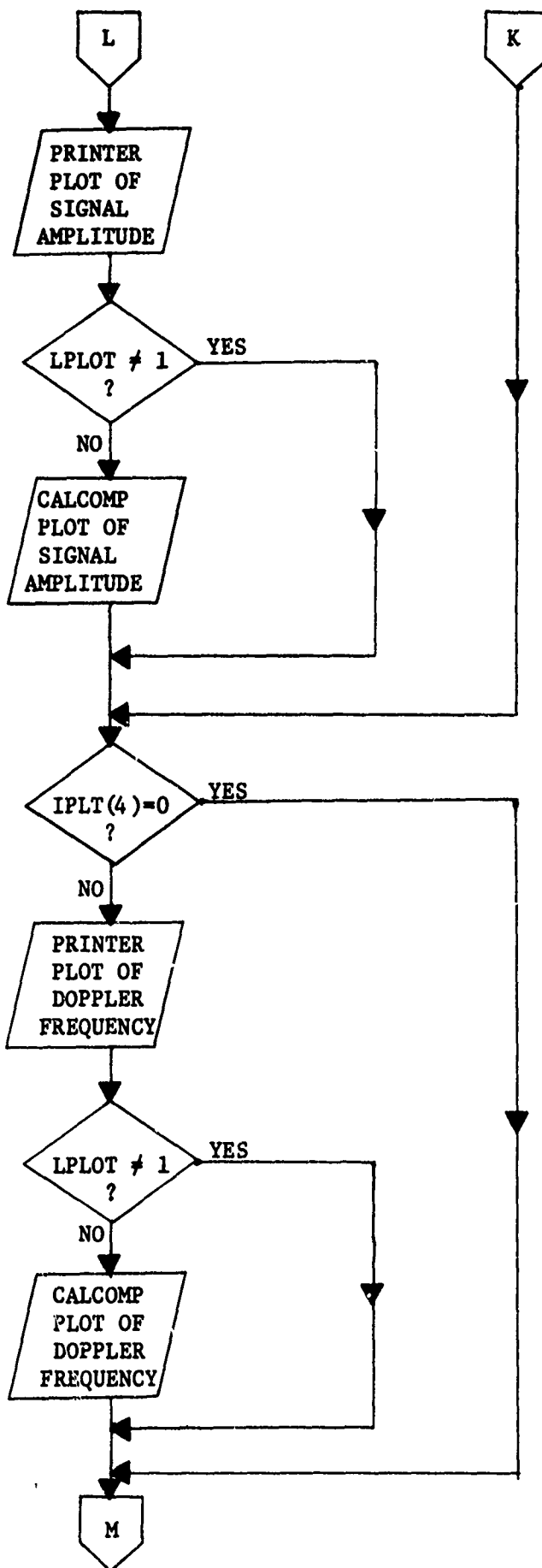


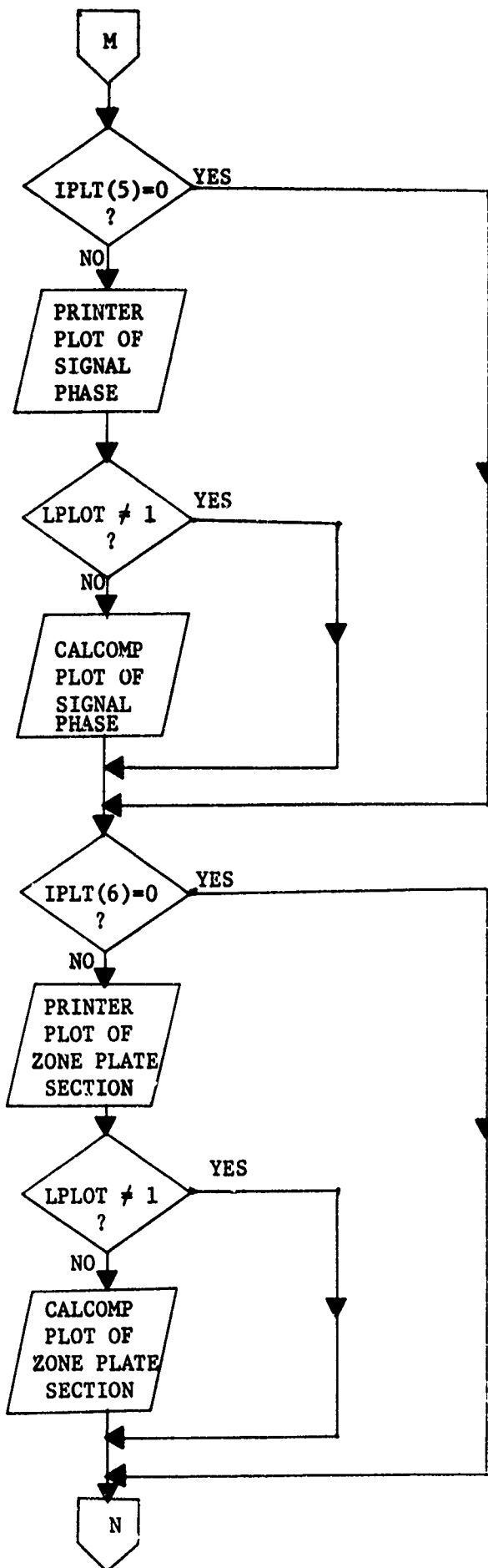
Note 10: If the preset focus option is evoked a new reference function value is not generated.

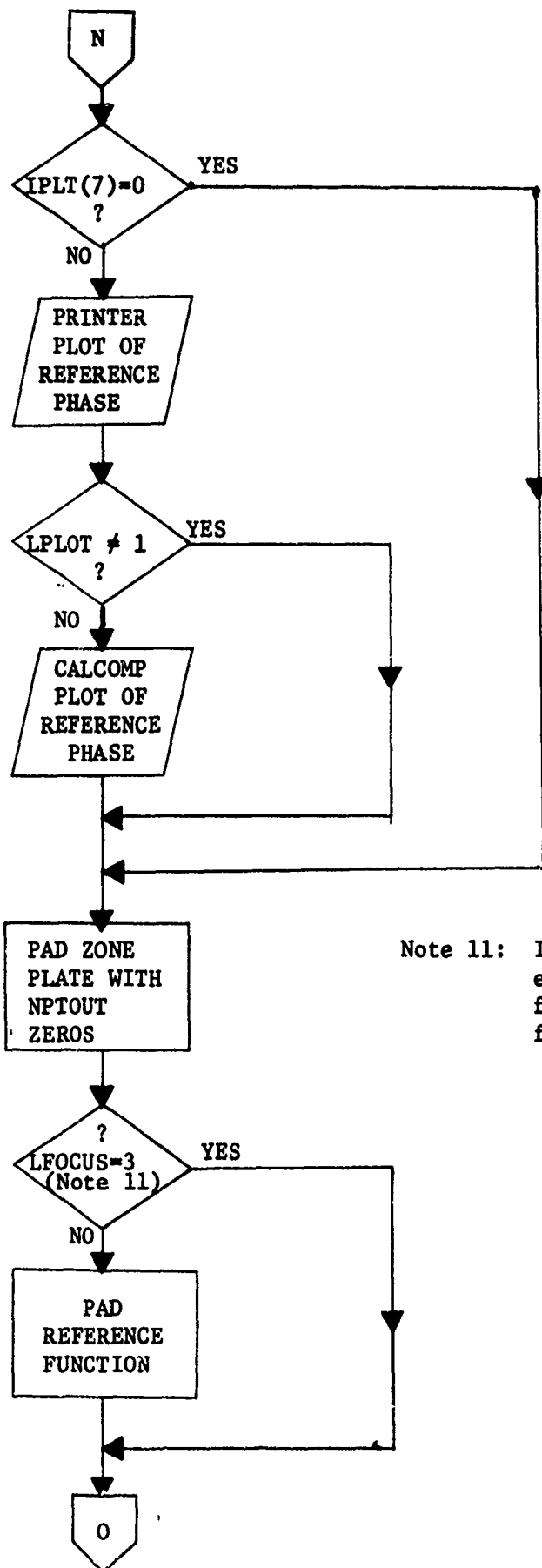




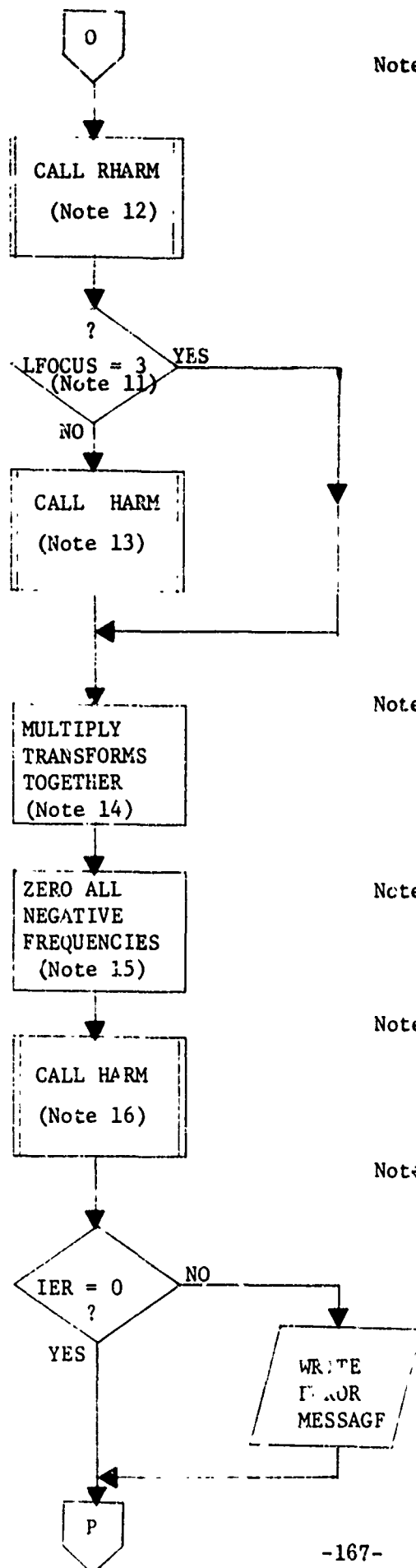








Note 11: If preset focus option is evoked skip reference function padding and transforming.



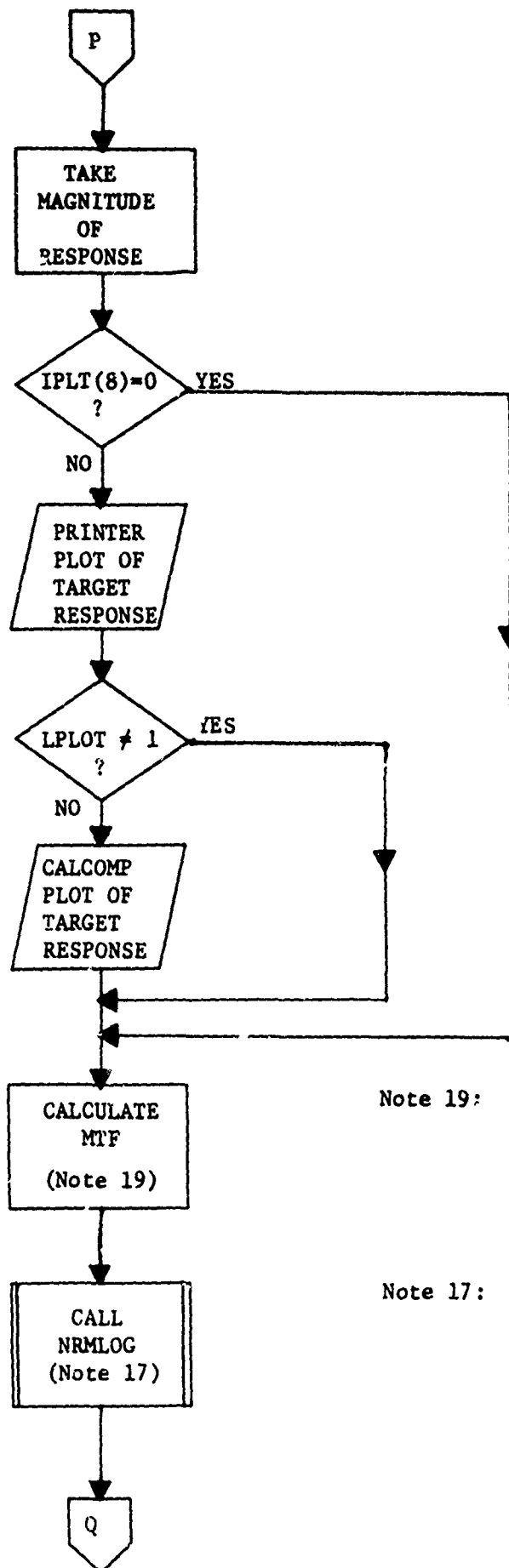
Note 12: Real Fourier transform of zone plate section (one-dimensional) in preparation for convolution.

Note 13: Complex Fourier transform of reference function in preparation for convolution.

Note 14: Multiply positive frequencies of transforms together to achieve complex convolution of reference and radar signals.

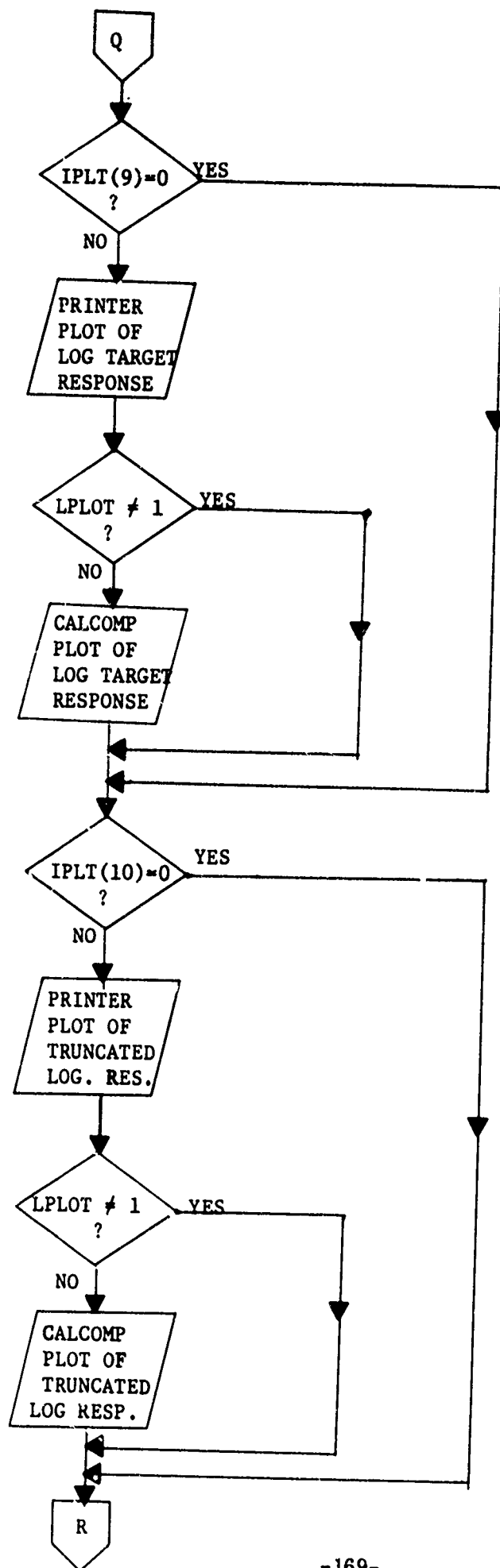
Note 15: Those negative frequencies resulting from real transform of signal are set to zero to insure complex processing.

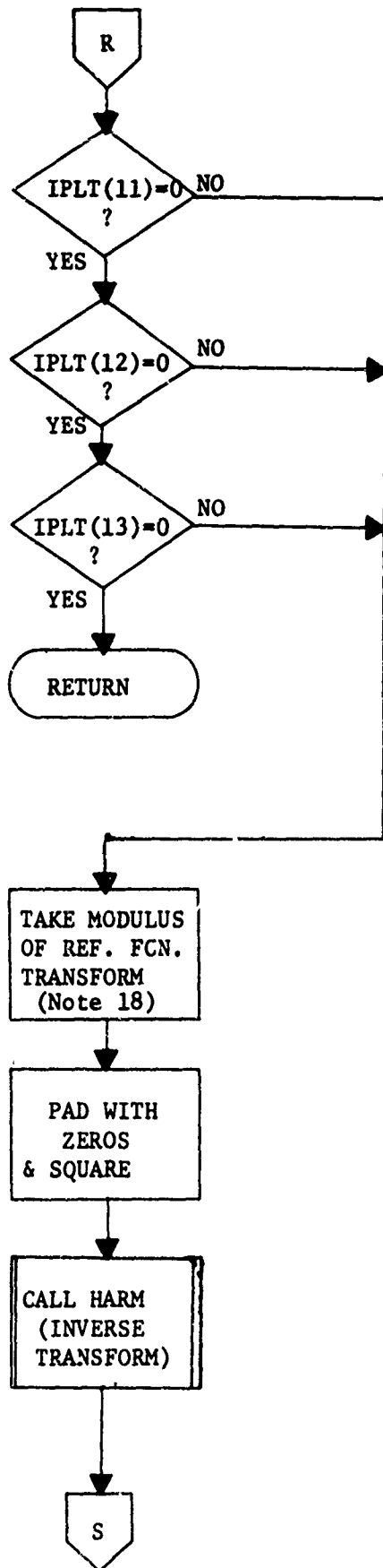
Note 16: Inverse transform to complete the convolution.



Note 19: The Modulation Transfer Function is the Modulus of the Fourier transform of the intensity impulse response. The MTF is generated and returned in an array to the main program.

Note 17: NRMLLOG clips the response below a specified threshold, takes 20 times the log of each point, and finds the locations of maximum value and 1st point above threshold. The data is normalized such that maximum is 0.0 db.





Note 18: To get ideal response one convolves reference function with itself. This is equivalent to taking the modulus squared of the reference function transform and performing an inverse transform.

